

Cyclohexane photo-catalytic oxidation on  $\text{TiO}_2$ ,  
an in situ ATR-FTIR mechanistic and kinetic study



Cyclohexane photo-catalytic oxidation on  $\text{TiO}_2$ ,  
an in situ ATR-FTIR mechanistic and kinetic study

**Proefschrift**

ter verkrijging van de graad van doctor  
aan de Technische Universiteit Delft,  
op gezag van de Rector Magnificus Prof. ir. K. C. A. M. Luyben,  
voorzitter van het College voor Promoties,  
in het openbaar te verdedigen  
op 1 november 2010 om 10:00 uur

door

Ana Rita Martins Guerreiro Rocha Almeida

Licenciada em Engenharia Química, Universidade Nova de Lisboa  
geboren te Lissabon, Portugal

Dit proefschrift is goedgekeurd door de promotoren:

Prof. dr. J. A. Moulijn

Prof. dr. G. Mul

Samenstelling promotiecommissie:

Rector Magnificus	voorzitter
Prof. dr. J.A. Moulijn	Technische Universiteit Delft, promotor
Prof. dr. G. Mul	Universiteit Twente, promotor
Prof. dr. F. Kapteijn	Technische Universiteit Delft
Prof. dr. I. W. C. E. Arends	Technische Universiteit Delft
Prof. dr. B. M. Weckhuysen	Universiteit Utrecht
Prof. dr. J. A. Anderson	University of Aberdeen
Dr. F. Tielens	Université Pierre et Marie Curie
Prof. dr. H. van Bekkum	Technische Universiteit Delft (reservelid)

The research reported in this thesis was carried out at the Catalysis Engineering Group, ChemE, Faculty of Applied Science, Delft University of Technology (Julianalaan 136, 2628 BL, Delft, The Netherlands), with financial support of Project DPC.7065 of the Stichting Technologische Wetenschappen (STW).

Proefschrift, Technische Universiteit Delft

met samenvatting in het Nederlands

ISBN 978-90-5335-335-6

Copyright © 2010 by Ana Rita Almeida

All rights reserved

Cover design: Ana Rita Almeida and Robert Kaners

Printed by Ridderprint B. V., Ridderkerk, The Netherlands

*Para a minha avó,  
que me ajudou a cá chegar mas não me viu acabar*



# Contents

<b>Preface</b>	<b>1</b>
<b>Chapter 1. Introduction</b>	<b>3</b>
1.1. Background	4
1.2. Problem statement	12
1.3. Aim and approach	13
1.4. Outline	17
<b>Chapter 2. <i>In situ</i> ATR-FTIR study on the selective photo-oxidation of cyclohexane</b>	<b>23</b>
2.1. Introduction	24
2.2. Experimental	25
2.3. Results	27
2.4. Discussion	37
2.5. Conclusions	42
<b>Chapter 3. Improved performance of TiO<sub>2</sub> in the selective photocatalytic oxidation of cyclohexane by increasing the rate of desorption through surface silylation</b>	<b>45</b>
3.1. Introduction	46
3.2. Experimental	47
3.3. Results	49
3.4. Discussion	58
3.5. Conclusions	64
<b>Chapter 4. Combined ATR-FTIR and DFT study of cyclohexanone adsorption on hydrated TiO<sub>2</sub> anatase surfaces</b>	<b>67</b>
4.1. Introduction	68
4.2. Experimental	69

4.3. Computational methods	70
4.4. Results	72
4.5. Discussion	88
4.6. Conclusions	91
<b>Chapter 5. Cyclohexane photo-catalytic oxidation over TiO<sub>2</sub>: a novel interpretation of temperature dependent performance</b>	<b>93</b>
5.1. Introduction	94
5.2. Experimental methods	95
5.3. Theoretical methods	96
5.4. Results	102
5.5. Discussion	114
5.6. Conclusions	118
5.7. Appendix	120
<b>Chapter 6. Cyclohexane photo-catalytic oxidation on TiO<sub>2</sub>: evidence for a Mars-van Krevelen mechanism</b>	<b>125</b>
6.1. Introduction	126
6.2. Experimental	127
6.3. Results	129
6.4. Discussion	140
6.5. Conclusions	144
<b>Chapter 7. Summary and outlook</b>	<b>147</b>
7.1. Summary	148
7.2. Outlook	151
<b>Samenvatting</b>	<b>153</b>
<b>List of acronyms</b>	<b>159</b>
<b>List of publications and presentations</b>	<b>161</b>
<b>Curriculum Vitae</b>	<b>165</b>
<b>Acknowledgements</b>	<b>167</b>



# PREFACE

Selective photo-catalysis has been considered as an alternative for conventional oxidation reactions, in particular when ‘thermal’ catalysis does not provide the desired product selectivities. The possibility of operating an oxidation reaction at room temperature and ambient pressures, by using a photon-activated catalyst is very attractive, but still far from industrial application. The question remains whether the use of sunlight, as an activating agent for a photo-oxidation reaction, can induce the selective formation of primary oxidation products with the required yields. Cyclohexane photo-oxidation to cyclohexanone was used as a model reaction for such study, using *in situ* Attenuated Total Reflection Fourier Transform Infrared (ATR-FTIR) spectroscopy. This spectroscopic technique allows for the analysis of the solid-liquid interface of heterogeneous photo-catalyzed reactions, and is therefore very informative for mechanistic and kinetic studies. This thesis presents a chronological sequence of the research performed on the cyclohexane photo-catalytic oxidation, with the objective of resolving the following issues:

- (i) Understand the reaction mechanism of cyclohexane photo-oxidation over  $\text{TiO}_2$ , including the determination of the intermediate steps towards cyclohexanone formation
- (ii) Reduce the known tendency for catalyst deactivation in the selective photo-oxidation of cyclohexane
- (iii) Determine kinetic parameters of this reaction

The first issue is reported in Chapter 2, where a preliminary reaction mechanism of the photo-catalytic oxidation of cyclohexane on  $\text{TiO}_2$  is proposed based on *in situ* ATR-FTIR results. In this chapter, cyclohexyl hydroperoxide is proposed as the reaction intermediate, but in Chapter 6 further studies on the reaction mechanism proved that this proposal needs adjustments. Isotopic labeling combined with Infrared Spectroscopy provided evidence for a Mars-van Krevelen mechanism, indicating that oxygen

incorporated in cyclohexane to form cyclohexanone originates from the  $\text{TiO}_2$  surface rather than from dissolved  $\text{O}_2$ .

The second issue is discussed in Chapters 3 and 5. The rate of catalyst deactivation was found to reduce when increasing the hydrophobic character of the  $\text{TiO}_2$  catalyst (Chapter 3). This was achieved by anchoring trimethylsilyl groups on the  $\text{TiO}_2$  surface, which increases the rate of cyclohexanone desorption. The rate of cyclohexanone desorption is also increased operating the reaction at slightly elevated temperatures ( $T < 50\text{ }^\circ\text{C}$ ), although this reduces selectivity due to the thermal enhancement of reactions leading to deactivation (Chapter 5).

The third issue is discussed in Chapters 4 and 5, where kinetic parameters are obtained by using the combination of ATR-FTIR spectroscopy data with theoretical methods. By Density Functional Theory (DFT) calculations, the adsorption enthalpies of cyclohexanone on different  $\text{TiO}_2$  surface planes, with various adsorbed  $\text{H}_2\text{O}$  layers, were calculated (Chapter 4). The combination of Infrared spectroscopy with a microkinetic model allowed for the quantification of the spectroscopic results and calculation of the kinetic and thermal parameters of the parallel routes of formation of cyclohexanone and deactivating species, respectively (Chapter 5).

Chapter 7 summarizes the most important findings with respect to the mechanism and kinetics of cyclohexane photo-catalytic oxidation and provides insight in how to reduce the rate of  $\text{TiO}_2$  deactivation. Although the research in this thesis was performed using artificial UV light, recommendations are given on how to efficiently use sunlight illumination to activate the photo-catalytic reaction.

# *Chapter 1*

## Introduction

Chemical processes are generally operated at elevated temperatures and pressures, and energy intensive separations are usually necessary. This thesis focuses on the production of cyclohexanone, which is an intermediate of high commercial importance as a result of its use in nylon-6 and nylon-6,6 production. Using  $\text{TiO}_2$  based photo-catalysis is a promising alternative to the inefficient commercial process of cyclohexanone production, producing cyclohexanone very selectively at ambient conditions. Furthermore, potentially the catalyst can be activated by a free energy source, i.e. sunlight. However, low yields and severe catalyst deactivation prevent the photo-catalytic alternative to be industrially applied. The work presented in this thesis aims at providing further insight in the mechanism and kinetics of cyclohexane photo-catalytic oxidation to cyclohexanone, by looking closely at the surface phenomena. Attenuated Total Reflection Fourier Transform Infrared (ATR-FTIR) which allows for the analysis of adsorbed reagents, intermediates and products at the catalyst surface, combined with isotopic substitution and modeling tools, is highly informative. This chapter provides a theoretical basis for understanding the various topics within this thesis. The aim and approach chosen to conduct this research are presented, and a description of the structure of the thesis is provided.

## 1.1. BACKGROUND

### 1.1.1. Cyclohexane oxidation

Cyclohexane oxidation is of large commercial importance, with a capacity of  $\sim 10^6$  tons a year. In this process a series of liquid phase reactors operate in a range of 130-180 °C and 8-12 bar pressure, in the presence of a homogeneous catalyst (cobalt or manganese naphthenate). Conversion of cyclohexane is in the range of 3-8% with selectivity to cyclohexanone and cyclohexanol of 70-80%. The conversion is usually kept below 5% in order to minimize the formation of byproducts (e.g. adipic acid and 6-hydroxyhexanoic acid). A variety of other compounds are formed, such as hydroperoxides, which are thermally or catalytically decomposed to produce extra cyclohexanone and cyclohexanol. The final products are used to produce  $\epsilon$ -caprolactam and adipic acid, which are monomers of nylon-6 and nylon-6,6 respectively, which explains the high commercial interest in this process. However, the industrially applied process has disadvantages, namely:

- the energy intensive recycling of unreacted cyclohexane;
- the energy intensive separation of the alcohol and ketone by distillation;
- and for the cases where specific caprolactam production is preferred, a higher cyclohexanone selectivity is desired and an energy intensive cyclohexanol dehydrogenation step is therefore necessary [1-4].

Overall, a high cyclohexanone to cyclohexanol ratio is preferred, which is not directly achieved by the industrial process. Furthermore, the industrially applied process due to its extreme conditions has led to serious accidents. The Flixborough disaster was an explosion at a cyclohexane oxidation plant in England, in the year of 1974. Two months prior to the explosion, a crack had been discovered in one of the reactors. A temporary pipe was installed to bypass the leaking reactor and allowing continued operation of the plant while reparations were made. The temporary bypass pipe (containing cyclohexane at 150 °C and 10 bar) ruptured, cyclohexane leaked and formed a vapour cloud, which exploded, completely destroying the plant. This accident killed 28 people and seriously injured 36 [5].

A safer and more selective alternative to cyclohexanone production is needed.

### *1.1.2. Heterogeneous photo-catalysis*

In a conventional heterogeneously catalyzed reaction, a solid catalyst is thermally activated, while in a heterogeneous photo-catalyzed reaction, activation occurs by light, i.e. by photons. A photo-catalyst is usually a semiconductor material like a metal oxide or sulfide, such as  $\text{TiO}_2$ ,  $\text{ZnO}$ ,  $\text{ZrO}_2$ ,  $\text{CeO}_2$ ,  $\text{CdS}$ ,  $\text{ZnS}$ , etc. of which  $\text{TiO}_2$  is the most widely applied.

Light absorbing semiconductors have been studied since 1921, when  $\text{TiO}_2$  was found to reduce, upon exposure to sun light, in the presence of an organic compound [6]. But it was only in 1972, that Fujishima and Honda [7] found that under UV illumination, a titanium dioxide electrode immersed in water, yields the formation of oxygen, with hydrogen formation occurring on a platinum counter electrode. After this finding, many research groups have dedicated their work to achieving sustainable hydrogen production by water splitting under solar light illumination. Besides this very important application many other practical applications of photo-catalysis have been discovered. Some of the most important ones are related to environmental applications, such as water purification [8,9] and air purification [10,11], both using  $\text{TiO}_2$  as photo-catalyst. Furthermore,  $\text{TiO}_2$  is now broadly applied in self-cleaning and self-sterilizing surfaces, as well as for cosmetic purposes as sun-blocking cream, where the function of  $\text{TiO}_2$  is to absorb the harmful UV radiation from the solar spectrum [12]. Most commercial photo-catalytic applications are based on complete depletion of organic pollutants, but there is also growing scientific interest in the possibility to use photo-catalytic redox transformations in practice, i.e. to selectively synthesize commercially interesting organic compounds. Heterogeneous photo-catalysis enables a large variety of selective mild oxidation reactions, dehydrogenations, hydrogen transfer reactions,  $^{16}\text{O}_2$ - $^{18}\text{O}_2$  isotopic exchange, and alkane-deuterium exchange [13,14].

### *1.1.3. Mechanism of photo-catalytic reactions*

Both in gas phase and liquid phase (organic or aqueous) applications, a photo-catalytic reaction is composed of several steps:

1. Mass transfer of reactants to the catalyst surface
2. Adsorption of the reactants

3. Light absorption by the solid catalyst, creating electrons ( $e^-$ ) and holes ( $h^+$ )
4. Transport of photo-generated charges to the adsorption sites,
5. Reaction of the adsorbed species,
6. Desorption of products
7. Mass transfer of products through the bulk [15]

When a  $\text{TiO}_2$  particle, or any other photo-catalyst, is illuminated by photons with energies exceeding the bandgap energy of the material, an electron ( $e^-$ ) is excited from the valance band to the conduction band, while a hole ( $h^+$ ) is created in the valence band, which corresponds to an electronic vacancy. The following reaction represents such electron hole separation:



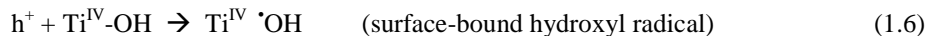
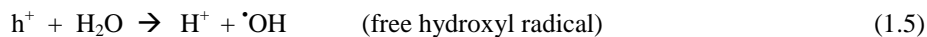
The holes and electrons formed after the charge-carrier generation participate in several pathways in photo-catalysis. The electron-hole pair can rapidly recombine, especially when the concentration of  $e^-$  and  $h^+$  in the catalyst particle is high. This recombination reduces the efficiency of photo-catalytic processes, with energy being lost as heat:



In the presence of adsorbed species, like molecular oxygen, the photo-generated electrons, with redox potential of -0.52 V, are able to reduce oxygen to a superoxide radical ( $\text{O}_2^-$ ):



The superoxide radical is an effective oxidizing agent that attacks neutral substrates as well as surface-adsorbed radicals and/or radical ions. The photo-generated holes created on the catalyst valence band are highly oxidizing, with redox potential of +2.53 V, and can receive electrons from donors. The  $h^+$  can oxidize water to hydrogen peroxide ( $\text{H}_2\text{O}_2$ ) or free hydroxyl radicals, or a  $\text{TiO}_2$  surface hydroxide to form surface bound hydroxyl radicals, respectively:



The surface-bound hydroxyl radical, one of the most powerful oxidizing species [16], is assumed to be the primary oxidizing species in the photo-catalytic oxidation of organic compounds [14,17]. Both surface-bound and free hydroxyl radicals can react with an adsorbed organic compound, via abstraction of H atoms by the  $\cdot\text{OH}$  radical, through a C-H bond cleavage:



Consequently, the resulting radical can react with  $\text{O}_2$ ,  $\text{O}_2^{\cdot-}$  or an  $\cdot\text{OH}$  radical to form oxygenated compounds, which is followed by a radical chain mechanism that can eventually lead to the mineralization of the organic compound to  $\text{CO}_2$  and  $\text{H}_2\text{O}$ . Figure 1.1 shows a schematic representation of the electron hole separation for a  $\text{TiO}_2$  particle leading to the initial steps of redox conversion of adsorbates.

Equations (1.1) through (1.7) summarize the important initial steps of catalyst activation by photons [17]. Each photo-activated state has a characteristic time, which was determined by flash photolysis for a  $\text{TiO}_2$  catalyst [18] and is shown in Table 1.1. According to this table, recombination of electron-hole pairs (10-100 ns) is faster than the reactions at the surface (100 ns to ms scale), contributing to the low quantum efficiencies of photo-catalytic reactions.

After the photon-activation of an adsorbed organic on the photo-catalyst surface, redox conversions take place, but the mechanisms involved remain far from clear. Over the past 20 years, new spectroscopic techniques have been developed to access the solid/liquid interface and carry on *in situ* mechanistic studies [19], which will be discussed further in this chapter.

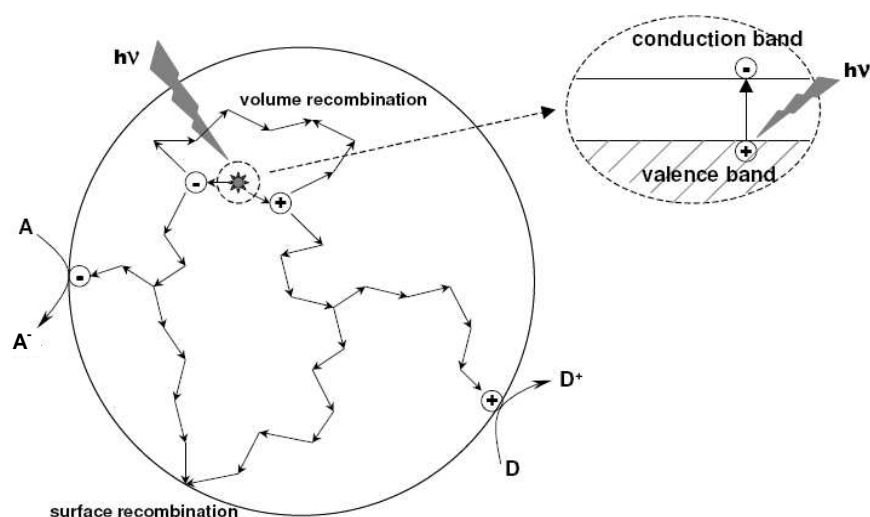


**Figure 1.1.** Fate of electrons and holes within a spherical  $\text{TiO}_2$  particle, under UV illumination, in the presence of an electron acceptor (A) and electron donor (D) (left); and energy band diagram of a  $\text{TiO}_2$  particle (right) [15].

**Table 1.1.** Characteristic times of  $\text{TiO}_2$  photon activated states [18].

Primary Process	Characteristic time
Generation of electron/hole pair:	
$\text{TiO}_2 + h\nu \rightarrow \text{TiO}_2 (e^- + h^+)$	fs (very fast)
Trapping of electron/hole pairs:	
$h^+ + \text{Ti}^{\text{IV}}\text{-OH} \rightarrow \{\text{Ti}^{\text{IV}}\text{OH}^{*+}\}$	10 ns (fast)
$e^- + \text{Ti}^{\text{IV}}\text{-OH} \rightarrow \{\text{Ti}^{\text{III}}\text{-OH}\}$	100 ps (shallow trap)
$e^- + \text{Ti}^{\text{IV}} \rightarrow \text{Ti}^{\text{III}}$	10 ns (deep trap)
Electron/hole recombination:	
$e^- + \{\text{Ti}^{\text{IV}}\text{OH}^{*+}\} \rightarrow \text{Ti}^{\text{IV}}\text{-OH}$	100 ns (slow)
$h^+ + \{\text{Ti}^{\text{III}}\text{OH}\} \rightarrow \text{Ti}^{\text{IV}}\text{-OH}$	10 ns (fast)
Reaction at the surface:	
$\{\text{Ti}^{\text{IV}}\text{OH}^{*+}\} + \text{organic} \rightarrow \text{Ti}^{\text{IV}}\text{-OH} + \text{oxidized organic}$	100 ns (slow)
$\{\text{Ti}^{\text{III}}\text{-OH}\} + \text{O}_2 \rightarrow \text{Ti}^{\text{IV}}\text{-OH} + \text{O}_2^{\bullet -}$	ms (very slow)



#### 1.1.4. $\text{TiO}_2$ photo-catalyst

$\text{TiO}_2$  can exist in three major crystalline phases anatase, rutile and brookite, of which anatase and rutile are photo-catalytically active with bandgaps of 3.2 and 3.0 eV, respectively [18]. Anatase is the most photo-catalytically active phase, but is the least stable of the two phases, transforming into rutile at temperatures higher than 600 °C. Anatase  $\text{TiO}_2$  has a bipyramid structure exhibiting 95% of the surface as (101) surfaces, truncated by (001) facets [20], with tetragonal dimensions of  $a = b = 3.782 \text{ \AA}$ ;  $c = 9.502 \text{ \AA}$  [21]. The bulk structure and equilibrated truncated octahedral shape of an anatase  $\text{TiO}_2$  particle is shown in Figure 1.2.

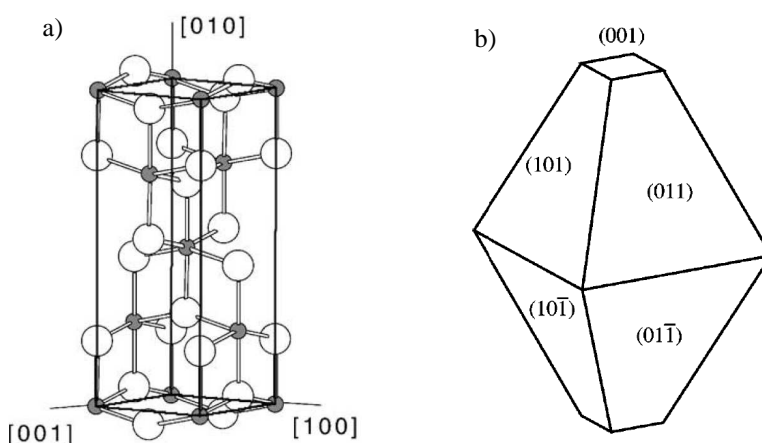


**Figure 1.2.** a) Bulk structure of anatase  $\text{TiO}_2$ , with the titanium atoms in grey and the oxygen atoms in white [21] and b) equilibrium shape of an anatase  $\text{TiO}_2$  crystal, according to the Wulff construction [20].

The activity of  $\text{TiO}_2$  photo-catalysts is dependent on various aspects. Extrinsic aspects are the catalyst morphology (powder, slurry or thin film), the light harvesting method and reactor design. Intrinsic aspects, which can be tuned with the applied catalyst synthesis method, are the crystalline structure (anatase or rutile), catalyst surface area, density of surface OH sites, surface acidity, surface defects and adsorption/desorption characteristics, such as hydrophilicity.

The activity of  $\text{TiO}_2$  photo-catalysts is more enhanced by increasing the OH concentration than surface area. An increase in the surface area in general results in an increase of surface defects and larger times of electron-hole recombination, but an increase in Ti-OH groups is more beneficial, since they act as both adsorption sites for  $\text{H}_2\text{O}$  and organics, and they are a source of  $\cdot\text{OH}$  radicals (upon hole scavenging), which are the primary oxidation agents in photo-catalytic reactions.

The surface hydrophilicity is also an important parameter;  $\text{TiO}_2$  catalysts are known to be very hydrophilic, with up to three hydrogen bonded water layers at ambient conditions, of which some are strongly adsorbed [22,23]. Water adsorption reduces the number of available Ti-OH sites for adsorption, and it also contributes to a higher concentration of  $\cdot\text{OH}$  radicals under UV illumination, inducing total oxidation of organics to  $\text{CO}_2$  and  $\text{H}_2\text{O}$  [24]. A systematic study of water adsorption on  $\text{TiO}_2$  was done by Density Functional Theory (DFT) calculations [25]. However in most DFT studies the effect of UV illumination is not taken into account. It is known that under UV irradiation the  $\text{TiO}_2$  catalyst undergoes surface modifications, especially in the presence of adsorbed water. The UV induced so-called super-hydrophilicity effect is the incorporation of adsorbed water molecules in the  $\text{TiO}_2$  structure with formation of new Ti-OH sites. This was observed by a placing a droplet of water on a  $\text{TiO}_2$  film; UV illuminating this droplet reduces the contact angle to  $\sim 0^\circ$  [12]. The reverse reaction, consisting in the removal of the photon induced OH sites with the formation of adsorbed  $\text{H}_2\text{O}$  was found to be a much slower process, in the order of days [26]. Given the strong hydrophilic character of  $\text{TiO}_2$  surfaces, the absorption characteristics measured under dark conditions will hardly relate to the UV illumination conditions, which will be discussed in Chapter 5.

In this research, a commercial  $\text{TiO}_2$  catalyst Hombikat UV 100 from Sachtleben Chemie was used. Hombikat UV 100 is synthesized by the ‘sulfate’ technology where ilmenite ( $\text{FeTiO}_3$ ) is leached by sulfuric acid and the formed  $\text{TiOSO}_4$  is decomposed by steam into  $\text{TiO}_2$  [27]. Properties of Hombikat UV 100 are resumed in Table 1.2.

**Table 1.2.** Properties of Hombikat UV 100 [28].

Hombikat UV 100	
Properties	High photo-catalytic activity per unit weight
Crystalline phase	100% anatase
Primary particle size	< 10nm
Agglomerates in H <sub>2</sub> O	1 µm
Surface area (m <sup>2</sup> /g)	337
Total surface-OH (mmol/g)	1.21
Acidic-OH (mmol/g)	0.92
Acidic-OH/basic-OH	3.3
Surface-OH density (1/nm <sup>2</sup> )	2.2
Acidity of surface-OH	Weak Lewis acidity

#### 1.1.5. Kinetics of photo-catalytic reactions

Most kinetic models used in photo-catalytic reactions are based on the Langmuir-Hinshelwood-Hougen-Watson (LHHW) models [9,29,30]. These models describe the reaction kinetics between two adsorbed species, a free radical and an adsorbed substrate, or alternatively a surface-bound radical and a free substrate. The initial rate of substrate removal ( $R_i$ ) varies proportionally with the surface coverage ( $\theta$ ), and the adsorption equilibrium of the substrate ( $K$ ) follows a Langmuir isotherm, as described in equation (1.8).

$$R_i = k\theta = \frac{kKC_i}{1 + KC_i} \quad (1.8)$$

where  $C_i$  is the initial concentration of the substrate and  $k$  is the Langmuir-Hinshelwood reaction constant. The kinetics of a photo-catalytic reaction depends on several aspects such as catalyst loading, wavelength of the UV light, light intensity,

temperature and pH [15]. Among the referred aspects, the particular effect of temperature on the selective photo-catalytic cyclohexane oxidation is discussed in Chapter 5. The effect of temperature on the activation energy of a photo-catalytic reaction is expected to be small. Activation energies in the range of 5-13 kJ/mol have been determined by pulse radiolysis, for the formation of  $\cdot\text{OH}$  radicals, or super-oxide anions [31,32], which is much lower than usually observed catalytically for thermally activated reactions. The apparent activation energies, generally calculated from a log plot of rate constant and reciprocal absolute temperature, tend to be affected by the adsorption enthalpies of reagents or products. At low temperatures higher apparent activation energies are commonly a result of product desorption limitations, while at higher temperatures negative apparent activation energies are usually ascribed to adsorption limitations of the reagent [15,33].

#### *1.1.6. Cyclohexane photo-catalytic oxidation*

Contrarily to the industrial cyclohexane oxidation process, the photo-catalytic process using a  $\text{TiO}_2$  based photo-catalyst, shows very high cyclohexanone selectivity [28]. Various aspects of the photo-catalytic oxidation of cyclohexane to cyclohexanone have received attention in the open literature, including the effect of illumination wavelength [34], photo-catalyst structure [33] and presence of solvents in the reaction [35-37]. Furthermore, various catalytic cycles have been proposed to explain the photo-catalytic conversion of cyclohexane to cyclohexanone on the  $\text{TiO}_2$  surface. However, so far little evidence is available to support the proposed reaction mechanisms.

### **1.2. PROBLEM STATEMENT**

The very high selectivity of  $\text{TiO}_2$ -catalyzed cyclohexane photo-oxidation to cyclohexanone is of interest for the possible industrial application of this reaction, as replacement of the currently applied industrial process. However, the low yields of cyclohexane oxidation by photo-catalysis make this process economically unviable. A widely known problem of  $\text{TiO}_2$  photo-catalysts is very fast deactivation under organic

reaction conditions [11,38], which induces short reaction life times and low yields. Until now, little understanding exists on mechanistic reaction steps occurring on the  $\text{TiO}_2$  surface, including its deactivation. In order to improve the performance of cyclohexane photo-catalytic oxidation on  $\text{TiO}_2$ , a deeper understanding of the mechanistic reaction steps is absolutely necessary.

### 1.3. AIM AND APPROACH

Though reaction mechanisms for cyclohexane photo-oxidation on  $\text{TiO}_2$  have been proposed [28,34], little *in situ* spectroscopic evidence is available to support these pathways. The aim of this doctoral research is to obtain actual mechanistic evidence and improve the knowledge of this specific photo-reaction, in order to understand its pitfalls and to design new improvement methods, both on reaction operation and catalyst functionalization. To obtain this knowledge, different techniques and methods were used, which will be described in the following.

#### 1.3.1. Time resolved *in situ* ATR-FTIR spectroscopy

Heterogeneously catalyzed liquid-phase reactions are conventionally analyzed by sample withdrawal from the reaction medium, followed by off-line characterization techniques, such as GC, HPLC, NMR or MS. Besides being time consuming, these techniques cannot analyze labile intermediates or adsorbates on the catalyst surface [39]. Attenuated Total Reflection Fourier Transform Infrared (ATR-FTIR) spectroscopy allows for the investigation of the solid-liquid interface under actual reaction conditions. *In situ* ATR-FTIR studies on photo-catalysis have mostly focused on  $\text{TiO}_2$  catalyzed photo-degradation of water-solved organic pollutants [40-47], and on photo-activation of water [48,49]. In general, these studies have shown that ATR-FTIR provides a sensitive tool for the analysis of surface adsorbed molecules, adsorbed reaction intermediates and allows estimation of its molecular structure, molecular orientation and adsorption strength. Furthermore, kinetic and mechanistic information can be extracted [50].

ATR is a type of internal reflection spectroscopy in which the sample is placed in contact with an internal reflection element (IRE) of high refractive index. Infrared radiation is focused onto the edge of the IRE, reflected through the IRE, and then directed to a suitable detector [19]. Although complete internal reflection occurs at the sample/IRE interface, an evanescent wave penetrates a short distance ( $d_p$ , nm) into the sample, depending upon the wavelength ( $\lambda$ , nm) of the incident light, where it can be absorbed. An absorption spectrum of the sample in contact with the IRE can be obtained, the spectrum being dependent on the angle of incidence ( $\theta$ ) and the refractive indices of the IRE material ( $n_1$ ) and the sample ( $n_2$ ), according to equation (1.9).

$$d_p = \frac{\lambda}{2\pi n_1 \sqrt{\sin^2 \theta - (n_2 / n_1)^2}} \quad (1.9)$$

The propagating light passing through the IRE forms a standing wave perpendicular to the total reflecting surface. If the sample absorbs radiation, the propagating wave interacts with the sample and becomes attenuated. A representation of a typical ATR cell and a focus on the evanescent wave is represented in Figure 1.2.

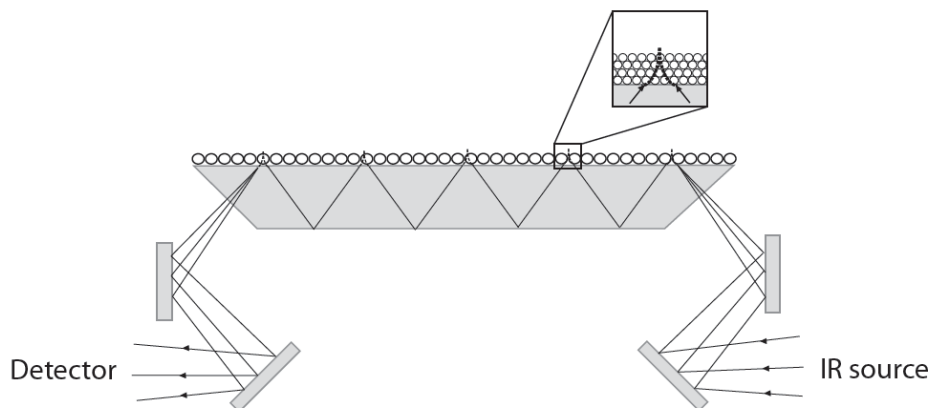


**Figure 1.2.** Typical ATR cell equipped with a horizontal IRE, coated with a solid catalyst. The inset represents the penetration depth of the evanescent wave.

The choice of IRE material is dependent upon a number of factors. These include the spectral range of interest, the adsorbent/adsorbate system under investigation, the nature of the solvent being used, the pH of the system, the physical and chemical properties of the different crystal materials available, and lastly, their respective cost. Some of the most important properties of the ZnSe and Diamond ATR crystals, which were used throughout this research, can be seen in Table 1.3. [19].

**Table 1.3.** Physical properties of ZnSe and Diamond IRE materials [19].

IRE	n	Hardness (kg/nm <sup>2</sup> )	Transmission (cm <sup>-1</sup> )
ZnSe	2.4	137	20000-700
Diamond	2.4	7000	4500-2500; 1667-33

The main advantage of ATR-FTIR spectroscopy is the sensitivity enhancement in comparison to conventional time-resolved spectra. However, the high sensitivity of this technique can also become a limitation, because ATR infrared spectra may simultaneously provide information on dissolved and adsorbed reactants and products, adsorbed intermediates, by-products, spectator molecules and the catalyst itself. The unspecific character of ATR-FTIR may therefore induce very complicated spectral analysis [51]. Also the time resolution of the spectral collection can be a limitation, when photo-catalytic reactions with very labile radical intermediates are analyzed. As shown in Table 1.1, the lifetime of photon-activated states ranges from femtosecond to millisecond time scales. Steps from femtosecond to microsecond time scales are too fast to be analyzed by most infrared spectroscopic techniques. Some photon induced steps in the millisecond and second range may be analyzed continuously by ATR-FTIR spectroscopy. Nakamura *et al.* applied ATR-FTIR spectroscopy to analyze surface intermediates of photo-catalytic reactions, formed by O<sub>2</sub> reduction [52] and water photo-oxidation [53]. These authors proposed a mechanism of O<sub>2</sub> photo-evolution, based on *in situ* analysis of short lived surface peroxo species, Ti(O<sub>2</sub>) and TiOOH. In this thesis, radical intermediates could not be measured with ATR-FTIR spectroscopy, but reaction steps in the scale of seconds, like adsorption, desorption, thermal decomposition and molecular rearrangement could be analyzed.

### 1.3.2. Isotopic labeling

The combination of ATR-FTIR with isotopic labeling is a powerful approach to obtain mechanistic and kinetic information on catalytic reactions. Isotopic substitution is a useful tool for assigning frequencies to bonds in adsorbed species, because the bond strength decreases with isotopic labeling and the IR frequencies shift to lower wavenumbers. The IR redshift can be predicted by the harmonic oscillator equation, as described in equation (1.10).

$$\nu = \frac{1}{2\pi} \sqrt{\frac{k}{\mu}} \quad (1.10)$$

with  $\nu$  ( $\text{cm}^{-1}$ ) corresponding to the frequency of the vibration,  $k$  ( $\text{cm}^{-2} \cdot \text{g}^{-1}$ ) to the force constant of the bond and  $\mu$  ( $\text{g}^{-1}$ ) to the reduced mass. The latter is determined based on the mass of each vibrating atoms, according to equation (1.11) [54].

$$\frac{1}{\mu} = \frac{1}{m_1} + \frac{1}{m_2} \quad (1.11)$$

Besides aiding the spectral interpretation, isotopic substitution also provides kinetic information, with the comparison between the rates of labeled and unlabeled product formation providing indication for the rate-limiting step of the reaction.

Isotopic substitutes which are commonly used are: deuterium ( $^2\text{H}$ ), an isotope of  $^1\text{H}$ ;  $^{18}\text{O}$ , an isotope of  $^{16}\text{O}$ ; and  $^{13}\text{C}$ , an isotope of  $^{12}\text{C}$ . The two first isotopes are used in this thesis for mechanistic and kinetic studies of cyclohexane photo-catalytic oxidation, and are discussed in Chapters 2 and 6.

### 1.3.3. Modeling

To study the kinetics of a heterogeneous catalyzed reaction, measurements of reaction rates and knowledge on the reaction mechanism, including reaction intermediates, are crucial. The reaction rates and activation enthalpies may vary depending on the reaction conditions of a heterogeneously catalyzed reaction, explained by a change in reaction pathway or rate limiting step, for example. To obtain this



information, the combination of *in situ* spectroscopy, isotopic labeling and computational methods is very useful [55]. As referred to previously, ATR-FTIR spectroscopy is a very sensitive technique able to simultaneously provide information on all the reaction agents. Molecular modeling, in particular Density Functional Theory (DFT) calculations, can be used for the interpretation of vibration frequencies obtained experimentally, and aids the analysis of ATR-FTIR results [46]. Furthermore, with molecular modeling, adsorption enthalpies of organics on modeled catalyst surfaces, which resemble experimental conditions, can also be estimated [56].

## 1.4. OUTLINE

The research described in this thesis focuses on the understanding of the reaction mechanism and kinetics of cyclohexane photo-catalytic oxidation over  $\text{TiO}_2$ , mainly by *in situ* ATR-FTIR spectroscopy, combined with molecular and kinetic modeling. Based on the obtained knowledge, modification of the  $\text{TiO}_2$  catalyst was performed to improve the performance in cyclohexane photo-catalytic oxidation.

In Chapter 2, a preliminary reaction mechanism of the photo-catalytic oxidation of cyclohexane on  $\text{TiO}_2$  is proposed based on *in situ* ATR-FTIR spectroscopic results. A first attempt is made to determine the rate determining step in the photo-oxidation of deuterated cyclohexane. In Chapter 3 the surface properties of the catalyst were modified, by silylation, to increase hydrophobicity and improve product desorption. The catalyst synthesis method and the mechanistic and kinetic effect of  $\text{TiO}_2$  silylation on cyclohexane photo-oxidation were studied.

The experimental results obtained by ATR-FTIR are compared with theoretical methods, on a molecular level and on a microkinetic level. Chapter 4 studies the infrared absorption features of cyclohexanone adsorbed on hydrated  $\text{TiO}_2$  surfaces, by a Density Functional Theory (DFT) calculation, in order to aid spectral interpretation and calculate adsorption enthalpies. In Chapter 5, the effect of temperature on cyclohexane photo-catalytic oxidation is analyzed, and the obtained experimental results are fitted to a microkinetic model, which allows for the quantification of ATR-FTIR results and

determination of kinetic and thermal parameters of cyclohexanone formation, as well surface deactivation.

Due to the many uncertainties still existing in relation to the mechanism of cyclohexanone formation, as well as the formation of deactivating species, further isotopic studies were developed and are discussed in Chapter 6, with the use of labeled oxygen ( $^{18}\text{O}_2$ ). This provided information on the mechanism of oxygen incorporation in products, and on the occurrence of a kinetic isotope effect for the formation of species inducing catalyst deactivation.

Chapter 7 summarizes the most important findings and includes recommendations for improvement of cyclohexane photo-oxidation. A schematic overview of the structure of the thesis is given in Figure 1.3.

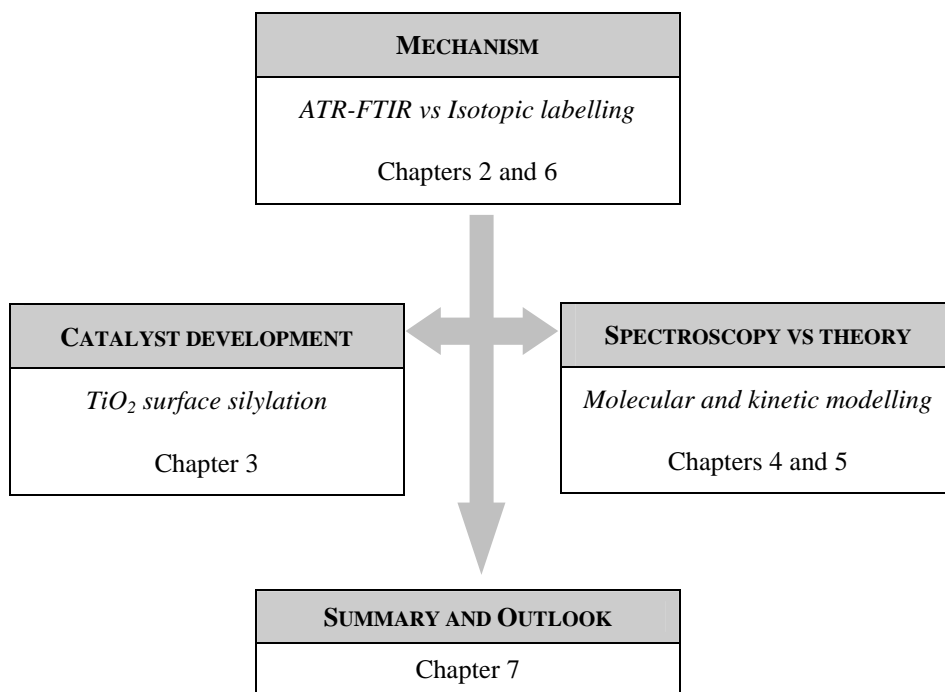


**Figure 1.3.** Schematic overview of the thesis.

## REFERENCES

- [1] E.J.Murray L.O.Winstrom, US3671588-A (1972), ALLIED CHEM CORP.
- [2] C.Summer, R.J.Gartside, M.Greene, I, US6008415-A (1999), ABB LUMMUS GLOBAL INC.
- [3] P.Saji, V, C.Ratnasamy, S.Gopinathan, US6392093-B1 (2002), COUNCIL SCI & IND RES.
- [4] I.Hermans, P.Jacobs, J.Peeters, Chem. -Eur. J. 13 (2007) 754.
- [5] [http://en.wikipedia.org/wiki/Flixborough\\_disaster](http://en.wikipedia.org/wiki/Flixborough_disaster)
- [6] A.Fujishima, X.T.Zhang, D.A.Tryk, Surf. Sci. Rep. 63 (2008) 515.
- [7] A.Fujishima, K.Honda, Nature 238 (1972) 37.
- [8] E.Pelizzetti, M.Borgarello, C.Minero, E.Pramauro, E.Borgarello, N.Serpone, Chemosphere 17 (1988) 499.
- [9] A.Mills, R.H.Davies, D.Worsley, Chem. Soc. Rev. 22 (1993) 417.
- [10] J.Peral, D.F.Ollis, J. Catal. 136 (1992) 554.
- [11] J.Peral, X.Domenech, D.F.Ollis, J. Chem. Technol. Biotechnol. 70 (1997) 117.
- [12] A.Fujishima, X.T.Zhang, C. R. Chim. 9 (2006) 750.
- [13] J.M.Herrmann, Helv. Chim. Acta 84 (2001) 2731.
- [14] M.A.Fox, M.T.Dulay, Chem. Rev. 93 (1993) 341.
- [15] J.M.Herrmann, Top. Catal. 34 (2005) 49.
- [16] O.Legrini, E.Oliveros, A.M.Braun, Chem. Rev. 93 (1993) 671.
- [17] C.S.Turchi, D.F.Ollis, J. Catal. 122 (1990) 178.
- [18] A.Mills, S.LeHunte, J. Photochem. Photobiol. A 108 (1997) 1.
- [19] A.R.Hind, S.K.Bhargava, A.McKinnon, Adv. Colloid Interface Sci. 93 (2001) 91.
- [20] M.Lazzeri, A.Vittadini, A.Selloni, Phys. Rev. B 63 (2001) 155409.
- [21] U.Diebold, Surf. Sci. Rep. 48 (2003) 53.
- [22] J.Soria, J.Sanz, I.Sobrados, J.M.Coronado, A.J.Maira, M.D.Hernandez-Alonso, F.Fresno, J. Phys. Chem. C 111 (2007) 10590.
- [23] A.Y.Nosaka, Y.Nosaka, Bull. Chem. Soc. Jpn. 78 (2005) 1595.
- [24] J.T.Carneiro, Application of TiO<sub>2</sub> semiconductor photocatalysis for organic synthesis, Thesis (2010), Technical University of Delft.
- [25] C.Arrouvel, M.Digne, M.Breyse, H.Toulhoat, P.Raybaud, J. Catal. 222 (2004) 152.

- [26] N.Sakai, A.Fujishima, T.Watanabe, K.Hashimoto, J. Phys. Chem. B 107 (2003) 1028.
- [27] P.Du, Catalysis Engineering of Light Induced Dye Degradation and Cyclohexane Photo-oxidation, Thesis (2009), Technical University of Delft.
- [28] P.Du, J.A.Moulijn, G.Mul, J. Catal. 238 (2006) 342.
- [29] M.R.Hoffman, S.T.Martin, W.Choi, D.W.Bahnmann, Chem. Rev. 95 (1995) 69.
- [30] J.M.Herrmann, Catal. Today 53 (1999) 115.
- [31] A.J.Elliot, A.S.Simons, Rad. Phys. Chem. 24 (1984) 229.
- [32] A.J.Elliot, D.R.McCracken, G.V.Buxton, N.D.Wood, J. Chem. Soc. Faraday Trans 86 (1990) 1539.
- [33] W.Mu, J.M.Herrmann, P.Pichat, Catal. Lett. 3 (1989) 73.
- [34] M.A.Brusa, M.A.Grela, J. Phys. Chem. B 109 (2005) 1914.
- [35] P.Boarini, V.Carassiti, A.Maldotti, R.Amadelli, Langmuir 14 (1998) 2080.
- [36] C.B.Almquist, P.Biswas, Appl. Catal. , A 214 (2001) 259.
- [37] M.A.Brusa, Y.Di Iorio, M.S.Churio, M.A.Grela, J. Mol. Catal. A 268 (2007) 29.
- [38] H.Einaga, S.Futamura, T.Ibusuki, Appl. Catal. B 38 (2002) 215.
- [39] G.Mul, G.M.Hamminga, J.A.Moulijn, Vib. Spectrosc. 34 (2004) 109.
- [40] G.N.Ekstrom, A.J.McQuillan, J. Phys. Chem. B 103 (1999) 10562.
- [41] J.M.Kesselman-Truttmann, S.J.Hug, Environ. Sci. Technol. 33 (1999) 3171.
- [42] I.Dolamic, T.Burgi, J. Phys. Chem. B 110 (2006) 14898.
- [43] A.E.Regazzoni, P.Mandelbaum, M.Matsuyoshi, S.Schiller, S.A.Bilmes, M.A.Blesa, Langmuir 14 (1998) 868.
- [44] P.Z.Araujo, C.B.Mendive, L.A.G.Rodenas, P.J.Morando, A.E.Regazzoni, M.A.Blesa, D.Bahnmann, Colloid Surf. A 265 (2005) 73.
- [45] C.B.Mendive, D.W.Bahnmann, M.A.Blesa, Catal. Today 101 (2005) 237.
- [46] C.B.Mendive, T.Bredow, M.A.Blesa, D.W.Bahnmann, Phys. Chem. Chem. Phys. 8 (2006) 3232.
- [47] W.Z.Xu, D.Rafty, J.S.Francisco, J. Phys. Chem. B 107 (2003) 4537.
- [48] D.S.Warren, A.J.McQuillan, J. Phys. Chem. B 108 (2004) 19373.
- [49] R.Nakamura, A.Imanishi, K.Murakoshi, Y.Nakato, J. Am. Chem. Soc. 125 (2003) 7443.
- [50] T.Burgi, A.Baiker, J. Phys. Chem. B 106 (2002) 10649.
- [51] T.Burgi, A.Baiker, Adv. Catal. 50 (2006) 227.

- [52] R.Nakamura, A.Imanishi, K.Murakoshi, Y.Nakato, J. Amer. Chem. Soc. 125 (2003) 7443.
- [53] R.Nakamura, Y.Nakato, J. Amer. Chem. Soc. 126 (2004) 1290.
- [54] J.W.Niemantsverdriet, in Spectroscopy in Catalysis, Wiley-VCH (2000).
- [55] H.Lynggaard, A.Andreasen, C.Stegelman, P.Stoltze, Prog. Surf. Sci. 77 (2004) 71.
- [56] C.B.Mendive, T.Bredow, A.Feldhoff, M.A.Blesa, D.Bahnemann, Phys. Chem. Chem. Phys. 11 (2009) 1794.



# Chapter 2

## *In situ* ATR-FTIR study on the selective photo-oxidation of cyclohexane over anatase TiO<sub>2</sub>

Anatase-catalyzed photo-oxidation of cyclohexane was analyzed by *in situ* ATR-FTIR spectroscopy. A set of seven UV-LEDs (375 nm), with a photon flux of  $8.98 \times 10^{-9}$  Einstein.cm<sup>-2</sup>.s<sup>-1</sup> (at the catalyst surface) was used to initiate the photo-reaction. Surface adsorbed cyclohexanone and water are the primary products of the photo-catalytic reaction, formed with a photonic efficiency of 0.5 mmol.Einstein<sup>-1</sup>, through a cyclohexyl hydroperoxide intermediate. Desorbed cyclohexanone, and surface carboxylates and carbonates become dominant in the subsequent stages of the reaction, leading to deactivation of the catalyst. The carboxylates and carbonates are most likely formed through non-selective peroxide oxidation and consecutive oxidation of adsorbed cyclohexanone by hydroxyl radicals. In the photo-catalytic oxidation of D<sub>12</sub>-cyclohexane, D<sub>10</sub>-cyclohexanone (in the adsorbed state and dissolved in cyclohexane) was formed at comparable rates as cyclohexanone. The absence of a kinetic isotope effect suggests that the reaction is not limited by activation of cyclohexane, but rather by activation of oxygen. Desorbed D<sub>10</sub>-cyclohexanone was observed at earlier stages and in higher quantities as compared to desorbed cyclohexanone. This is tentatively explained by a higher water content of the applied D<sub>12</sub>-cyclohexane compared to cyclohexane, inducing cyclohexanone desorption. Suggestions for improvement of the process are provided on the basis of the acquired scientific information.

This chapter is based on the following publication: A.R.Almeida, J.A.Moulijn, G.Mul, J. Phys. Chem. C 112 (2008) 155.

## 2.1. INTRODUCTION

The oxidation of cyclohexane is an important commercial reaction to convert cyclohexane via cyclohexanone in caprolactam, a monomer for nylon-6 production. For caprolactam production a low cyclohexanol/cyclohexanone ratio is desired, because the consecutive step of cyclohexanol dehydrogenation is costly and energy consuming.  $\text{TiO}_2$  based catalysts have been identified to be active in the photo-catalytic conversion of cyclohexane, with high ketone selectivity [1]. Various aspects of the photo-catalytic reaction have received attention in the open literature, including the effect of wavelength [2], catalyst constitution [3] and solvents [4-6]. Furthermore, various catalytic cycles have been proposed to explain the conversion of cyclohexane. However, little *in situ* spectroscopic evidence is available to support these pathways. Moreover, although deactivation of  $\text{TiO}_2$  has been reported previously [7,8], the reasons hereof have been given little attention.

Attenuated Total Reflection Fourier Transform Infrared (ATR-FTIR) spectroscopy provides a viable means of investigating the kinetics of light-induced heterogeneous oxidation. By using this technique, reactions can be monitored in real time and *in situ*. ATR-FTIR studies on photo-catalysis focused mostly on the  $\text{TiO}_2$  catalyzed photo-degradation of water-solved organic pollutants [9-16], or photo-activation of water [17,18]. In general, these studies have shown that ATR-FTIR spectroscopy provides a sensitive tool for analysis of surface adsorbed molecules, making it a powerful technique for mechanistic studies. To the best of our knowledge, ATR-FTIR spectroscopy has never been used to study selective photo-catalytic oxidations. In this chapter we present the results of such study on selective photo-oxidation of cyclohexane, with the aim to: i) analyze the processes leading to deactivation of  $\text{TiO}_2$  in the selective photo-oxidation of cyclohexane, and ii) by using  $\text{D}_{12}$ -cyclohexane, to investigate the kinetically relevant steps in the reaction. Ultraviolet light-emitting diodes (UV-LEDs) were used as UV source, with a characteristic single peak light emission at 375 nm wavelength. The results of the study are discussed, and guidelines for improvements of the process conditions for the selective liquid phase photo-oxidation of cyclohexane are presented.



## 2.2. EXPERIMENTAL

### 2.2.2. TiO<sub>2</sub> coating preparation

The photo-catalyst used was Hombikat UV 100 TiO<sub>2</sub> (Sachtleben) of 100% anatase crystallinity (determined by XRD), a  $S_{\text{BET}}$  of 337 m<sup>2</sup>/g and a primary particle size of approximately 5 nm [1]. Hombikat was heated to 120°C for 1 h in static air and suspended in distilled water at a concentration of 1.47 g/l. The suspension was treated for 30 min in a 35 kHz Elmasonic ultrasonic bath, 2 mL of this suspension was spread on the ZnSe crystal and dried in vacuum overnight. The conditions used were such to obtain an approximate 1.7 µm thick coating, as determined by calculations based on pure anatase density.

### 2.2.3. ATR-FTIR setup

A scheme of the ATR-FTIR setup is shown in Figure 2.1. The ATR-FTIR setup consists of a Harrick Horizon multiple internal reflections accessory, coupled to a 4 mL flow-through cell containing a ZnSe crystal on the bottom plate, and a quartz window on the top plate. The 45° internal reflection element of 50x10x2 mm allows 11 infrared bounces. The Fourier transform infrared measurements were performed on a Nicolet 8700 FT-IR apparatus equipped with a DTGS detector. An assembly of 7 UV LEDs (Roithner Lasertechnik) fitting on the top of the cell, provided illumination to the reaction mixture through the quartz window. The 375 nm wavelength UV LEDs were placed 2 cm above the ZnSe crystal and had a specific angle of 15°, allowing complete illumination of the cell. The intensity of each UV-LED was measured by a photodiode and, for 375 nm wavelength, an incident photon flux at the surface of TiO<sub>2</sub> corresponding to 8.98x10<sup>-9</sup> Einstein.cm<sup>-2</sup>.s<sup>-1</sup>, was determined. The low energy dissipation of this type of light source, allows typically up to 90% of its energy to be transformed into photon energy.

Cyclohexane was saturated with O<sub>2</sub> by dry air bubbling at 7.65 mL/min flow. The oxygen-saturated cyclohexane was flown at 4 mL/min through the ATR cell by means of a series II High-Performance Liquid Chromatography (HPLC) pump. The outflow of

the cell went through a chilling bath to maintain the liquid at room temperature. The temperature was monitored in the oxygenation vessel by a thermocouple.

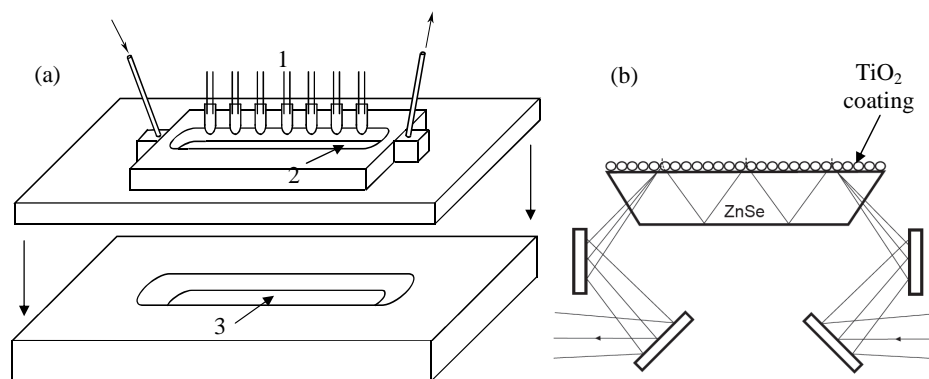


**Figure 2.1.** a) Scheme of the ATR-FTIR cell, including the UV LED assembly (1), the quartz window on the top plate (2) and the internal reflection element (3); b) Representation of the IR path and penetration into the  $\text{TiO}_2$  coating. In practice 11 bounces were allowed by the crystal dimensions, rather than the 3 bounces shown.

#### 2.2.4. Cyclohexane and deuterated cyclohexane photo-oxidation

A volume of 30 mL of cyclohexane 99.0% from J. T. Baker was used for photo-oxidation reactions. Cyclohexane was dried over Molsieve type 4A overnight before use, to remove traces of water. Cyclohexane- $\text{D}_{12}$ , 99.6 atom % D (Sigma-Aldrich), was used as received. Prior to the photo-catalytic oxidation experiments, adsorption of cyclohexane on the  $\text{TiO}_2$  coating at  $8.75 \text{ mL} \cdot \text{min}^{-1}$  was monitored for 100 min. A mirror velocity of 0.6329 and a resolution of  $4 \text{ cm}^{-1}$  were used for all measurements. The spectra during cyclohexane adsorption are shown relative to a background of  $\text{TiO}_2$  in air. After 100 min, a spectrum of adsorbed cyclohexane on  $\text{TiO}_2$  was collected as background for the photo-oxidation experiments. UV-induced oxidation of cyclohexane was continued for 100 min, taking a spectrum every minute. The background and the sample spectra were averaged from 64 and 32 spectra, respectively.

### 2.3. RESULTS

The spectral development upon equilibrating cyclohexane or deuterated cyclohexane with the TiO<sub>2</sub> surface is shown in Figures 2.2a and 2.2b, respectively. Decreasing peaks at 3630-3030 cm<sup>-1</sup> and 1630 cm<sup>-1</sup> correspond to the removal of residual adsorbed water from the TiO<sub>2</sub> surface. The former broad band is assigned to the stretching vibrations of adsorbed H<sub>2</sub>O and the latter to the corresponding H<sub>2</sub>O bending mode [19]. The symmetric and asymmetric stretching vibrations of the CH<sub>2</sub> groups in cyclohexane (Figure 2.2a) can be observed around 2924 and 2850 cm<sup>-1</sup>, with the corresponding CD<sub>2</sub> vibrations in deuterated cyclohexane located at around 800 cm<sup>-1</sup> lower wavenumbers (2194 and 2090 cm<sup>-1</sup>). Spectra of adsorbing cyclohexane and deuterated cyclohexane in the region below 1500 cm<sup>-1</sup> are shown in Figure 2.3.

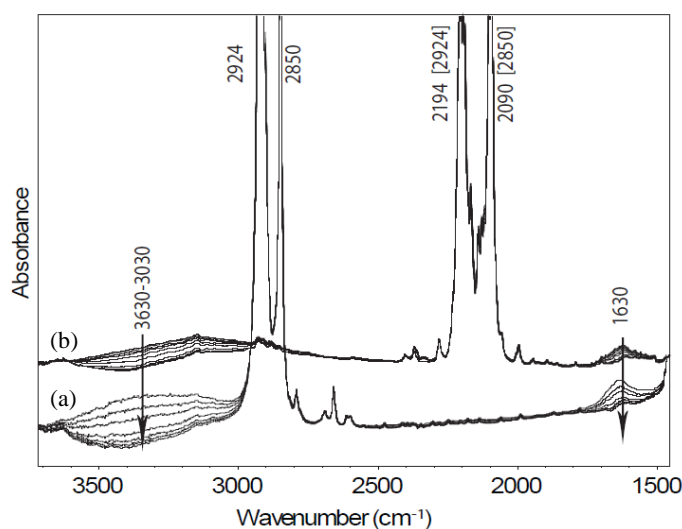


**Figure 2.2.** ATR-FTIR spectra of a) C<sub>6</sub>H<sub>12</sub> and b) C<sub>6</sub>D<sub>12</sub> (7.85 mL/min flow) adsorption on anatase TiO<sub>2</sub> coated on ZnSe (the background used was the spectrum of the TiO<sub>2</sub> coating in air). Wavenumbers in brackets indicate the corresponding C<sub>6</sub>H<sub>12</sub> absorptions. Spectra were recorded after 0.5, 2, 6, 10, 20, 40, 60, 80 and 100 min.

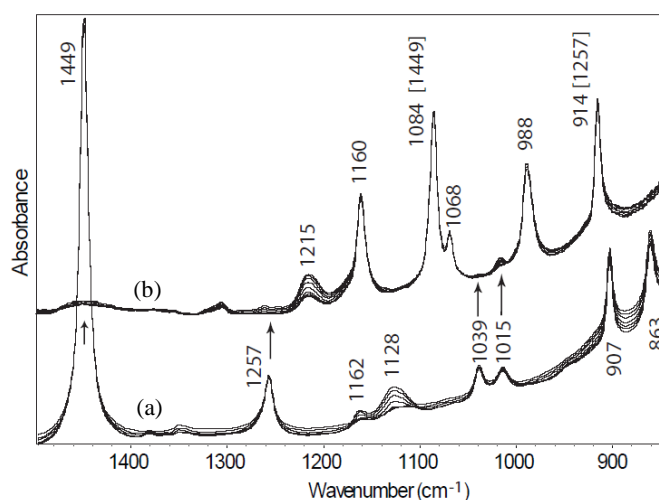


**Figure 2.3.** ATR-FTIR spectra of a)  $\text{C}_6\text{H}_{12}$  and b)  $\text{C}_6\text{D}_{12}$  (7.85 mL/min flow) adsorption on anatase  $\text{TiO}_2$  coated on ZnSe (the background used was the spectrum of the  $\text{TiO}_2$  coating in air). Wavenumbers in brackets indicate the corresponding  $\text{C}_6\text{H}_{12}$  absorptions. Spectra recorded after 0.5, 2, 6, 10, 20, 40, 60, 80 and 100 min.

The peaks at  $1449$  and  $1257\text{ cm}^{-1}$ , corresponding to the  $\text{CH}_2$  bending vibration in cyclohexane (Figure 2.3a), appear to be shifted to  $1084$  and  $914\text{ cm}^{-1}$  respectively, in the deuterated cyclohexane spectrum (Figure 2.3b). Infrared bands of cyclohexane located below  $1257\text{ cm}^{-1}$  (Figure 2.3a), have shifted in the spectrum of deuterated cyclohexane outside the spectral range of the measurement. The harmonic oscillator equation [20] was applied to support the assignment of the shifted infrared bands for deuterated cyclohexane. The obtained experimental wavenumbers are deviating less than  $15\text{ cm}^{-1}$  from the calculated values. The bands at  $1160$ ,  $1068$  and  $988\text{ cm}^{-1}$  have been assigned in the literature to rocking and twisting  $\text{CD}_2$  vibrations [21].

The presence of adsorbed water on the catalyst in the beginning of cyclohexane- $\text{D}_{12}$  adsorption could lead to isotopic exchange. This phenomenon occurs only to a small extent, as is evident from a slight increase of the bands at  $1257$ ,  $1039$  and  $1015\text{ cm}^{-1}$ , assigned to different types of  $\text{CH}_2$  vibrations (Figure 2.3b).

Two peaks at  $1162$  and  $1128\text{ cm}^{-1}$  show a continuous growth in time during cyclohexane adsorption (Figure 2.3a). Apparently the bands of cyclohexane at  $1157$  and  $1090\text{ cm}^{-1}$  [21] have shifted to higher frequencies upon adsorption. The harmonic

oscillation theory predicts the appearance of similar deuterated cyclohexane vibrations around 853 and 828 cm<sup>-1</sup>, but due to strong absorptions of the crystal and the TiO<sub>2</sub> coating these are not apparent. There is however one peak growing during D<sub>12</sub>-cyclohexane adsorption, at 1215 cm<sup>-1</sup> wavenumbers, assigned to the CD<sub>2</sub> wagging vibration of adsorbed deuterated cyclohexane.

The spectrum recorded after 100 min of cyclohexane adsorption on the surface of TiO<sub>2</sub> was used as background for the spectra recorded during the photo-catalyzed reaction. The UV-induced products of cyclohexane oxidation are shown in Figures 2.4 and 2.5, and were recorded during 100 min of reaction.

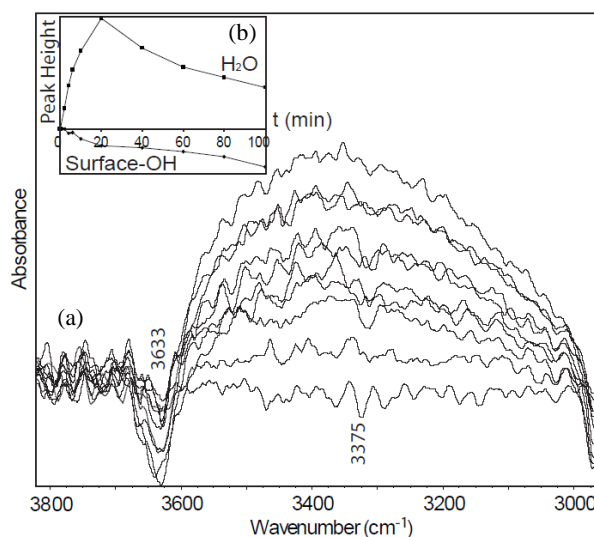


**Figure 2.4.** a) ATR-FTIR spectra recorded during cyclohexane (4 mL/min flow) photo-oxidation on anatase TiO<sub>2</sub> coated on ZnSe. Spectra recorded at 0.5, 2, 6, 10, 20, 40, 60, 80 and 100 min. b) Surface-OH group (3633 cm<sup>-1</sup>) and H<sub>2</sub>O (3375 cm<sup>-1</sup>) peak height evolution.

In Figure 2.4a two absorptions are visible that may be assigned to the most acidic Ti(IV)O-H sites (3633 cm<sup>-1</sup>) [22] and the OH stretching vibration of adsorbed water molecules (centered at 3375 cm<sup>-1</sup>). The irregular shape of the water band indicates the presence of an additional absorption around 3512 cm<sup>-1</sup> typical for the O-H stretching vibration of hydroperoxides, which might be indicative of a hydroperoxide intermediate in the reaction [19]. The surface coverage of TiO<sub>2</sub> with OH groups and H<sub>2</sub>O is changing

during the photo-catalytic oxidation, which can be followed by the peak height evolution, shown in Figure 2.4b. A strong increase in the amount of adsorbed water is observed in the first 20 min followed by a continuous decrease, while the OH-surface groups on  $\text{TiO}_2$  show a continuous decrease in time. The behavior of the hydroperoxide contribution is hard to evaluate due to the strong overlap with the water absorptions.

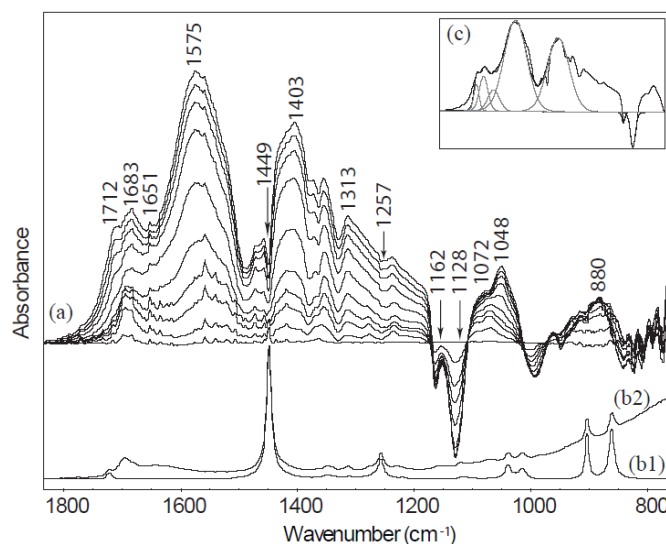


**Figure 2.5.** a) ATR-FTIR spectrum of cyclohexane (4 mL/min flow) photo-oxidation on anatase  $\text{TiO}_2$  coated on ZnSe. Spectra recorded at 0.5, 2, 6, 10, 20, 40, 60, 80 and 100 min.; b) ATR-FTIR spectrum (100 times reduced) of 0.06 M cyclohexanone in cyclohexane solution over the ZnSe crystal (b<sub>1</sub>) and over the  $\text{TiO}_2$  coated ZnSe crystal (b<sub>2</sub>); c) peak deconvolution of the 100 min spectrum of cyclohexane photo-catalytic oxidation.

A very broad range of infrared absorptions develops in time between 1800 and 800  $\text{cm}^{-1}$ , consisting of several overlapped peaks (Figure 2.5a). For the analysis of these results, it has to be taken into account that besides products yielding positive peaks, also negative peaks at 1162 and 1128  $\text{cm}^{-1}$  are present due to photo-catalytic conversion of adsorbed cyclohexane. The negative peaks at 1449, 1257 and 902  $\text{cm}^{-1}$  are characteristic of the scissoring, twisting and rocking vibrations of  $\text{CH}_2$  groups in cyclohexane [21]. Cyclohexanone synthesis may be followed by the peaks at 1712, 1683 and 1313  $\text{cm}^{-1}$ . The desorbed cyclohexanone molecules are identified by the growing 1712 and 1313

cm<sup>-1</sup> absorptions. The former peak corresponds to the C=O stretching vibration and the later one arises from bending modes of CH<sub>2</sub> groups as a result of the C=O stretching motion [23]. Adsorbed cyclohexanone molecules on TiO<sub>2</sub> lead to a less energetic C=O stretching vibration, that can be followed, in Figure 2.5a, by the 1683 cm<sup>-1</sup> peak intensity. To better exemplify the red shift of the C=O peak in cyclohexanone adsorbed state; a spectrum of a cyclohexanone in cyclohexane solution (0.06 M) with and without TiO<sub>2</sub> coating layer is presented (Figure 2.5b). Under dissolved conditions the C=O stretching peak occurs isolated at 1712 cm<sup>-1</sup>, but in the presence of the TiO<sub>2</sub> coating, the appearance of a second peak is a clear indication of adsorbed cyclohexanone. The ‘noise’ observed around 1651 cm<sup>-1</sup> is due to rotational modes of H<sub>2</sub>O, and is a result of slightly different levels of humidity during the background and sample collection. The broad peak at 1575 cm<sup>-1</sup> can be assigned to the C=O stretching vibration of adsorbed carboxylates [13,24]. Also adsorbed carbonate species are visible in the spectra, and induce the 1403 cm<sup>-1</sup> band, and features in the 1072-1048 cm<sup>-1</sup> region [24,25]. An irregular peak, formed at 880 cm<sup>-1</sup> wavelength during the photo-catalytic reaction, has been assigned to surface peroxides [26]. The irregular shape of this peak is due to overlapping negative cyclohexane modes, which make the trend hard to analyze. However, we feel that the presence of this band is further evidence for the formation of an intermediate peroxide (cyclohexyl hydroperoxide), since the kinetics of the intensity is more or less similar to that of the band around 3512 cm<sup>-1</sup> (shown in Fig. 2.4a).

Further knowledge of the evolution of product formation can be derived from the spectra by analyzing the peak area by deconvolution, as shown in Figure 2.5c. In the deconvolution, the bending mode of adsorbed water was taken into account. The peak area evolution of cyclohexanone (1712, 1683 cm<sup>-1</sup>), carboxylate (1562 cm<sup>-1</sup>), carbonate (1409 cm<sup>-1</sup>), as well as cyclohexane (1128 cm<sup>-1</sup>) during the photo-catalytic oxidation is shown in Figure 2.6. In the first 2 min of reaction the most prominent species adsorbed on the catalyst surface is cyclohexanone (1683 cm<sup>-1</sup>). In the following time intervals partial desorption of cyclohexanone from the surface into cyclohexane (represented by the 1712 cm<sup>-1</sup> peak) is apparent, while also products of further oxidation are formed, the carboxylates and carbonates (1575, 1403 cm<sup>-1</sup>). The negative peak intensity at 1128 cm<sup>-1</sup>, representing the decrease in cyclohexane coverage, is constant after 40 min of reaction, indicating that the initially adsorbed cyclohexane is completely converted.

After 100 min of photo-oxidation, the surface carboxylate bands have the highest intensity, followed by the carbonate species.

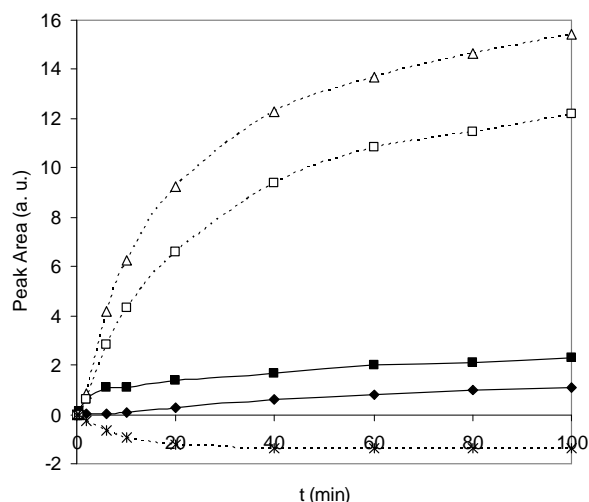


**Figure 2.6.** Evolution of the most prominent infrared peaks formed upon 100 min cyclohexanone photo-oxidation (4 mL/min flow) on anatase TiO<sub>2</sub> coated on ZnSe. Bulk cyclohexanone (◆), adsorbed cyclohexanone (■), carboxylates (Δ), carbonates (□), and adsorbed cyclohexanone (\*). Lines are only used as reference guide.

The area of the 1712 and 1683 cm<sup>-1</sup> peaks provides quantitative information on the relative ratio of dissolved and adsorbed cyclohexanone molecules formed during photocatalytic oxidation. A Langmuir curve was constructed to correlate the peak area (1683 cm<sup>-1</sup>) to the concentration of adsorbed cyclohexanone. The bulk cyclohexanone, on the other hand, was calibrated by a linear correlation between concentrations and 1712 cm<sup>-1</sup> peak area (Figure 2.7). The production of cyclohexanone during the photo-catalytic oxidation could thereby be followed, which is shown in Figure 2.8. A high initial rate of adsorbed cyclohexanone formation is apparent in the first 10 min of reaction, until steady state is reached. This is followed by the formation of dissolved cyclohexanone, initially at comparable rates as adsorbed cyclohexanone, and then showing a continuously decreasing rate in the time span of the reaction.



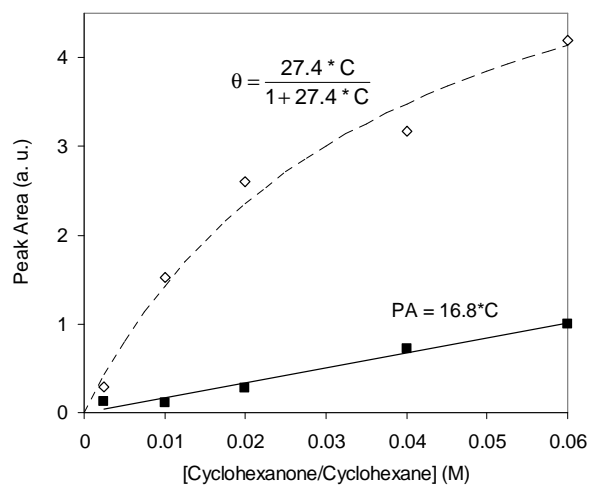


**Figure 2.7.** Peak area calibration of cyclohexanone adsorbed on TiO<sub>2</sub> (◇) and bulk cyclohexanone (■).

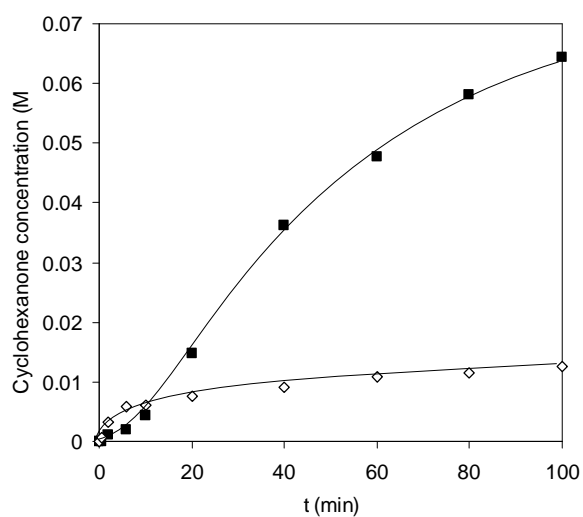


**Figure 2.8.** Concentrations (mol.L<sup>-1</sup>) of adsorbed cyclohexanone (◇) and bulk cyclohexanone (■) formed during the photo-catalytic oxidation of cyclohexane.

Based on these data, i.e. the initial rate of adsorbed cyclohexanone formation, the photonic efficiency of this process at 375 nm wavelength could be determined. Considering that the UV light penetrates through the whole thickness of the powder layer [27], a photonic efficiency ( $\Phi_h$ ) of  $0.5 \text{ mmol.Einstein}^{-1}$ , was determined [28]. Besides the detailed qualitative information, *in situ* ATR-FTIR is thus also quantitative.

Photo-catalytic oxidation of deuterated cyclohexane was performed to determine the presence or absence of a kinetic isotope effect. The trends in infrared absorption intensities can be seen in Figures 2.9 and 2.10 for the higher ( $4000\text{--}2000 \text{ cm}^{-1}$ ) and lower frequencies ( $1800\text{--}1000 \text{ cm}^{-1}$ ), respectively.

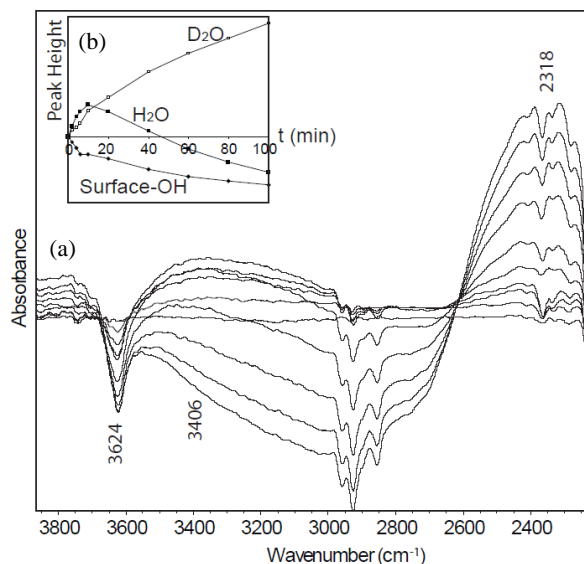


**Figure 2.9.** a) ATR-FTIR spectrum of deuterated cyclohexane (4 mL/min flow) photo-oxidation on anatase  $\text{TiO}_2$  coated on ZnSe. Spectra recorded at 0, 2, 6, 10, 20, 40, 60, 80 and 100 min. b) Acidic surface-OH groups ( $3624 \text{ cm}^{-1}$ ),  $\text{H}_2\text{O}$  ( $3406 \text{ cm}^{-1}$ ) and  $\text{D}_2\text{O}$  ( $2318 \text{ cm}^{-1}$ ) peak height evolution.

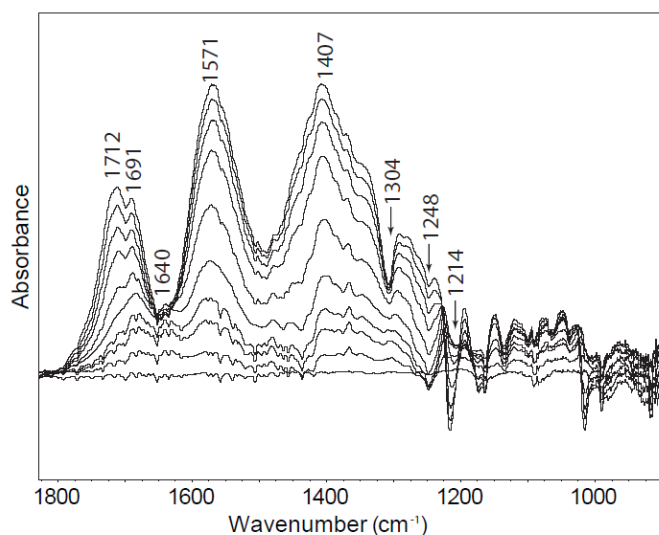


**Figure 2.10.** ATR-FTIR spectrum of deuterated cyclohexane (4 mL/min flow) photo-oxidation on anatase TiO<sub>2</sub> coated on ZnSe. Spectra recorded at 0, 2, 6, 10, 20, 40, 60, 80 and 100 min.

The photo-catalytic oxidation of deuterated cyclohexane shows in the high frequency range not only the decreasing intensity of the OH-surface groups and a trend in adsorbed H<sub>2</sub>O, but also the OD stretching vibrations of adsorbed D<sub>2</sub>O (at 2318 cm<sup>-1</sup>). Figure 2.9b shows the peak height evolution of these bands. The decrease in the intensity of the OH surface group at 3624 cm<sup>-1</sup> is similar to that observed during cyclohexane photo-oxidation (Figure 2.4b). Although the assignment of the 3406 band is ambiguous, it can be postulated that the increase in this absorption is associated with the formation of the cyclohexyl peroxide intermediate and water. A strong decrease in the spectral intensity of adsorbed H<sub>2</sub>O (and peroxide) is observed in the later stages of the experiment, with a continuous increase in D<sub>2</sub>O intensity.

Comparing Figure 2.10 and Figure 2.5a, spectral features of cyclohexanone (1713 cm<sup>-1</sup>), adsorbed cyclohexanone (1691 cm<sup>-1</sup>) as well as carboxylates (1571 cm<sup>-1</sup>) and carbonates (1407 cm<sup>-1</sup>) are very similar during oxidation of cyclohexane and cyclohexane-D<sub>12</sub>. The negative peaks, related to adsorbed C<sub>6</sub>D<sub>12</sub> consumption have shifted outside the region of the carbonate absorptions. At 1214 cm<sup>-1</sup> wavenumbers, the consumption of the reagent may be followed, which shows a very similar trend as the corresponding 1128 cm<sup>-1</sup> peak of cyclohexane (Figure 2.5a).

The time evolution of the adsorbed and desorbed cyclohexanone peak areas during cyclohexane and cyclohexane-D<sub>12</sub> experiments are shown in Figure 2.11. For the time evolution of the adsorbed carboxylate and carbonate peak areas the comparison is shown in Figure 2.12. The formation of surface D<sub>10</sub>-cyclohexanone occurs at a slower rate than H<sub>10</sub>-cyclohexanone. On the other hand, dissolved D<sub>10</sub>-cyclohexanone forms almost immediately after the onset of the reaction, whereas dissolved H<sub>10</sub>-cyclohexanone shows an apparent initiation period. For the carboxylate and carbonate species, a decrease in peak intensity is observed during the deuterated experiment vs cyclohexane oxidation.

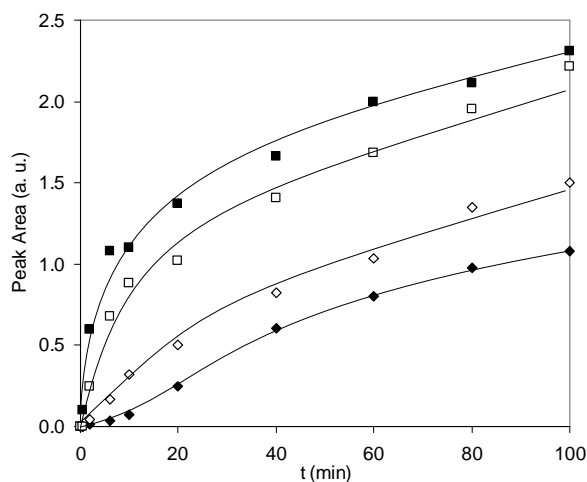


**Figure 2.11.** Peak area growth upon 100 min cyclohexane and deuterated cyclohexane photo-oxidation (4 mL/min flow) on anatase TiO<sub>2</sub> coated on ZnSe. Adsorbed cyclohexanone (■), bulk cyclohexanone (◆), adsorbed D<sub>10</sub>-cyclohexanone (□) and bulk D<sub>10</sub>-cyclohexanone (◇). Lines are only used as reference guide.

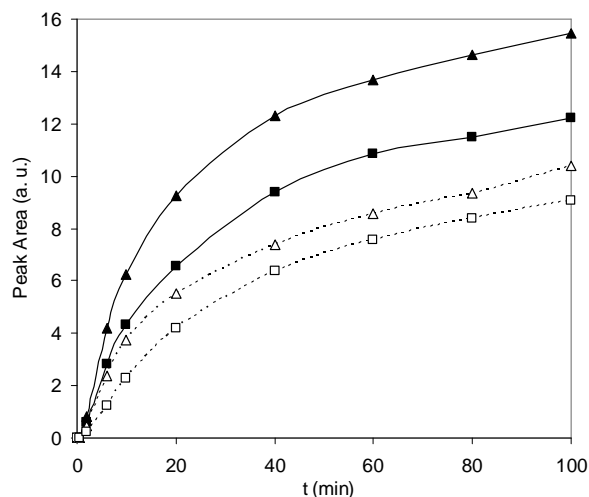


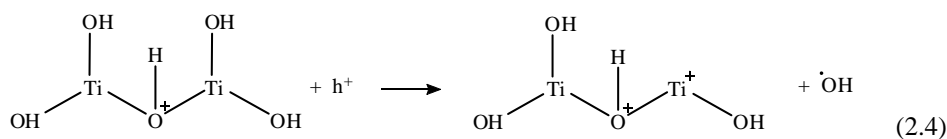
**Figure 2.12.** Peak area growth upon 100 min cyclohexane and deuterated cyclohexane photo-oxidation (4 mL/min flow) on anatase TiO<sub>2</sub> coated on ZnSe. Adsorbed carboxylates (▲), adsorbed carbonates (■), adsorbed deuterated carboxylates (Δ) and adsorbed deuterated carbonates (□). Lines are only used as reference guide.

## 2.4. DISCUSSION

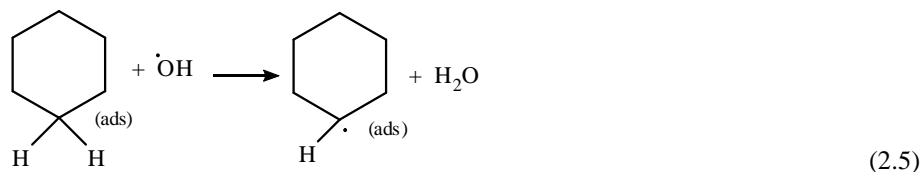
Reaction mechanisms of the photo-catalytic oxidation of cyclohexane to cyclohexanone over TiO<sub>2</sub> have been proposed [1,2,4,5], but spectroscopic evidence is scarce, and the products of further oxidation are generally not taken into account. Based on the *in situ* ATR-FTIR spectra of the photo-catalytic oxidation of cyclohexane reported in this study, a mechanism is proposed including consecutive photo-oxidation to surface carbonates/carboxylates.

In Figure 2.2, it has been shown that residual water on the TiO<sub>2</sub> surface is removed and cyclohexane adsorption is apparent by the bands at 1162 and 1128 cm<sup>-1</sup>. The reaction of adsorbed cyclohexane is initiated by light. The physical processes upon absorption of light by TiO<sub>2</sub> have been discussed extensively in the literature, and it is clear that both holes and electrons, after reaching the surface, can interact with species present on the surface of the catalyst. In this case, the photo-generated holes, if not recombining with electrons, can react with the OH groups on the catalyst surface (with

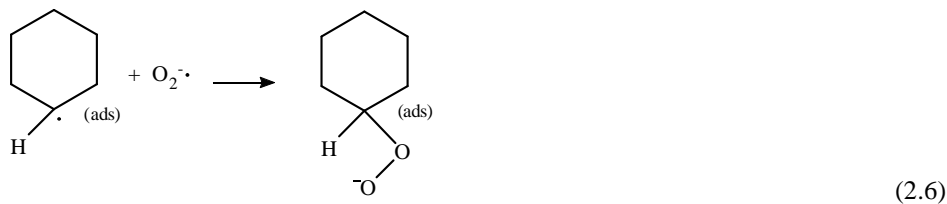
hydroxyl radical formation), or react directly with the adsorbed cyclohexane molecules (with cyclohexyl radical formation). Most scientists favor the activation of the OH surface groups on the catalyst, which we have assumed in our mechanistic pathway as well. Electrons are generally assumed to react with  $O_2$ , yielding  $O_2^{\cdot-}$ :

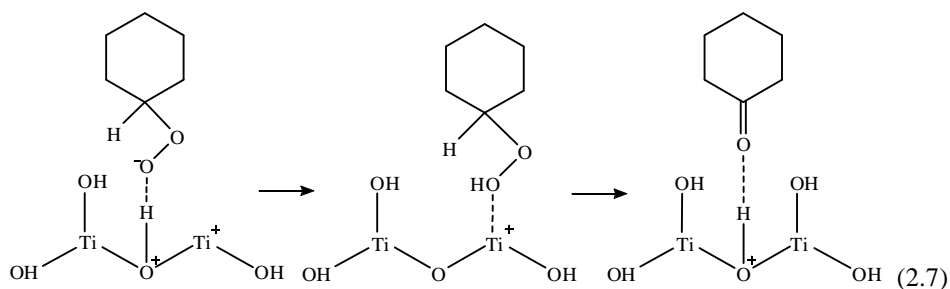


The surface hydroxyl radical is very reactive and immediately reacts with the surface adsorbed cyclohexane to a (surface adsorbed) cyclohexyl radical and water:



This is then followed by the reaction of the cyclohexyl radical and the superoxide ion to yield an adsorbed peroxide intermediate:





Finally reaction (2.7) shows the acid catalyzed peroxide decomposition and formation of cyclohexanone, with regeneration of the hydroxyl group. This mechanism is largely supported by our spectroscopic data. First, surface adsorbed water is clearly formed at comparable initial rates as cyclohexanone, while the features in the absorption bands around 3512 cm<sup>-1</sup> and around 800 cm<sup>-1</sup> are also consistent with the formation of a peroxide. Second, involvement of a surface hydroxyl group in interactions with intermediates and products (reaction (2.7)) is shown by the decreasing intensity of the 3633/3624 cm<sup>-1</sup> absorption. The mechanism would indicate that in the oxidation of D<sub>12</sub>-cyclohexane, HOD would be formed in the initial stages of the reaction (through reaction (2.5)), while H<sub>2</sub>O is observed. In view of the large quantity of acidic OH groups on the surface in the beginning of the reaction, this is most likely the result of isotopic exchange of HOD with O-H, yielding H<sub>2</sub>O and O-D. The decrease in OH-surface groups is indeed faster during the C<sub>6</sub>D<sub>12</sub> photo-oxidation experiment (Figure 2.9b), consistent with the formation of OD sites and surface isotopic exchange. Spectroscopic evidence for the O-D groups is ambiguous, with the expected absorption around 2600 cm<sup>-1</sup> strongly overlapping with the broad features of the D<sub>2</sub>O absorptions. Still, a shoulder could be present at the high frequency tail of the D<sub>2</sub>O absorption (Figure 2.9a), in particular in the initial stages of the reaction.

Following these initial stages of the reaction, the surface becomes progressively saturated with water, peroxides, and cyclohexanone, leading to secondary processes. Cyclohexanone desorption is observed (Figure 2.6), facilitated by the competitive adsorption of water molecules formed in the reaction. (Figure 2.4b). The slow initial rate of cyclohexanone desorption, is absent in the trend of bulk D<sub>12</sub>-cyclohexanone (Figure 2.11). Different initial water concentrations in cyclohexane *vs* deuterated cyclohexane are proposed to affect the different trend in the formation of dissolved C<sub>6</sub>H<sub>10</sub>O and dissolved C<sub>6</sub>D<sub>10</sub>O. The 1712 cm<sup>-1</sup> peak area in the deuterated experiment

shows a faster growth, suggesting a slightly higher concentration of H<sub>2</sub>O (or D<sub>2</sub>O) competing with the catalyst surface sites and facilitating D<sub>10</sub>-cyclohexanone desorption. Despite this beneficial effect, there is however a secondary effect of the increasing surface coverage of water, being the formation of additional ·OH radicals (and protons), consistent with the decreasing water peak in the final stages of the reaction (Figure 2.9b). These are most likely involved in the secondary non-selective reactions, as will be discussed later.

#### *2.4.1. Rate determining step*

The initial aim of the use of deuterated cyclohexane was to evaluate the presence of a kinetic isotope effect. Slight deviations in spectral intensity are expected, since the refractive indexes of C<sub>6</sub>H<sub>12</sub> and C<sub>6</sub>D<sub>12</sub> are slightly different, but this is a minor effect. Comparing the reactivity profiles in Figures 2.11 and taking into account the sum of the adsorbed and dissolved amount of cyclohexanone, in the beginning stages of the C<sub>6</sub>H<sub>12</sub> and C<sub>6</sub>D<sub>12</sub> photo-catalytic oxidation, a similar reactivity is observed. The reaction rate is therefore not affected by the isotopic exchange, and reaction steps involving C-D bond breaking (like reaction (2.5) or (2.7) in the proposed mechanism) are not rate limiting the formation of the cyclohexanone. The kinetics of cyclohexanone formation by photo-catalytic oxidation thus seem to be limited by another reaction, like for example the activation of O<sub>2</sub>, which depends on free electron availability and adsorbed O<sub>2</sub> concentrations. The solubility of O<sub>2</sub> in cyclohexane is low, and a limitation in O<sub>2</sub> availability is not unlikely. Experiments at higher O<sub>2</sub> pressures are planned to verify this hypothesis and to enhance the reaction rate.

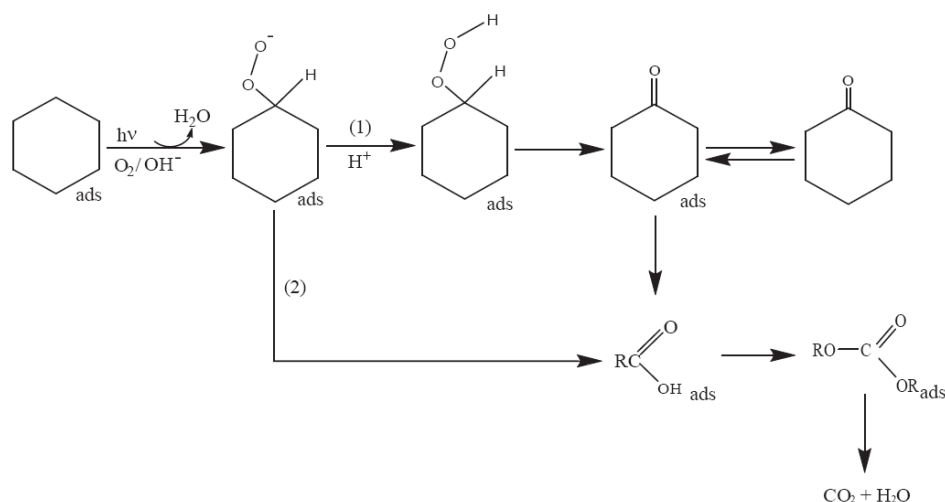
#### *2.4.2. Formation of carbonates and carboxylates*

After two min of reaction, the formation of carboxylate (1575 cm<sup>-1</sup>) and carbonate (1403 cm<sup>-1</sup>) species is already apparent. Based on the spectroscopic data, a scheme for the formation of secondary products can be drawn (Scheme 2.1). The adsorbed cyclohexanone molecules are proposed to be the major reagent forming the carboxylate compounds. Carboxylates can further oxidize to carbonates or even completely to CO<sub>2</sub>



and H<sub>2</sub>O. Besides consecutive reaction of cyclohexanone, also a non-selective route of peroxide decomposition to carbonates and/or carboxylates might exist, due to deactivation of acidic OH groups on TiO<sub>2</sub>. Dissolved cyclohexanone formation shows a very similar time dependence as the carbonate/carboxylate formation, and it is thus concluded that these species are inducing the catalyst deactivation. Carbonate species, in particular, have been considered detrimental for photo-catalytic processes, due to their competition to adsorption sites and photo-generated holes [29].

**Scheme 2.1.** Steps of cyclohexane photo-catalytic oxidation, including the formation of carboxylates, carbonates and finally, the products of total oxidation. Step (1) occurs over totally hydroxylated TiO<sub>2</sub> surface. On deactivated catalyst, step (1) and (2) occur simultaneously.



Isotopic exchange has a clear effect on the formation of carboxylate and carbonate compounds, of which the intensity of absorption is clearly lower than in the H<sub>12</sub>-cyclohexane photo-oxidation (Figure 2.12). Again, an effect of the refractive indexes of C<sub>6</sub>H<sub>12</sub> and C<sub>6</sub>D<sub>12</sub>, which are slightly different, is contributing, but not enough to completely explain the difference. It is apparent from the experiment that the surface cyclohexanone coverage is lower in the C-D experiment than in the C-H experiment (Figure 2.11), which is consistent with the lower amount of carbonates/carboxylates if consecutive cyclohexanone oxidation is leading to the formation of these non-selective

oxidation products. Another explanation is related to the kinetic isotope effect: multiple C-H or C-D bonds need to be broken for carboxylate and carbonate formation, which might contribute to the lower rate. Finally, formation of OD radicals might be slower than the formation of OH radicals, as a result of the stability of  $D_2O$  vs  $H_2O$ .

The apparently different carboxylate/carbonate ratio intensity for the  $C_6H_{12}$  (Figure 2.5a) and  $C_6D_{12}$  (Figure 2.10) photo-oxidation, is most likely an artifact, induced by the negative contribution of the  $1449\text{ cm}^{-1}$  peak to the carbonate intensity in the  $C_6H_{12}$  experiment.

#### 2.4.3. Cyclohexanol formation

Cyclohexanol has often been reported as one of the mono-oxygenated products of the cyclohexane photo-catalytic oxidation, and has also been proposed as an intermediate in cyclohexanone formation [5]. The presence of cyclohexanol has, however, not been detected under our experimental conditions. The characteristic cyclohexanol absorption peaks between  $1500$  and  $800\text{ cm}^{-1}$  were absent. Therefore, the formation of this mono-oxygenated compound, if any, must occur at very low and undetectable concentrations, under our experimental conditions.

### 2.5. CONCLUSIONS

The photo-catalytic oxidation of cyclohexane was performed over anatase  $TiO_2$  with a photonic efficiency of  $0.5\text{ mmol.Einstein}^{-1}$ . In the first min, the reaction was very selective towards cyclohexanone formation, however, desorption of this compound from the  $TiO_2$  surface is slow, making it feasible to react further towards carboxylate and carbonate-like compounds. The strong adsorption of these compounds on the catalyst surface strongly decreases the rate of cyclohexanone formation.

No kinetic isotope effect was observed for the formation of cyclohexanone, so the formation of this compound is proposed to be limited by the  $O_2$  pressure. A faster cyclohexanone desorption was observed during the deuterated cyclohexane photo-oxidation, possibly due to an increased competitive adsorption of  $H_2O$  and  $D_2O$ .

ATR-FTIR showed to be applicable for *in situ* analysis of selective photo-catalyzed reactions, allowing a better understanding of the reaction mechanism of selective photo-oxidation of cyclohexane. Quantitative analysis of the selective oxidation product and the photo-catalytic efficiency are possible.

## REFERENCES

- [1] P.Du, J.A.Moulijn, G.Mul, J. Catal. 238 (2006) 342.
- [2] M.A.Brusa, M.A.Grela, J. Phys. Chem. B 109 (2005) 1914.
- [3] W.Mu, J.M.Herrmann, P.Pichat, Catal. Lett. 3 (1989) 73.
- [4] P.Boarini, V.Carassiti, A.Maldotti, R.Amadelli, Langmuir 14 (1998) 2080.
- [5] C.B.Almquist, P.Biswas, Appl. Catal. A 214 (2001) 259.
- [6] M.A.Brusa, Y.Di Iorio, M.S.Churio, M.A.Grela, J. Mol. Catal. A 268 (2007) 29.
- [7] J.Peral, X.Domenech, D.F.Ollis, J. Chem. Technol. Biotechnol. 70 (1997) 117.
- [8] H.Einaga, S.Futamura, T.Ibusuki, Appl. Catal. B 38 (2002) 215.
- [9] G.N.Ekstrom, A.J.McQuillan, J. Phys. Chem. B 103 (1999) 10562.
- [10] J.M.Kesselman-Truttmann, S.J.Hug, Environ. Sci. Technol. 33 (1999) 3171.
- [11] I.Dolamic, T.Burgi, J. Phys. Chem. B 110 (2006) 14898.
- [12] A.E.Regazzoni, P.Mandelbaum, M.Matsuyoshi, S.Schiller, S.A.Bilmes, M.A.Blesa, Langmuir 14 (1998) 868.
- [13] P.Z.Araujo, C.B.Mendive, L.A.G.Rodenas, P.J.Morando, A.E.Regazzoni, M.A.Blesa, D.Bahnmann, Colloid Surf. A 265 (2005) 73.
- [14] C.B.Mendive, D.W.Bahnmann, M.A.Blesa, Catal. Today 101 (2005) 237.
- [15] C.B.Mendive, T.Bredow, M.A.Blesa, D.W.Bahnmann, Phys. Chem. Chem. Phys. 8 (2006) 3232.
- [16] W.Z.Xu, D.Raftery, J.S.Francisco, J. Phys. Chem. B 107 (2003) 4537.
- [17] D.S.Warren, A.J.McQuillan, J. Phys. Chem. B 108 (2004) 19373.
- [18] R.Nakamura, A.Imanishi, K.Murakoshi, Y.Nakato, J. Am. Chem. Soc. 125 (2003) 7443.
- [19] G.Socrates, in Infrared Characteristic Group Frequencies Tables and Charts, Wiley, New York (1994).

- [20] J.W.Niemantsverdriet, in Spectroscopy in Catalysis, Wiley-VCH (2000).
- [21] T.Shimanouchi, in National Bureau of Standards (Eds.), Tables of Molecular Vibrational Frequencies Consolidated Volume I, Tokyo (1972).
- [22] S.H.Szczepankiewicz, A.J.Colussi, M.R.Hoffmann, J. Phys. Chem. B 104 (2000) 9842.
- [23] L.J.Bellamy, in The Infrared Spectra of Complex Molecules Advances in Infrared Group Frequencies, Chapman and Hall Ltd., London (1975).
- [24] D.J.Yates, J. Phys. Chem. 65 (1961) 746.
- [25] P.A.Connor, K.D.Dobson, A.J.McQuillan, Langmuir 15 (1999) 2402.
- [26] G.N.Ekstrom, A.J.McQuillan, J. Phys. Chem. B 103 (1999) 10562.
- [27] W.Wang, Y.Ku, Chemosphere 50 (2003) 999.
- [28] G.Sagawe, R.J.Brandi, D.Bahnmann, A.E.Cassano, Chem. Eng. Sci. 58 (2003) 2587.
- [29] I.Dolamic, T.Burgi, J. Catal. 248 (2007) 268.

# *Chapter 3*

## Improved performance of $\text{TiO}_2$ in the selective photo-catalytic oxidation of cyclohexane by increasing the rate of desorption through surface silylation

The effect of silylation on the performance of an anatase  $\text{TiO}_2$  catalyst, in the selective photo-oxidation of cyclohexane was investigated using Attenuated Total Reflection Fourier Transform Infrared (ATR-FTIR) spectroscopy and an illuminated slurry reactor. The rate of cyclohexanone formation showed a dependency on the availability of surface active OH-sites, and on the desorption rate of cyclohexanone. Two classes of catalysts could be identified: (1) those containing less than 1.0 wt% Si where the cyclohexanone formation rate is decreased by silylation due to a decrease in OH availability, and (2) those containing more than 1.0 wt% Si where the improved desorption rate becomes dominant over the decreasing OH availability, and the cyclohexanone formation rate observed in an illuminated slurry reactor is increased. ATR-FTIR spectroscopic results confirmed the linear increase in the rate of cyclohexanone desorption as a function of increasing silicon content of the  $\text{TiO}_2$  surface. Because of this enhanced desorption, silylation also resulted in a decrease in rate of formation of surface deactivating carbonate and carboxylate species on  $\text{TiO}_2$ .

This chapter is based on the following publication: A.R.Almeida, J.T.Carneiro, J.A.Moulijn, G.Mul, J. Catal. 273 (2010) 116.

### 3.1. INTRODUCTION

Photo-catalysis is widely applied in the decomposition of contaminants from water and air [1]. Among various semiconductor materials,  $\text{TiO}_2$  is the most investigated catalyst, and used in commercial water purification [2]. The use of  $\text{TiO}_2$  to selectively synthesize organic compounds at mild conditions is also of interest [3]. However, low conversions and strong deactivation of  $\text{TiO}_2$  catalysts prevent these photo-catalytic processes from being commercially applied [4-8]. The reason for  $\text{TiO}_2$  deactivation is the formation of surface bound carbonates and carboxylates, as observed in ATR-FTIR spectroscopy studies. The formation of these species in the selective cyclohexane oxidation was proposed to be the result of slow desorption of cyclohexanone, which leads to overoxidation [8]. Transient studies confirmed that cyclohexanone desorption is slow: to desorb 90% of adsorbed cyclohexanone from a pre-illuminated  $\text{TiO}_2$  catalyst in cyclohexane, requires almost 30 min in the dark [9]. In order to decrease the rate of deactivation in cyclohexane oxidation, desorption of cyclohexanone should be stimulated. Several strategies could be followed to achieve this, such as the use of solvents [10-12], the use of elevated temperatures [13] or catalyst modification. In this research the last option has been evaluated, in particular the modification of the  $\text{TiO}_2$  surface by silylation. This method is commonly applied for Ti-substituted mesoporous silica catalysts, to reduce desorption limitations of polar products in oxidation reactions [14-16]. In these cases, silanol groups from the mesoporous support are exchanged with methylated silane groups, like trimethylsilanes. But also silylation of commercial  $\text{TiO}_2$  has been applied and in general a decrease in surface hydrophilicity and affinity to polar molecules has been observed [17,18]. It will be demonstrated in the present paper by data obtained from *in situ* ATR-FTIR studies that the hydrophilicity of a commercial  $\text{TiO}_2$  catalyst is indeed decreased by coupling trimethylsilane groups to its surface, stimulating desorption of cyclohexanone formed by photo-catalytic cyclohexane oxidation, and thus reducing the rate of catalyst deactivation.

## 3.2. EXPERIMENTAL

### 3.2.1. Catalyst synthesis

The photo-catalyst used in this study was Hombikat UV100 TiO<sub>2</sub> (Sachtleben) of 100% anatase crystallinity (determined by XRD), a  $S_{\text{BET}}$  of 337 m<sup>2</sup>/g and a primary particle size of approximately 5 nm [7]. Hexamethyldisilazane (HMDS) from Fluka was chosen as the silylating agent, because of its high reactivity [19,20]. The silylation method applied is similar to the one described by Fadeev et al. [21]. The catalyst was dried overnight at 120°C, and 0.5 g of TiO<sub>2</sub> was mixed with different volumes of HMDS in 10 mL of toluene (99.5% from Sigma Aldrich), in a magnetically stirred round bottom flask with a reflux cooler. The synthesis was carried out at room temperature for 24 h, after which the silylated TiO<sub>2</sub> materials were filtered, washed with toluene and dried overnight at 120°C. Four silylation batches were made with 0.02, 0.06, 0.08 and 0.15 g of HMDS.

### 3.2.2. Catalyst characterization

X-Ray Fluorescence (XRF) measurements were performed on a Panalytical PW 1480 spectrometer and the silicon content (wt%) in the silylated TiO<sub>2</sub> catalysts was calculated with the so-called Superq routine. The silylated TiO<sub>2</sub> catalysts were characterized by Diffuse Reflectance Infrared Spectroscopy (DRIFTS) on a Bruker IFS 66 spectrometer. The catalyst powders were introduced into a DRIFTS cell (Spectratech) and dried for 30 min at 120°C. All absorbance and single beam spectra were collected with 128 averaged scans and 4 cm<sup>-1</sup> spectral resolution against a KBr background. Thermogravimetric analysis (TGA) was performed on a Mettler Toledo TGA/SDTA851e. The samples were heated from 25-600°C at a heating rate of 10 K/min under 10 mL/min He flow. Solid state <sup>29</sup>Si Magic Angle Spinning Nuclear Magnetic Resonance (<sup>29</sup>Si MAS NMR) was performed on a Bruker Avance 400 spectrometer, using a 5 mm zirconia rotor, with spinning speed of 11 kHz. The spectral window was 25063 Hz, with 50 ms acquisition time and 15 s acquisition delay.

### 3.2.3. Cyclohexane photo-catalytic oxidation – ATR-FTIR

The catalysts were dried at 120°C for 1 h in static air and suspended in toluene at a concentration of 3.67 g/L. The suspensions were treated for 30 min in a 35 kHz Elmasonic ultrasonic bath; 2 mL of this suspension was spread on a ZnSe crystal and dried in vacuum overnight.

The *in situ* ATR-FTIR setup used for the photo-catalytic oxidation of cyclohexane is described in detail elsewhere [8]. Briefly, a volume of 50 mL of cyclohexane 99.0% from Sigma Aldrich was used for the photo-oxidation reactions. Cyclohexane was dried over Molsieve (type 4A) overnight before use, to remove traces of water, and saturated with O<sub>2</sub> by bubbling dry air at 7.65 mL/min. The oxygen saturated cyclohexane was flown at 4 mL/min through the ATR cell by means of a series II high performance liquid chromatography pump. Prior to the photo-catalytic oxidation experiments, adsorption of cyclohexane on the TiO<sub>2</sub> coating was monitored for 60 min. A spectrum of adsorbed cyclohexane on TiO<sub>2</sub> was collected as background for the photo-oxidation experiment. UV-induced oxidation of cyclohexane was continued for 90 min, taking a spectrum every min. The photo-catalytic reaction was initiated by an assembly of 7 UV LEDs with 375 nm wavelength emission with an incident photon flux of  $9 \times 10^{-9}$  Einstein.cm<sup>-2</sup>.s<sup>-1</sup> at the surface of the catalyst coating. The first minute of collection was performed in the dark. The background and the sample spectra were averaged from 64 and 32 spectra, respectively. A mirror velocity of 0.6329 cm s<sup>-1</sup> and a resolution of 4 cm<sup>-1</sup> were used for all measurements. All the spectra were corrected by subtracting the features of the rotational modes of water vapor.

### 3.2.4. Cyclohexane photo-catalytic oxidation – Slurry reactor

Photo-catalytic tests were performed in a slurry reactor illuminated from the top, which will be referred to as top illumination reactor and is described elsewhere [22]. The pyrex reactor contained 100 mL of cyclohexane and 1 g/L of catalyst on all measurements. Air, pre-saturated with cyclohexane was bubbled through the liquid at a flow rate of 30 mL/min, assuring constant saturation of cyclohexane with O<sub>2</sub> (0.012 mol/L). Illumination was provided by a 50 W high pressure mercury lamp (HBO50W from ZEISS), with incident photon flux of  $2.10 \times 10^{-7}$  Einstein cm<sup>-2</sup> s<sup>-1</sup> in all



measurements. The reaction was carried out for 100 min and liquid GC samples were analyzed by a flame ionization detector (Chromopack CPwax 52CB).

### 3.3. RESULTS

#### 3.3.1. Catalyst characterization

The applied variation of the silylation method yielded a series of materials with different silicon loading on TiO<sub>2</sub>: TiSi0.1, TiSi1.0, TiSi1.6 and TiSi2.1, which contain 0.1, 1.0, 1.6 and 2.1 wt% Si, as determined by XRF analysis. Bare Hombikat, of 100% anatase crystallinity, is referred to as TiSi0. The TGA analysis of TiSi0, TiSi1.0, TiSi1.6 and TiSi2.1 recorded in He are shown in Figure 3.1. The negative contributions in this figure correspond to the weight loss divided by initial mass of catalyst, and are displayed as a function of increasing temperature. At temperatures below 120°C, weakly adsorbed water is removed from the catalyst surface [15]. More strongly adsorbed water is removed at temperatures between 120-300°C [23], where particle sintering also starts to occur. In the range of 150-400°C an extra contribution related to decomposition of HMDS residue may contribute to the weight loss [19]. Above 400°C a negative feature is observed for the silylated catalysts, which corresponds to the decomposition of trimethylsilyl groups from the silylated surface [19].

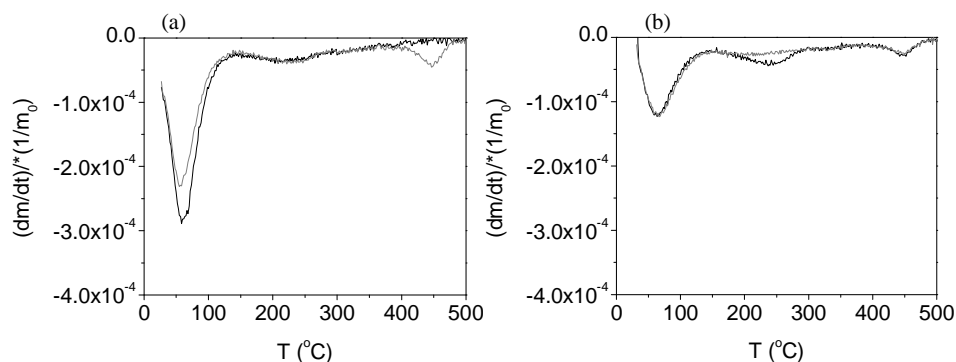


**Figure 3.1.** Thermogravimetric analysis (TGA) under He flow of a) TiSi0 (black line), TiSi1.0 (grey line), b) TiSi1.6 (black line) and TiSi2.1 (grey line).

$^{29}\text{Si}$  MAS NMR was performed on the TiSi1.6 catalysts to understand which type of Si bonding was induced by the synthesis method. In Figure 3.2, a single peak is observed at 11.69 ppm that corresponds to  $(\text{TiO})\text{Si}(\text{CH}_3)_3$  [14,16,19]. Additional NMR features were absent, like those of Si-OH and Si-O-Si groups, so neither hydroxylation nor polymerization of surface silane groups has occurred to a large extent in the synthesis.

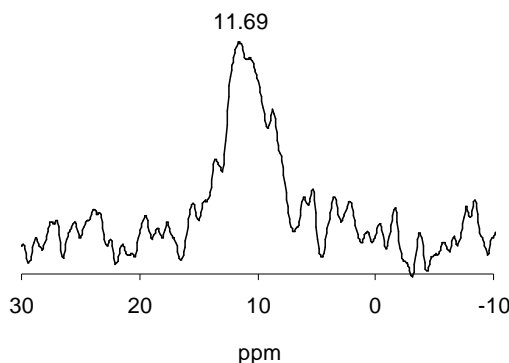
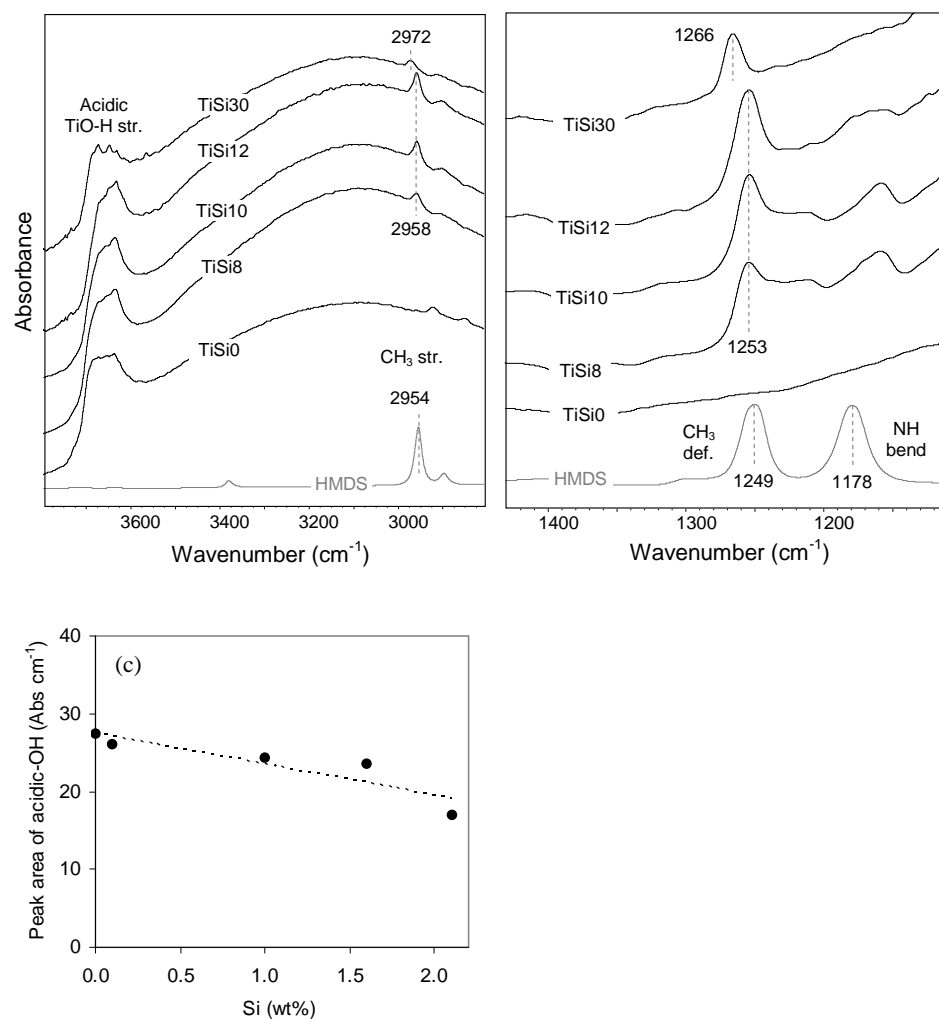


**Figure 3.2.**  $^{29}\text{Si}$  MAS NMR of the TiSi1.6 catalyst.

The DRIFTS analysis of the catalysts is shown in Figure 3.3(a) and (b). Though different OH active sites have been identified on commercial  $\text{TiO}_2$  surfaces, for simplicity we refer to the surface active sites as acidic or basic-OH. The surface OH density was determined by the  $\text{Fe}(\text{acac})_3$  adsorption method [24], which accounts for all types of OH sites, of which an acidic contribution was measured by  $\text{NH}_3$ -TPD [7]. The remaining contribution will be referred to as basic-OH groups. An acidic/basic OH ratio of 3.3 has been reported for this commercial  $\text{TiO}_2$  [7], corresponding to ~75% surface coverage by acidic-OH sites. Stretching vibrations of the acidic-OH appear in all spectra, as a number of overlapping bands in the  $3690\text{--}3630\text{ cm}^{-1}$  region [25] (Figure 3.3(a)). A broad contribution of  $\text{H}_2\text{O}$  is also apparent in the  $3600\text{--}3000\text{ cm}^{-1}$  region. The basic-OH group is H-bridged with adsorbed water molecules, and its stretching vibration is expected to absorb around  $3415\text{ cm}^{-1}$ , but is overlapped by strong water contributions [25]. The peak area of the acidic-OH is represented in Figure 3.3(c) as a

function of silicon content, and a decreasing trend can be observed. The TiSi0 sample shows small methyl vibrations below 3000 cm<sup>-1</sup>, characteristic of this commercial TiO<sub>2</sub>. A reference spectrum of liquid HMDS is shown in Figure 3.3(a) with specific CH<sub>3</sub> stretching vibrations at 2954 and 2897 cm<sup>-1</sup>. The silylated materials show similar IR bands, but shifted to higher wavenumbers, 2958 and 2905 cm<sup>-1</sup>. The shift is more intense for TiSi2.1, in which the CH<sub>3</sub> stretching vibrations of silane occur at 2972 and 2915 cm<sup>-1</sup>. The typical Si-OH stretching vibration expected at 3675 cm<sup>-1</sup> [26], is not visible in any of the silylated catalysts, in agreement with the <sup>29</sup>Si MAS NMR result.

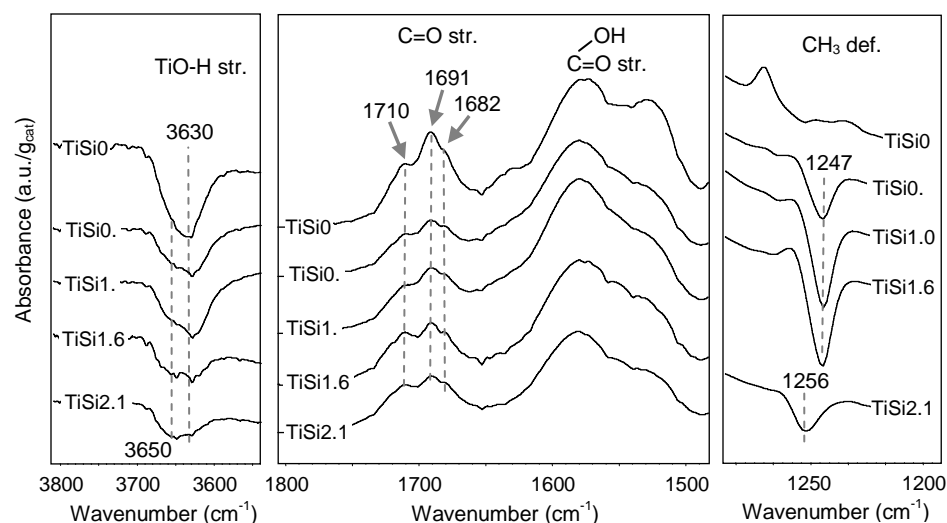
The spectral features of the samples in the range of 1450-1100 cm<sup>-1</sup> are shown in Figure 3.3(b). TiSi0 does not show any particular band in this region, besides the broad feature of strong Ti-O-Ti stretching modes below 1000 cm<sup>-1</sup>. The silylated TiO<sub>2</sub> catalysts show additional IR bands, which are indicative of the presence of surface silane. The reference spectrum of HMDS has specific IR bands at 1249 and 1178 cm<sup>-1</sup>, which correspond to a CH<sub>3</sub> group deformation mode [27] and to NH bending modes [28], respectively. The silylated TiO<sub>2</sub> materials show the CH<sub>3</sub> group deformation mode [27] at 1253 cm<sup>-1</sup>, and a number of overlapping bands at lower wavenumbers, of which the one occurring at 1158 cm<sup>-1</sup> is the most pronounced. These bands occur in the NH bending region and are probably related to small amounts of adsorbed NH<sub>3</sub> [28,29]. TiSi2.1 shows only the CH<sub>3</sub> group deformation mode [27] at 1266 cm<sup>-1</sup> and no clear NH<sub>3</sub> contribution. Other important vibrations like Si-C rocking around 860 cm<sup>-1</sup> [27], Ti-O-Si stretching vibration at 910-960 cm<sup>-1</sup> or Si-OH at 980 cm<sup>-1</sup> [30] are not visible due to the strong absorption modes of TiO<sub>2</sub>.



**Figure 3.3.** DRIFTS measurements recorded in He flow of TiSi0, TiSi0.1, TiSi1.0, TiSi1.6 and TiSi2.1 at RT after heating to 120°C, including a reference spectrum of liquid HMDS, measured by ATR-FTIR spectroscopy in the (a) 3800 to 2800  $\text{cm}^{-1}$  wavenumber region and (b) the 1450 to 1100  $\text{cm}^{-1}$  wavenumber region. In (c) the peak area of the acidic TiO-H stretching vibrations is represented as a function of silicon content.

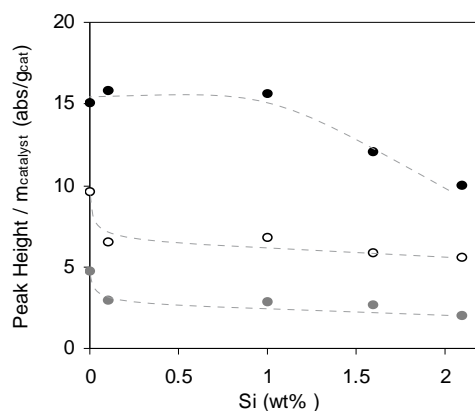
### 3.3.2. Photo-catalytic cyclohexane oxidation

Figure 3.4 shows the ATR-FTIR absorption spectra of the catalysts in cyclohexane flow after 90 min of UV illumination. The acidic-OH sites on TiO<sub>2</sub> are depleted during the photo-catalytic reaction [8], as witnessed for TiSi0 by the negative vibration centered at 3630 cm<sup>-1</sup>. The same feature is present in the spectra of the silylated samples, with the higher the silicon content, the lower the extent of depletion. The center of the (negative) acidic-OH peak shifts from 3630 cm<sup>-1</sup> on TiSi0, to 3650 cm<sup>-1</sup> on silylated catalysts, and the relative contribution of this shifted band increases with silicon content. In the infrared fingerprint region, below 1800 cm<sup>-1</sup>, the main products formed during reaction can be observed. The band observed at 1710 cm<sup>-1</sup> corresponds to the C=O stretching vibration of cyclohexanone, when this molecule is desorbed and dissolved in the reaction mixture. The bands observed at 1691 and 1682 cm<sup>-1</sup> are also corresponding to the C=O stretching vibration of cyclohexanone, but indicate that the molecule is adsorbed on the catalyst surface through hydrogen bonding [8]. The relative absorption of bulk/adsorbed carbonyl bands depends on the degree of silylation. In TiSi0 the bulk cyclohexanone band is much lower than the bands corresponding to adsorbed cyclohexanone. Silylated samples show a similar bulk cyclohexanone band as observed for TiSi0, but lower contributions of adsorbed cyclohexanone. The formation of other species is also apparent in the region below 1600 cm<sup>-1</sup>, where a broad absorption of at least three main bands is apparent. Different species can contribute to these absorptions, including symmetric vibrations of carboxylates [31,32], carbonates (around 1589 cm<sup>-1</sup>) [33], and bicarbonates (around 1555 cm<sup>-1</sup>) [34]. These species adsorb strongly on the TiO<sub>2</sub> surface and are therefore referred to as deactivating species. The CH<sub>3</sub> bending vibration of the silane groups shows a negative absorption after the photo-catalytic reaction. The position of these negative bands is at 1247 cm<sup>-1</sup> for samples of low silane content, and at 1256 cm<sup>-1</sup> for TiSi2.1. These bands are slightly red shifted in comparison to the ones observed in Figure 3.3.



**Figure 3.4.** ATR-FTIR spectrum after 90 min of cyclohexane photo-oxidation on TiSi0, TiSi0.1, TiSi1.0, TiSi1.6 and TiSi2.1.

The peak heights of the 1691, 1579 and 3630  $\text{cm}^{-1}$  bands after 90 min of photocatalytic reaction, were determined for all catalysts and are shown in Figure 3.5, as a function of silicon content. The band height for adsorbed cyclohexanone decreases with silicon content. The peak height of the acidic-OH depletion is represented by positive values, showing a decrease with surface silicon concentration. Both adsorbed cyclohexanone and acidic-OH depletion show a similar trend. From the intensity of the band of deactivating species represented by the absorption at 1579  $\text{cm}^{-1}$ , it can be concluded that the amount of deactivating species formed decreases only above 1.0% silicon content.



**Figure 3.5.** ATR-FTIR bands after 90 min of cyclohexane photo-oxidation for TiSi0, 0.1, 1.0, 1.6 and 2.1 divided by the mass of catalyst. The black symbols correspond to deactivating species (1579 cm<sup>-1</sup>), the empty symbols to adsorbed cyclohexanone (1691 cm<sup>-1</sup>) and the grey symbols to the positive values of acidic-OH depletion (3630 cm<sup>-1</sup>).

### 3.3.3. Cyclohexanone and water desorption under dark conditions

Cyclohexanone and water desorption were analyzed after reaction in the ATR-FTIR set-up, by continuing the cyclohexane flow under dark conditions. Cyclohexanone desorption is characterized by a decay in the intensity of the 1691 cm<sup>-1</sup> band in time, which is shown in Figure 3.6(a), for the TiSi0, TiSi1.0 and TiSi2.1 catalysts. Although carboxylates and water might have a small contribution to the peak height of the 1691 cm<sup>-1</sup> band, exponential curves could be well fitted through the data, allowing estimation of the desorption constants of cyclohexanone through the following equation:  $H = H_0 \exp(-k_{\text{des}} t) + H_{\text{end}}$ , where  $k_{\text{des}}$  is the desorption constant of cyclohexanone, measured in 1/min, while  $H$  is the 1691 cm<sup>-1</sup> peak height in time,  $H_0$  the peak height at  $t = 0$  min, and  $H_{\text{end}}$  the peak height at  $t = 60$  min, all determined in absorbance units per g<sub>catalyst</sub>. TiSi0 starts from a larger value of  $H_0$  but for all cases a similar  $H_{\text{end}}$  is reached after 60 min of dark desorption. The  $k_{\text{des}}$  values deduced from the exponential decay in all catalysts are represented in Figure 3.6(b) as a function of silicon content, and a linear relation was obtained.

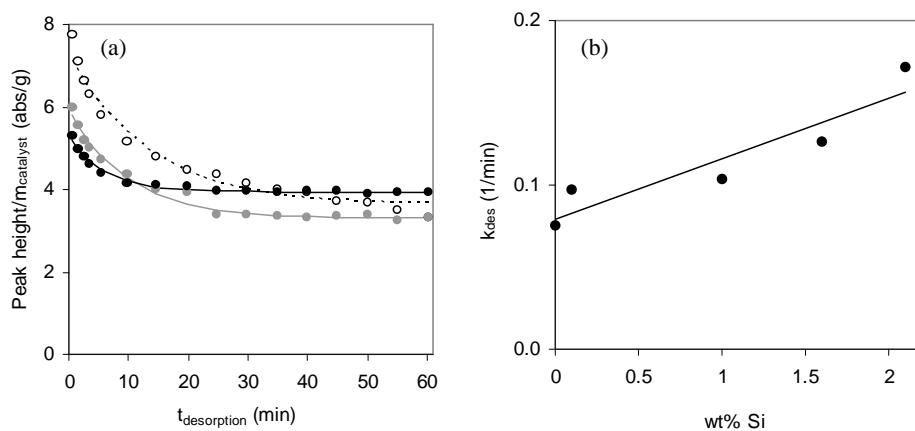


**Figure 3.6.** (a) Cyclohexanone desorption (dark conditions) on TiSi0 (open symbols), TiSi1.0 (grey symbols) and TiSi2.1 (black symbols) measured by the  $1691\text{ cm}^{-1}$  band height divided by catalyst mass (the lines correspond to exponential fits); (b) cyclohexanone desorption constant (determined from the exponential curves) as a function of silicon content (wt%).

A similar result was obtained for water desorption after reaction, shown in Figure 3.7(a). The amount of water desorbing from TiSi0 is much larger than for silylated materials, indicating a higher degree of surface hydration. The exponential curves fitted through the data provide an estimate for the desorption constant of water from the surface, which is represented in Figure 3.7(b) as a function of silicon content. As for cyclohexanone, it can be observed that  $k_{\text{des}}$  for water correlates linearly with surface silylation.



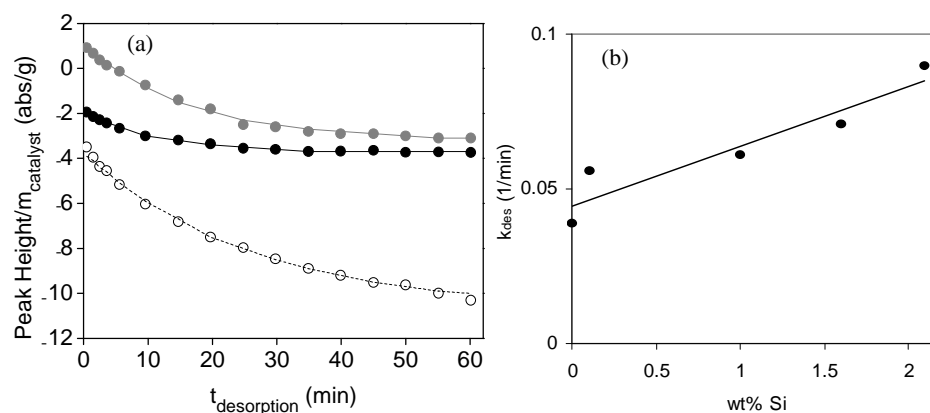


**Figure 3.7.** (a) Water desorption (dark conditions) from TiSi0 (open symbols), TiSi1.0 (grey symbols) and TiSi2.1 (black symbols) measured by the 3350 cm<sup>-1</sup> band height divided by catalyst mass (the lines correspond to exponential fits); (b) water desorption constant (determined from the exponential curves) as a function of silicon content (wt%).

### 3.3.4. Top illumination reactor

To compare the performance of the different catalysts in a quantitative way, cyclohexane photo-oxidation tests were performed in the top illumination reactor. Figure 3.8(a) shows the photo-catalytic formation of cyclohexanone in mmol, for TiSi0, TiSi1.0 and TiSi2.1. The initial rate of cyclohexanone formation increases in the following order: TiSi0 > TiSi2.1 > TiSi1.0. At illumination times longer than 40 min, the slope of the TiSi0 and TiSi1.0 curves decreases due to deactivation, and the rate of cyclohexanone formation for TiSi2.1 becomes the highest. Figure 3.8(b) shows the GC results after 100 min of reaction for all the catalysts, for both cyclohexanone and cyclohexanol (in mmol). The latter was not clearly observed in the ATR-FTIR spectroscopic results, but in the slurry reactor cyclohexanol is observed, though in very low amounts for all samples. Cyclohexanone formation decreases by partial trimethylsilylation on the TiO<sub>2</sub> surface, but over 1.0 wt% Si the amount of cyclohexanone formed increases again. For TiSi2.1 the ketone formed after 100 min of photo-oxidation is similar to that obtained for bare TiO<sub>2</sub>. The selectivity towards cyclohexanone formation is similar, ranging between 95 and 97%, suggesting that the reaction mechanism is not affected by silylation.

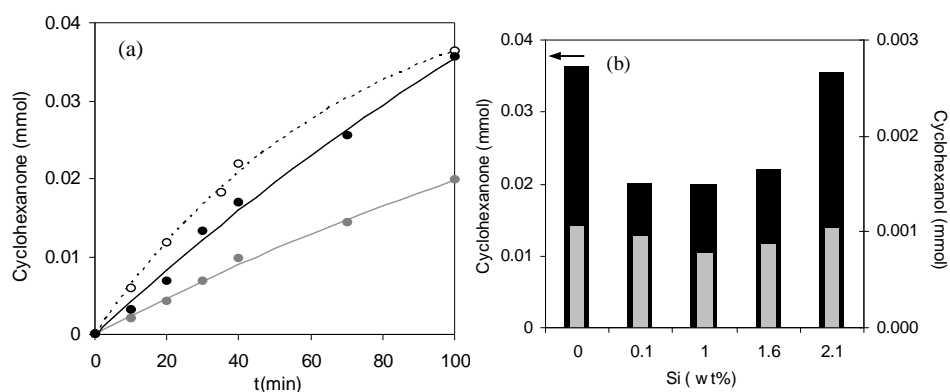


**Figure 3.8.** GC analysis of the products of cyclohexane photo-oxidation performed in a top illumination reactor. (a) formation of cyclohexanone (in mmol) vs. time for TiSi0 (open symbols), TiSi1.0 (grey symbols) and TiSi2.1 (black symbols); and (b) cyclohexanone (black) and cyclohexanol (grey) in mmol, formed after 100 min of reaction, for all catalysts.

### 3.4. DISCUSSION

HMDS is expected to react with the OH groups on the  $\text{TiO}_2$  surface, through the equation described in Figure 3.9 [18].

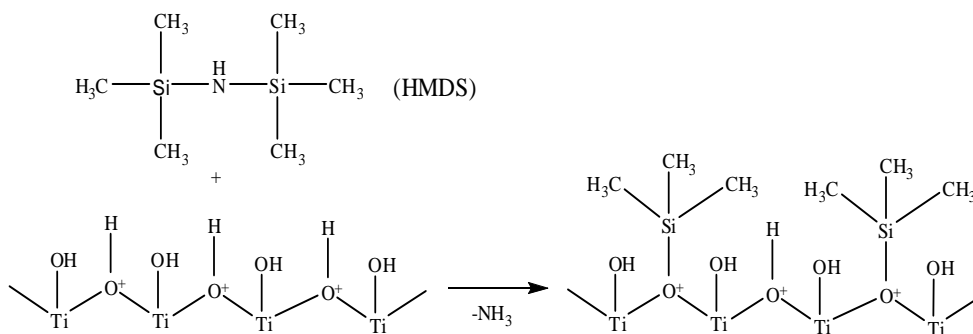


**Figure 3.9.** Expected reaction of hexamethyldisilazane (HMDS) with  $\text{TiO}_2$ , producing a partially silylated  $\text{TiO}_2$  surface and ammonia.

We provide significant evidence that indeed this reaction has occurred on the Hombikat surface. The XRF analysis proves the presence of silicon on the TiO<sub>2</sub> surface, with a range of 0 up to 2.1 wt% Si-loading, corresponding to a maximum surface coverage of 60%. Silane coupling on the surface is furthermore demonstrated by the <sup>29</sup>Si MAS NMR (Figure 3.2) spectra, in which isolated Ti-O-Si(CH<sub>3</sub>)<sub>3</sub> groups were identified for TiSi1.6. Since not all catalysts were analyzed by <sup>29</sup>Si MAS NMR, other types of silane coupling for samples containing higher silane content cannot be excluded. Silylation is confirmed by DRIFTS analysis (Figure 3.3), where the presence of methyl groups with wavenumbers corresponding to those of HMDS on the surface is evident. Also secondary changes in the surface properties are in agreement with surface silylation. TGA analysis in Figure 3.1 shows a lower amount of weakly and strongly adsorbed water on the surface, indicating that TiO<sub>2</sub> catalysts become less hydrophilic after the silylation procedure. This is confirmed by the decreasing intensity of absorptions assigned to water vibrations in the DRIFT spectra (Figure 3.3). Furthermore, from the DRIFT spectra it can be deduced that acidic-OH groups are converted, the amount changing linearly with silicon content (Figure 3.3(c)). The analysis of basic-OH sites is not possible under the applied conditions, so the possibility of silylation of basic-OH sites cannot be fully ruled out. But knowing that (i) only ~25% of the OH sites existing on the surface are basic [7], and (ii) the maximum coverage with silylated species is 60 % (for TiSi2.1), and (iii) a linear relation with the amount of acidic sites exists, we conclude that mainly acidic sites are silylated. It is therefore proposed that silanes bind to the TiO<sub>2</sub> surface preferentially through the acidic OH sites, as demonstrated in Figure 3.9. It can be concluded that for TiSi2.1 the acidic-OH sites are not fully depleted upon silylation. This is important because both acidic and basic-OH sites are involved in cyclohexane photo-oxidation, as proposed in a previously reported reaction mechanism [8]. Another factor preventing full silylation, is the coverage of the TiO<sub>2</sub> surface with up to three hydrogen bonded water layers at ambient conditions, of which some is strongly adsorbed [23,35]. A pre-treatment at temperatures higher than 400°C, needed for complete dehydration (Figure 3.1), was not applied in this study, in order to prevent morphological changes and to maintain a comparable activity of the samples. Summarizing, the synthesis procedure leads to a successful partial silylation of the TiO<sub>2</sub> surface.

### 3.4.1. Cyclohexanone and water desorption

The main objective of this study was to decrease the surface hydrophilicity of  $\text{TiO}_2$ , by coupling hydrophobic groups on the surface and stimulate desorption of photocatalytically formed cyclohexanone. The polar character of cyclohexanone and water molecules leads to desorption times from  $\text{TiO}_2$  into an organic medium of over 30 min, under dark conditions [9]. As desired, the cyclohexanone and water desorption rates were significantly increased by silylation (Figure 3.6 and 3.7). Since the desorption constants of both cyclohexanone and water increase linearly with surface silicon content, we propose that the adsorption enthalpy of these molecules on surface OH sites decreases by the presence of neighboring silane groups. A progressive shift of the negative band from 3630 to 3650  $\text{cm}^{-1}$  with increasing silane content (Figure 3.4), suggesting a decrease in acid strength of the OH groups, is in agreement with weaker product adsorption involving H-bridges.

The increased rate of desorption indicated above, leads to a lower amount of deactivating species on the surface of catalysts with more than 1.0 wt% Si (Figure 3.4 and 3.5). This can be explained as follows. It has been previously proposed that the main route for carboxylate formation is through the oxidation of surface bound cyclohexanone by  $\cdot\text{OH}$  radicals [8]. The increased hydrophobicity of the surface decreases the amount of adsorbed water, thus decreasing the concentration of  $\cdot\text{OH}$  radicals formed during illumination. The smaller availability of  $\cdot\text{OH}$  radicals contributes to the observed larger surface selectivity.

Though the cyclohexanone desorption rates are increased and, as a consequence, catalyst deactivation is reduced, surface silanes proved to be unstable under photocatalytic conditions (Figure 3.4). The negative trend in the  $\text{CH}_3$  deformation vibration indicates that the silane groups are oxidized, as observed in previous publications [17]. Analyzing the catalyst coating before and after reaction (not shown), we observed that the decomposition of the silanes from the surface is not complete, explaining the observed remaining positive effects. No evidence was found for the recovery of OH sites characteristic of the (silane-free)  $\text{TiSiO}$  sample, upon UV-illumination of silylated catalysts. Perhaps the best strategy is to apply more stable silane groups e.g. fluorine-containing silylation agents, that have been confirmed to be very stable under photocatalytic conditions [36].

### 3.4.2. Effect of silylation on the reaction rate

In silylating the catalyst surface the number of available active OH-sites is reduced, so an effect on the rate of cyclohexanone formation is expected [22]. In Figure 3.10(a) the initial rate of cyclohexanone formation is compared to the rate over partially deactivated catalysts, as determined from the tangents of the exponential fits at  $t = 0$  min and  $t = 100$  min in Figure 3.8(a). The initial reaction rate is greatly decreased for catalysts with low silane content, but at silane loadings above 1.0% there is an increase in the initial rate of cyclohexanone formation. The large difference in initial rate observed for TiSi0 relative to the silylated samples suggests the presence of a fraction of highly reactive sites on the surface. These highly reactive sites are apparently preferentially converted to Ti-O-Si(CH<sub>3</sub>)<sub>3</sub> groups, or blocked by NH<sub>3</sub> adsorption during silylation (Figure 3.3). We conclude that these highly active sites are very susceptible to deactivation, explaining the large difference between initial cyclohexanone formation rate and the rate over partially deactivated TiSi0 catalyst, compared to the silylated materials. In the following we provide a simplified explanation for the trend in cyclohexanone formation rate over partially deactivated surfaces, on the basis of the trend in desorption rate constant, and availability of acidic OH sites, taken as a measure of the photo-catalytic sites (Fig. 3.10b).

The rate of cyclohexanone formation,  $r$  in mmol/min, can be described by equation (3.1):

$$r = k_f N_T \frac{K_{Cane} C_{Cane}}{1 + K_{Cane} C_{Cane} + K_{Cnone} C_{Cnone}} \quad (3.1)$$

where  $k_f$  (min/mmol) is the cyclohexanone formation constant,  $N_T$  the number of available active sites (OH-groups, lowered in amount by catalyst deactivation and precursors for the active site formed by light activation),  $K_{Cane}$ ,  $C_{Cane}$  (mmol/cm<sup>3</sup>) and  $K_{Cnone}$ ,  $C_{Cnone}$  (mmol/cm<sup>3</sup>) the Langmuir constants and concentrations of cyclohexane and cyclohexanone, respectively. Because of the low temperatures it is assumed that the occupancy is high, implying that the fraction of empty sites is negligible. Two limiting cases are considered.

When  $K_{Cane} C_{Cane} \gg [1 + K_{Cnone} C_{Cnone}]$ , equation (3.1) can be simplified to:

$$r = k_f N_T \quad (3.2)$$

When  $K_{C_{none}} C_{C_{none}} \gg [1 + K_{C_{cane}} C_{C_{cane}}]$ , equation (3.1) can be simplified to:

$$r = k_f N_T \frac{K_{C_{cane}} C_{C_{cane}}}{K_{C_{none}} C_{C_{none}}} \quad (3.3)$$

Cyclohexanone is expected to have a much stronger adsorption enthalpy than cyclohexane, so the second limiting case is most realistic and considered in the following. For simplicity we assume that on bare  $TiO_2$  only one set of OH sites determines the reaction rate in steady state conditions ( $N_{T,TiSi0} = N_1$ ). On a silylated surface three types of sites are distinguished: isolated OH sites ( $N_1$ ), OH sites with a neighboring silane group ( $N_2$ ) and silylated inactive sites ( $N_{Si}$ ),  $N_T = N_1 + N_2 + N_{Si}$ . So for a silylated surface  $[N_1 + N_2] < N_{T,TiSi0}$ . This leads to the following rate equation:

$$r = k_f N_1 \frac{K_{C_{cane}} C_{C_{cane}}}{K_{C_{none,1}} C_{C_{none}}} + k_f N_2 \frac{K_{C_{cane}} C_{C_{cane}}}{K_{C_{none,2}} C_{C_{none}}} \quad (3.4)$$

For  $TiSi0$  this reduces to:

$$r_{TiSi0} = k_f N_{T,TiSi0} \frac{K_{C_{cane}} C_{C_{cane}}}{K_{C_{none,1}} C_{C_{none}}} \quad (3.5)$$

The trends in surface OH sites ( $N_1 + N_2$ ), assuming that the acidic OH groups represent the active sites, and desorption constants ( $k_{des}$ ) as a function of silylation are shown in Figure 3.10(b). The data shows for  $TiSi2.1$ :  $(N_1 + N_2) = 0.6 N_{T,TiSi0}$ . It should, be noted that for  $TiSi2.1$ , a surface coverage of 60% was obtained and, as a consequence, the number of OH active sites which are neighboring a silane group are predominant, so  $N_2 \gg N_1$  and  $N_2 \sim 0.6 N_{T,TiSi0}$ . For the rate of desorption of  $TiSi2.1$  an analogous relation holds:  $k_{des,TiSi2.1} = 2.3 k_{des,TiSi0}$ , which corresponds to  $K_{C_{none,TiSi2.1}} = (1/2.3) K_{C_{none,TiSi0}}$  (when  $k_{ads}$  is constant). So Equation (3.4) for  $TiSi2.1$  can be simplified to:

$$r_{\text{TiSi2.1}} = k_f 0.6 N_{\text{T,TiSi0}} \frac{K_{\text{Cane}} C_{\text{Cane}}}{(1/2.3) K_{\text{Cnone,l}} C_{\text{Cnone}}} = 1.4 r_{\text{TiSi0}} \quad (3.6)$$

assuming that the cyclohexanone formation rate constant is the same for TiSi0 and TiSi2.1. So the rate of cyclohexanone formation is higher for TiSi2.1 than for TiSi0 due to the improved desorption constant, despite the decrease in available active sites. Accordingly, the available OH sites of TiSi2.1, taking into consideration that approximately 60% of the OH groups is converted by silylation, show a higher turnover frequency (TOF) than of TiSi0, i.e.  $9.3 \times 10^{-3} \text{ min}^{-1}$  compared to  $5.6 \times 10^{-3} \text{ min}^{-1}$ , respectively. The turnover numbers (TON) are 0.8 and 0.3 for TiSi2.1 and TiSi0 for the short illumination times applied here. Previous work has shown that TiSi0 at longer illumination times shows a TON above unity, and that (silylated) TiO<sub>2</sub> is indeed a catalyst for the target reaction, albeit deactivating.

As stated previously, equation (3.6) applies only to the rate of cyclohexanone formation at prolonged illumination times, after which a certain amount of active sites is deactivated. To analyze the initial rate of cyclohexanone formation on TiSi0, two sites should be considered: very reactive, rapidly deactivating OH-sites (N<sub>3</sub>), and the stable OH-sites contributing to the conversion over partially deactivated catalysts (N<sub>1</sub>). The cyclohexanone formation constant for N<sub>3</sub> (k<sub>3</sub>) is apparently considerably larger than for N<sub>1</sub> (k<sub>1</sub>). This has an effect on the photonic efficiency, determined by the ratio of the initial rate of product formation and the incident photon flux, which is higher for TiSi0 (0.0025 mol Einstein<sup>-1</sup>) than for TiSi2.1 (0.0016 mol Einstein<sup>-1</sup>). It should be mentioned that in the final stages of the reaction, the photonic efficiency is higher for TiSi2.1 (0.00108 mol Einstein<sup>-1</sup>), than for TiSi0 (0.00062 mol Einstein<sup>-1</sup>), the consequence of the much lower rate of deactivation of the silylated catalyst.

In summary, the data show that a relatively high level of silylation is required to create improved catalysts. Two regimes can be defined:

1) At Si content < 1.0 wt%, the rate of cyclohexanone formation follows the decrease in available OH sites. So the improvement in cyclohexanone desorption rate constant is not enough to compensate for the decrease in surface OH groups.

2) At Si content > 1.0 wt%, the rate of cyclohexanone formation increases as a result of a further increased cyclohexanone desorption rate constant. Under these conditions, the desorption rate becomes dominant and over-compensates the negative impact of the

decrease in surface OH groups. At higher silane content the still available OH sites are characterized by a higher turnover frequency than the original free OH sites on TiSi0.

There should be an optimum trimethylsilyl loading that combines the increased surface hydrophobicity, with a sufficient number of available surface active sites. Based on the data provided here, the silylation loading should be at least 2.1 wt%.

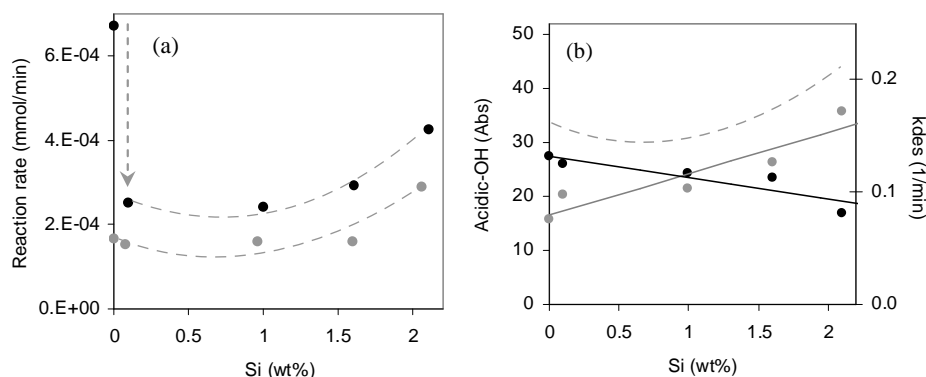


**Figure 3.10.** (a) Initial cyclohexanone formation rate (black symbols) and rate over partially deactivated surfaces (grey symbols) during photo-catalytic cyclohexane oxidation, as determined in the top illumination reactor. The arrow emphasizes the large difference in initial cyclohexanone formation rate between TiSi0 and TiSi0.1. (b) Peak area of acidic-OH (black) and cyclohexanone desorption constant (grey) as a function of silicon content, compared with the cyclohexanone formation rate over partially deactivated surfaces (dashed grey line).

### 3.5. CONCLUSIONS

A commercial TiO<sub>2</sub> catalyst was modified by coupling -Si(CH<sub>3</sub>)<sub>3</sub> groups to its surface. The trimethylsilyl groups, which seem to react preferentially with acidic-OH sites, increase the hydrophobicity of the silylated-TiO<sub>2</sub> catalysts. Desorption rates of cyclohexanone were increased by surface modification, and a linear relation between silane loading and cyclohexanone desorption rate constant was observed. Accordingly, during cyclohexane photo-oxidation, the silylated catalysts showed a lower tendency for deactivation. At low silane contents, the rate of cyclohexanone formation over partially deactivated surfaces decreased due to the dependency on the number of OH-groups.



However, for higher silane content (Si > 1.0 wt%), the increased desorption rate of cyclohexanone overcomes the lower number of surface OH sites with relatively high stability.

The silylated surface groups were not stable under photo-catalytic conditions. Improvement of the surface modification method should include the use of fluorine-containing silylation agents, which have been proven to resist photo-catalytic conditions.

## REFERENCES

- [1] A.Fujishima, X.T.Zhang, C. R. Chim. 9 (2006) 750.
- [2] A.Mills, R.H.Davies, D.Worsley, Chem. Soc. Rev. 22 (1993) 417.
- [3] M.A.Fox, M.T.Dulay, Chem. Rev. 93 (1993) 341.
- [4] J.Peral, X.Domenech, D.F.Ollis, J. Chem. Technol. Biotechnol. 70 (1997) 117.
- [5] H.Einaga, S.Futamura, T.Ibusuki, Appl. Catal. , B 38 (2002) 215.
- [6] S.A.Larson, J.L.Falconer, Catal. Lett. 44 (1997) 57.
- [7] P.Du, J.A.Moulijn, G.Mul, J. Catal. 238 (2006) 342.
- [8] A.R.Almeida, J.A.Moulijn, G.Mul, J. Phys. Chem. C 112 (2008) 1552.
- [9] T.J.A.Renckens, A.R.Almeida, M.R.Damen, M.T.Kreutzer, G.Mul, Catal. Today 155 (2010) 302.
- [10] C.B.Almquist, P.Biswas, Appl. Catal. A 214 (2001) 259.
- [11] M.A.Brusa, Y.Di Iorio, M.S.Churio, M.A.Grela, J. Mol. Catal. A 268 (2007) 29.
- [12] P.Boarini, V.Carassiti, A.Maldotti, R.Amadelli, Langmuir 14 (1998) 2080.
- [13] W.Mu, J.M.Herrmann, P.Pichat, Catal. Lett. 3 (1989) 73.
- [14] N.Igarashi, K.Hashimoto, T.Tatsumi, Microporous Mesoporous Mat. 104 (2007) 269.
- [15] M.V.Cagnoli, S.G.Casuscelli, A.M.Alvarez, J.F.Bengoa, N.G.Gallegos, M.E.Crivello, E.R.Herrero, S.G.Marchetti, Catal. Today 107-08 (2005) 397.
- [16] M.L.Pena, V.Dellarocca, F.Rey, A.Corma, S.Coluccia, L.Marchese, Microporous Mesoporous Mat. 44 (2001) 345.

- [17] S.Ikeda, Y.Kowata, K.Ikeue, M.Matsumura, B.Ohtani, *Appl. Catal. A* 265 (2004) 69.
- [18] M.I.Baron, L.Merhari, J. *Eur. Ceram. Soc.* 24 (2004) 1399.
- [19] X.F.Li, H.X.Gao, G.J.Jin, L.Chen, L.Ding, H.Y.Yang, Q.L.Chen, *J. Mol. Struct.* 872 (2008) 10.
- [20] A.Quintanilla, J.J.W.Bakker, M.T.Kreutzer, J.A.Moulijn, F.Kapteijn, *J. Catal.* 257 (2008) 55.
- [21] A.Y.Fadeev, R.Helmy, S.Marcinko, *Langmuir* 18 (2002) 7521.
- [22] J.T.Carneiro, C.C.Yang, J.A.Moma, J.A.Moulijn, G.Mul, *Catal. Lett.* 129 (2009) 12.
- [23] J.Soria, J.Sanz, I.Sobrados, J.M.Coronado, A.J.Maira, M.D.Hernandez-Alonso, F.Fresno, *J. Phys. Chem. C* 111 (2007) 10590.
- [24] J.A.Rob van Veen, Fred T.G.Veltmaat, Gert Jonkers, *J. Chem. Soc. Chem. Commun.* (1985) 1656.
- [25] G.Martra, *Appl. Catal. A* 200 (2000) 275.
- [26] T.A.Jurgens, J.W.Rogers, *J. Phys. Chem.* 99 (1995) 731.
- [27] L.J.Bellamy, in: (Eds.), *The Infrared Spectra of Complex Molecules Advances in Infrared Group Frequencies*, Chapman and Hall Ltd., London (1975).
- [28] G.Busca, H.Saussey, O.Saur, J.C.Lavalley, V.Lorenzelli, *Appl. Catal.* 14 (1985) 245.
- [29] K.Hadjiivanov, O.Saur, J.Lamotte, J.C.Lavalley, *Z. Phys. Chem.* 187 (1994) 281.
- [30] C.Beck, T.Mallat, T.Burgi, A.Baiker, *J. Catal.* 204 (2001) 428.
- [31] P.Z.Araujo, C.B.Mendive, L.A.G.Rodenas, P.J.Morando, A.E.Regazzoni, M.A.Blesa, D.Bahnemann, *Colloid Surf. A* 265 (2005) 73.
- [32] D.J.Yates, *J. Phys. Chem.* 65 (1961) 746.
- [33] W.G.Su, J.Zhang, Z.C.Feng, T.Chen, P.L.Ying, C.Li, *J. Phys. Chem. C* 112 (2008) 7710.
- [34] M.Primet, P.Pichat, M.V.Mathieu, *J. Phys. Chem.* 75 (1971) 1221.
- [35] A.Y.Nosaka, Y.Nosaka, *Bull. Chem. Soc. Jpn.* 78 (2005) 1595.
- [36] Y.Kuwahara, K.Maki, Y.Matsumura, T.Kamegawa, K.Mori, H.Yamashita, *J. Phys. Chem. C* 113 (2009) 1552.

# *Chapter 4*

## Combined ATR-FTIR and DFT study of cyclohexanone adsorption on hydrated TiO<sub>2</sub> anatase surfaces

The adsorption of cyclohexanone on different planes ((100), (101) and (001)) of anatase TiO<sub>2</sub>, with variable level of hydration, was evaluated by Density Functional Theory (DFT) calculations. Surface hydration was found to affect the cyclohexanone adsorption enthalpy and the calculated infrared absorption frequencies of the preferred adsorbed configurations considerably. A good correlation was found between two experimentally observed infrared absorption frequencies at 1694 cm<sup>-1</sup> and at 1681 cm<sup>-1</sup> of cyclohexanone adsorbed on TiO<sub>2</sub>, determined by Attenuated Total Reflection Fourier Transform Infrared (ATR-FTIR) spectroscopy, and frequencies calculated for configurations of cyclohexanone interacting with the (101) surface with low and intermediate levels of hydration, respectively. The corresponding adsorption enthalpies of these adsorbed configurations amount to -23.5 kJ/mol and -37.0 kJ/mol, respectively. In addition, DFT calculations show that cyclohexanone physisorption on the hydrated (100) plane of anatase yields an adsorption enthalpy of -89.4 kJ/mol. This might be a configuration contributing to irreversible adsorption of cyclohexanone known to occur experimentally after photo-catalytic activation of TiO<sub>2</sub>. Other phenomena of relevance to irreversible adsorption are also briefly addressed.

This chapter is based on the following publication: A.R.Almeida, M.Calatayud, F.Tielens, J.A.Moulijn, G.Mul (2010) submitted.

## 4.1. INTRODUCTION

Photo-catalytic reactions are generally operated at room temperature, where product desorption limitations are an issue [1]. Some of us have previously analyzed the selective formation of cyclohexanone by photo-oxidation of cyclohexane over  $\text{TiO}_2$ , using *in situ* ATR-FTIR spectroscopy. It was found that slow desorption of cyclohexanone from the  $\text{TiO}_2$  surface enhanced the formation of consecutively oxidized products, resulting in catalyst deactivation [2]. Two carbonyl-related absorption frequencies are always observed for cyclohexanone adsorbed on  $\text{TiO}_2$  surfaces. The configuration of adsorbed cyclohexanone, and the role of water in determining the adsorption modes, are of relevance in designing  $\text{TiO}_2$  surfaces with improved catalytic properties, but far from understood. Periodical Density Functional Theory (DFT) calculations, can aid infrared spectral interpretation [3] and the understanding of interactions between adsorbate and catalyst [4]. DFT calculations are based on model catalyst surfaces, which usually are very well representative for macroscopic anatase  $\text{TiO}_2$  particles, exhibiting 95% of the surface as (101) surfaces, truncated by (001) facets [5]. However, most commercial  $\text{TiO}_2$  catalysts are nanoparticles with a variety of surface facets and defects, like oxygen vacancies, which largely influence the reactivity of the  $\text{TiO}_2$  surface [6]. The large degree of hydration at operating conditions [7,8] is also of great importance, since the adsorption mode of a probe molecule is strongly affected by secondary interactions [9]. It is possible to approach more realistic conditions in DFT calculations, by introducing a hydration layer on the modeled  $\text{TiO}_2$  surface [4].

In this study interaction of cyclohexanone with (100), (101) and (001)  $\text{TiO}_2$  planes of different hydration levels was studied by periodic DFT calculations, in order to provide further insight in ATR-FTIR spectral interpretation and better understanding of the adsorption configurations of cyclohexanone leading to surface deactivation of  $\text{TiO}_2$  during photo-oxidation.

## 4.2. EXPERIMENTAL

### 4.2.1. Catalyst characterization

Solid state <sup>1</sup>H-MAS-NMR was performed on a Bruker Avance 400 spectrometer, using a 5 mm zirconia rotor, with spinning speed of 11 kHz. The spectral window was 25063 Hz, with 50 ms acquisition time and 15 s acquisition delay. Transmission Electron Microscopy (TEM) was performed using a FEI Tecnai TF20 electron microscope with a field emission gun as the source of electrons operated at 200 kV. Samples were mounted on Quantifoil® carbon polymer supported on a copper grid, by placing a few droplets of a suspension of ground sample in ethanol on the grid, followed by drying at ambient conditions. The crystal lattice distances were determined by Fast Fourier Transformation (FFT) of the TEM images, which were generated using Digital Micrograph 3 software.

### 4.2.2. Cyclohexanone adsorption reference

The photo-catalyst used in this study was Hombikat UV100 TiO<sub>2</sub> (Sachtleben) of 100% anatase crystallinity (determined by XRD), a S<sub>BET</sub> of 337 m<sup>2</sup>/g and a primary particle size of approximately 5 nm [10]. The catalyst was dried at 120°C for 1 h in static air and suspended in water at a concentration of 1.5 g/L. The suspension was treated for 30 min in a 35 kHz Elmasonic ultrasonic bath; 2 mL of this suspension was spread on a ZnSe crystal and dried in vacuum in a desiccator at room temperature overnight. The coating obtained was dried at 120°C for 1 h.

The *in situ* ATR-FTIR setup used for the cyclohexanone adsorption experiments, is described in detail elsewhere [2]. Cyclohexane 99.0% from Sigma Aldrich and cyclohexanone 99.8% Fluka Analytical were used. Cyclohexane and a solution of 0.05 M of cyclohexanone in cyclohexane were dried over Molsieve type 4A overnight before use. A volume of 50 mL of cyclohexane was flown through the TiO<sub>2</sub> coated ATR crystal during 1 h by means of a series II high performance liquid chromatography pump. After surface stabilization a spectrum was taken as background. For the measurement of the absorption spectrum for cyclohexanone, the inlet of the ATR cell was switched from pure cyclohexane to the solution of 0.05 M of cyclohexanone in

cyclohexane. A Nicolet 8700 spectrometer equipped with a TRS N<sub>2</sub>-cooled detector was used. The measurements were done with a mirror velocity of 1.8988 cm.s<sup>-1</sup> and a resolution of 4 cm<sup>-1</sup>. The background and the sample spectra were averaged from 64 and 32 spectra, respectively.

### 4.3. COMPUTATIONAL METHODS

Geometry optimization and molecular dynamics calculations were performed using the *ab initio* plane-wave pseudopotential approach as implemented in the Vienna *Ab Initio* Simulation Package (VASP code) [11,12]. Periodically repeated calculations with the Generalized Gradient Approximation (GGA) density functional by Perdew and Wang PW91 [13] were performed. The valence electrons were treated explicitly and their interactions with the ionic cores are described by the projector augmented-wave method (PAW), which allows a low energy cut off equal to 400 eV for the plane-wave basis.

The relaxation of the anatase (100), (101) and (001) planes used in this study, was discussed previously [14,15]. Each surface plane was optimized with different extents of adsorbed H<sub>2</sub>O, and the distribution of water layers over the TiO<sub>2</sub> planes was based on previous work by Arrouvel et al. [15]. Physisorbed cyclohexanone is stabilized by one or more H-bonds between the oxygen atom of cyclohexanone and a hydrogen atom of a surface active site or adsorbed H<sub>2</sub>O molecule. Cyclohexanone was chemisorbed on TiO<sub>2</sub> inducing a chemical bond between a coordinatively unsaturated titanium surface atom and the oxygen atom of cyclohexanone. The unit cell dimensions were determined for each plane in order to reduce the interaction between adsorbed cyclohexanone with adjacent unit cells. In Table 4.1 the characteristics of the surface planes, with variable levels of hydration and unit cell dimensions are shown.

Geometry optimization calculations were performed with the conjugate-gradient algorithm, at 0 K and at 3x2x1 k-point mesh and the partial occupancies are set for each wave function using the tetrahedron method with Blöchl corrections [16]. The positions of all the atoms in the super cell as well as the cell parameters are relaxed, in the potential energy determined by the full quantum mechanical electronic structure until the total energy differences between the loops is less than 10<sup>-4</sup> eV.

To explore the surface potential energy of our system we performed, initially, 0 K geometry optimizations on several intuitive starting configurations; the obtained systems were used as inputs for an *ab initio* Molecular Dynamics (MD) study within the micro-canonical ensemble in the microcanonical (NVE) approach, at  $T = 300$  K, to scan the possible configurations of the system. We considered several starting configurations (but no statistics was performed on them) and the run was stopped after  $t \geq 2$  ps. To avoid fluctuations associated to the large time step chosen (2.5 fs), the mass of H atoms was set to 3. The local minima found from Molecular Dynamics results were systematically re-optimized at 0 K, in order to achieve the absolute electronic minimum energy for each configuration. Molecular Dynamics were performed at  $1 \times 1 \times 1$  k-points mesh with an energy cutoff of 250 eV. For both optimization and molecular dynamic calculations, half of the slab was frozen and only the upper four TiO<sub>2</sub> layers were allowed to relax.

Vibrational spectra were calculated, with  $1 \times 1 \times 1$  k-points mesh, for a limited number of atoms within the harmonic approximation. Only the adsorbed cyclohexanone molecule and its neighboring or interacting OH groups on the surface were allowed to move, while the rest of the slab was kept frozen. The eigenvalues of the Hessian matrix after diagonalization lead to the frequency values. The assignment of the vibrational modes was done by inspection of the corresponding eigenvectors. A scaling factor was applied to the calculated carbonyl vibrations. The scaling factor was determined by the ratio between the experimentally observed carbonyl vibration ( $1722 \text{ cm}^{-1}$ ) of cyclohexanone dissolved in cyclohexane and the carbonyl vibration calculated by DFT, when the molecule is isolated. This approach is accurate for carbonyl vibrations [17]. Furthermore the scaling factor is dependent on the size of the unit cell (Table 4.1), so the scaling factor was adjusted for each TiO<sub>2</sub> plane, a similar procedure was successfully undertaken in ref [18].

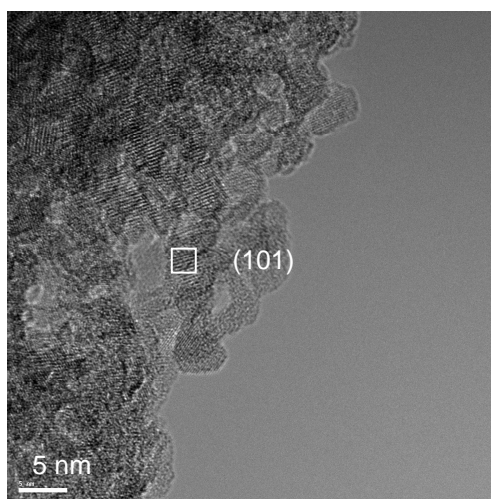
**Table 4.1.** Dimensions of (100), (101) and (001) unit cells and applied hydration levels.

Planes	Unit cell dimensions			Bare slab thickness (Å)	Hydration level		
	a (Å)	b (Å)	c (Å)		(H <sub>2</sub> O molecules/nm <sup>2</sup> )		
(101)	7.6	10.9	40	13.8	4.8	9.6	16.8
(100)	7.6	9.5	40	13.1	6.2	9.3	18.5
(001)	7.4	11.6	40	13.3	2.3	7.0	16.4

## 4.4. RESULTS

### 4.4.1. Catalyst characterization

Analysis of the applied commercial TiO<sub>2</sub> by X-ray Diffraction (XRD) was discussed previously [19], showing anatase crystallinity, with the diffraction lines of the (101) crystallographic phase being dominant. The bulk crystalline structure was also analyzed by TEM, as shown in Figure 4.1. The sample was further analyzed by determination of the lattice parameters, which were calculated by a Fast Fourier Transformation (FFT). The most common lattice distance in Figure 4.1 ranged from 0.34 to 0.36 nm, which is indicative of the presence of (101) surface exposed planes [20].

**Figure 4.1.** Transmission Electron microscopy (TEM) image of anatase TiO<sub>2</sub> UV-100.



The TiO<sub>2</sub> surface is known to be very hydrophilic, being covered with up to three hydrogen bonded water layers [21,22]. Before determining photo-catalytic activity, a pretreatment at 120°C is commonly applied. Thermo-gravimetric analysis in air reported elsewhere [23], shows that only 60% of the total amount of adsorbed water is removed by this 120°C pre-treatment. Under cyclohexane photo-oxidation conditions, the surface hydration is expected to be lower than under air conditions, but spectroscopic data clearly show the presence of water, remaining strongly adsorbed on the TiO<sub>2</sub> surface [2]. Furthermore, water is a byproduct of the photo-catalytic cyclohexane oxidation [2], and is expected to remain adsorbed on the anatase surface. So the effect of strongly adsorbed water on the TiO<sub>2</sub> surface must be considered for interpretation of spectroscopic data. <sup>1</sup>H-MAS-NMR measurements on TiO<sub>2</sub> under humid and dried conditions are shown in Figure 4.2. Under humid conditions (Figure 4.2a) mainly one narrow peak is visible, corresponding to adsorbed H<sub>2</sub>O on the TiO<sub>2</sub> surface. The fact that the peak is narrow suggests a high mobility of the protons measured. Therefore, these are not associated with surface active sites, but with layers of adsorbed water on the surface. When the catalyst is heated to 120°C (Figure 4.2b), the NMR signal intensity decreases and shifts slightly to lower fields. The broader signal obtained corresponds to either surface sites or more rigid water molecules with restricted mobility at the surface [8].

It is known from previous publications [24], that the surface-OH sites of anatase TiO<sub>2</sub> show <sup>1</sup>H-MAS-NMR peaks at chemical shifts of 2.3 and 6.4 ppm. The high field peak at 2.3 ppm is assigned to basic-OH sites, where the hydrogen atom binds to a terminal oxygen. The low field peak at 6.4 ppm corresponds to the positively charged more acidic protons located on bridged oxygen atoms and forming weak hydrogen bonds with adjacent oxygen atoms [24]. The position of the expected OH sites in the NMR spectra is represented in Figure 4.2b). One main peak is observed which occurs at 5.9 ppm, a similar position as in Figure 4.2a), corresponding to more rigid molecules of adsorbed water, which can be related to physisorbed H<sub>2</sub>O or Ti-H<sub>2</sub>O sites. The small shoulder around 2.3 ppm, corresponding to basic-OH sites, indicate that some of these sites are free. The acidic-OH site is not visible, so this site is probably H-bonded to adsorbed water molecules. Weak contributions of bridging and isolated OH sites indicate that they are either occupied by adsorbed water molecules or of low expression in the

surface. No explanation was found for the shoulder at 9.8 ppm, which could indicate the presence of a different kind of surface OH site, or surface contaminant.

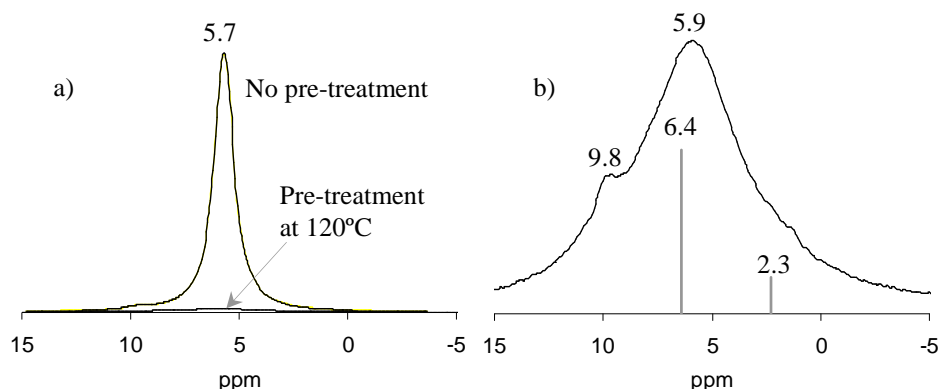


**Figure 4.2.**  $^1\text{H}$ -MAS-NMR of a)  $\text{TiO}_2$  UV-100 with no pre-treatment and with a pre-treatment of  $120^\circ\text{C}$  and b) focus on the measurement after pre-treatment at  $120^\circ\text{C}$ . The grey lines correspond to the expected position of  $\text{TiO}_2$  active OH-sites [24].

#### 4.4.2. Cyclohexanone adsorption – ATR-FTIR spectra

Cyclohexanone adsorption was induced by flowing a solution of 0.05 M of cyclohexanone in cyclohexane for two hours over the  $\text{TiO}_2$  surface. The changes in spectral intensities are shown in Figure 4.3a. The spectra of externally fed cyclohexanone are similar to those obtained at initial conditions of cyclohexane photo-oxidation [25], which suggests that the adsorption configurations are similar under UV and dark conditions. The range between  $1800$  and  $1600\text{ cm}^{-1}$  contains a band at  $1722\text{ cm}^{-1}$ , corresponding to the  $\text{C}=\text{O}$  stretching vibration of dissolved cyclohexanone, as confirmed by the spectrum obtained in the absence of the  $\text{TiO}_2$  coating. This study will focus on this vibration, since it is the only cyclohexanone absorption band, which red-shifts in the presence of  $\text{TiO}_2$ . The two contributions at  $1694$  and  $1681\text{ cm}^{-1}$ , correspond to the carbonyl vibration of cyclohexanone when H-bonded to the catalyst surface [2]. The isosbestic point with positive and negative contributions at  $1650$  and  $1615\text{ cm}^{-1}$  respectively, is related to a change in the configuration of  $\text{H}_2\text{O}$  adsorbed in the surface, due to cyclohexanone co-adsorption. A deconvolution method was applied to different

adsorption spectra, and the peak areas of the adsorbed cyclohexanone bands are presented in Figure 4.2b, as a function of adsorption time. The band at 1694 cm<sup>-1</sup> is the most prominent; its contribution decreases with a rise in the contribution of the 1681 cm<sup>-1</sup> peak (Figure 4.3b). The behavior of these two bands suggests a slow reorganization of cyclohexanone on the surface towards a preferred adsorption configuration, with a main absorption band at 1681 cm<sup>-1</sup>. After 120 min the ratio of the 1681 cm<sup>-1</sup> and 1694 cm<sup>-1</sup> bands is 60/40.

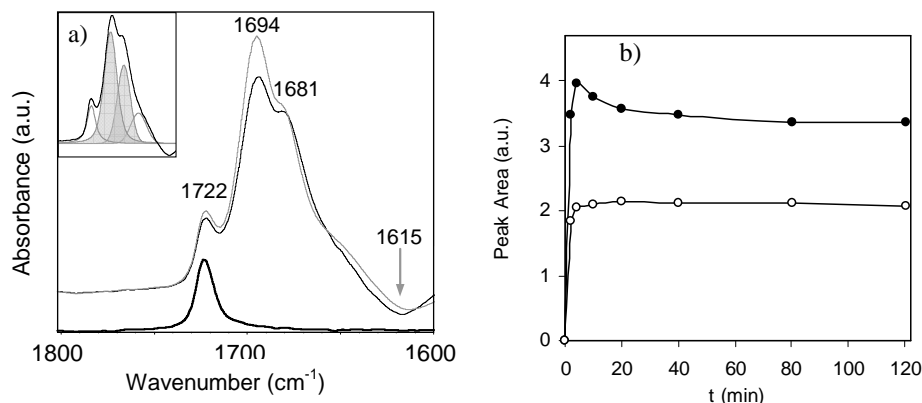


**Figure 4.3.** a) Spectrum of bulk cyclohexanone without TiO<sub>2</sub> (thick black), spectra of 0.05 M of cyclohexanone in cyclohexane adsorption on TiO<sub>2</sub> (background of cyclohexane adsorption on TiO<sub>2</sub>) for 5 min (grey) and 120 min (black), whose peak deconvolution is shown in the inset; b) Peak area profile of adsorbed cyclohexanone bands (full black symbols: 1694 cm<sup>-1</sup>; empty black symbols: 1681 cm<sup>-1</sup>).

#### 4.4.3. DFT calculations

In order to take the effect of adsorbed H<sub>2</sub>O on the interaction of cyclohexanone with TiO<sub>2</sub> surfaces into account, TiO<sub>2</sub> surfaces were modeled with different amounts of H<sub>2</sub>O molecules adsorbed per nm<sup>2</sup>, as discussed in previous publications [15,26]. In Table 4.2 the structures of the (100), (101), (001) TiO<sub>2</sub> surface planes, with different extents of water adsorption, are shown. The lowest hydration level includes only chemisorbed H<sub>2</sub>O molecules. The second hydration level includes physisorbed (H-bonded) H<sub>2</sub>O molecules on surface OH sites, and the highest hydration level contains an adsorbed

water layer. The adsorption energy of a water molecule ( $E_{\text{H}_2\text{O,ads}}$ , in kJ/mol) on each surface plane and at a specific surface hydration is shown in Table 4.2. This was calculated according to the following equation:

$$E_{\text{H}_2\text{O,ads}} = \frac{E_{\text{hydr. slab}} - E_{\text{bare slab}} - n_{\text{H}_2\text{O}} E_{\text{H}_2\text{O}}}{n_{\text{H}_2\text{O}}} \quad (4.1)$$

with  $E_{\text{bare slab}}$  corresponding to the calculated energy of the bare (dehydrated) slab,  $E_{\text{hydr. slab}}$  to the energy of the hydrated slab,  $E_{\text{H}_2\text{O}}$  to the energy of one gas-phase water molecule at its equilibrium geometry and  $n_{\text{H}_2\text{O}}$  to the number of water molecules added to the unit cell at each hydration level. The negative values presented in Table 4.2, indicate that the adsorption step is exothermic.

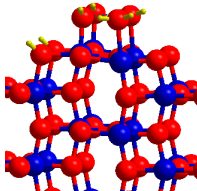
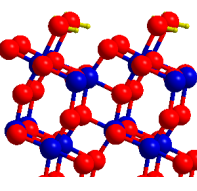
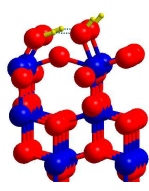
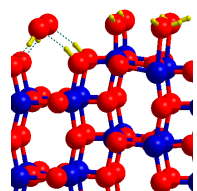
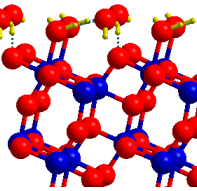
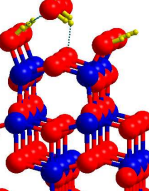
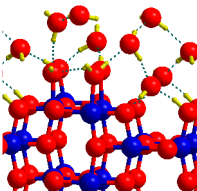
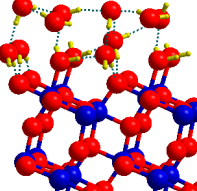
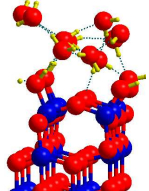
Water chemisorbs on the (100) surface plane at coverages up to 6.2 molecules/nm<sup>2</sup>. Some water molecules dissociate on free Ti sites and on bridging Ti-O-Ti sites of bare (100) surface, with the formation of Ti-OH sites and bridging Ti-OH-Ti sites, respectively. Undissociated water molecules chemisorb on free Ti sites and form Ti-H<sub>2</sub>O sites. Free Ti-O-Ti sites are also present at the lowest hydration level. Increasing the water coverage to 9.3 molecules/nm<sup>2</sup> leads to water physisorption on the bridging Ti-O-Ti sites, with a H<sub>2</sub>O adsorption energy of -61.7 kJ/mol. The formation of a layered H<sub>2</sub>O network is induced at surface hydration levels of 18.5 molecules/nm<sup>2</sup>, characterized by similar affinity of water to the surface, of -61.0 kJ/mol.

On the (101) plane, water chemisorbs without dissociation up to a surface coverage of 4.8 molecules/nm<sup>2</sup>. For this coverage, an adsorption enthalpy of -65.7 kJ/mol was determined with the formation of only Ti-H<sub>2</sub>O, leaving bridging Ti-O-Ti oxygen sites still free on the surface. A surface hydration increase to 9.6 H<sub>2</sub>O molecules per nm<sup>2</sup> induces molecular physisorption of H<sub>2</sub>O, H-bonded to Ti-O-Ti and neighboring Ti-H<sub>2</sub>O sites [26]. A decrease in adsorption enthalpy (-57.1 kJ/mol) is observed at higher hydration levels, where a multilayer of adsorbed water is formed.

The (001) surface plane in its bare state (OH free) contains Ti-O-Ti sites with the oxygen atom at a higher plane than the Ti atoms. Upon hydration one of the Ti-O-Ti bonds breaks and two Ti-OH sites are created. Of these two new OH sites, one contains an oxygen atom originally from the TiO<sub>2</sub> lattice structure. Under low surface hydration

(2.3 molecules/nm<sup>2</sup>), the created Ti-OH sites are H-bonded, and free Ti-O-Ti sites are still present [15,26]. On this TiO<sub>2</sub> plane the energy for dissociative water chemisorption is much higher (-184.7 kJ/mol). At a surface hydration level of 7.0 molecules/nm<sup>2</sup> H<sub>2</sub>O physisorption occurs, with H<sub>2</sub>O molecules H-bridging on the Ti-O-Ti sites, and a reduction of the H<sub>2</sub>O adsorption strength to -97.4 kJ/mol. The formation of H<sub>2</sub>O multi layers on the surface, at coverages of 16.4 H<sub>2</sub>O molecules per nm<sup>2</sup> is characterized by an adsorption energy of -72.6 kJ/mol.

**Table 4.2.** Adsorption energies of H<sub>2</sub>O on TiO<sub>2</sub> (100), (101) and (001) at different hydration levels.

	(100)	(101)	(001)
Structures			
Hydration (H <sub>2</sub> O/nm <sup>2</sup> )	6.2	4.8	2.3
Energy (kJ/mol)	-68.5	-65.7	-184.7
Structures			
Hydration (H <sub>2</sub> O/nm <sup>2</sup> )	9.3	9.6	7.0
Energy (kJ/mol)	-61.7	-67.1	-97.4
Structures			
Hydration (H <sub>2</sub> O/nm <sup>2</sup> )	18.5	16.8	16.4
Energy (kJ/mol)	-61.0	-57.1	-72.6

For each surface plane at a specific surface hydration level, the energy of cyclohexanone adsorption ( $E_{\text{Cnone,ads}}$ , in kJ/mol) is calculated according to the following equation:

$$E_{\text{Cnone,ads}} = E_{\text{Cnone,hydr. slab}} - E_{\text{hydr. slab}} - E_{\text{Cnone}} \quad (4.2)$$

with  $E_{\text{Cnone,hydr. slab}}$  corresponding to the calculated energy of cyclohexanone adsorbed on a hydrated slab,  $E_{\text{hydr. slab}}$  the energy of the hydrated slab,  $E_{\text{Cnone}}$  the energy of the isolated cyclohexanone molecule at its equilibrium geometry with one cyclohexanone molecule per slab ( $n_{\text{Cnone}} = 1$ ). The energy of adsorption of cyclohexanone on different (100)  $\text{TiO}_2$  active sites was calculated, and is shown in Table 4.3.

Depending on the surface plane and degree of hydration, different active sites will be available for cyclohexanone adsorption. For  $\text{TiO}_2$  (100) surface, three different adsorption sites can be considered, and each will present a different adsorption enthalpy for cyclohexanone. Also a chemisorption configuration can be considered, but this was not included in the Boltzmann distribution calculation. The population in the physisorbed configuration of greatest weight depends on the energy of state according to the Boltzmann distribution. For example, the probability of configuration I in Table 4.3, is given by the following relation:

$$\frac{\text{Configuration I}}{\text{Configuration i}} = \frac{\exp\left(-\frac{E_I}{RT}\right)}{\sum_i \exp\left(-\frac{E_i}{RT}\right)} \quad (4.3)$$

with  $i$  corresponding to all the cyclohexanone physisorbed configurations (I, II and III).

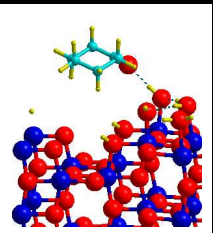
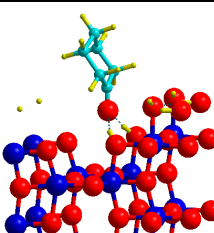
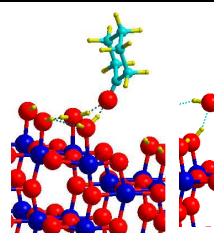
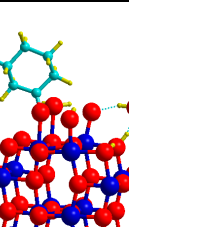
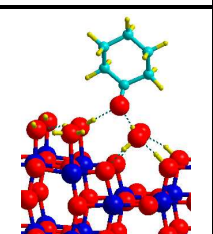
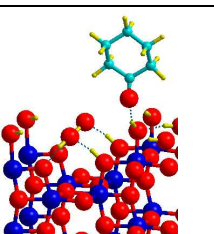
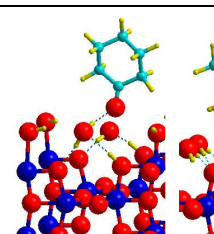
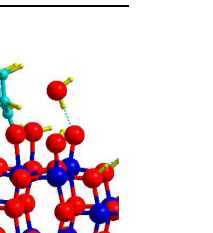
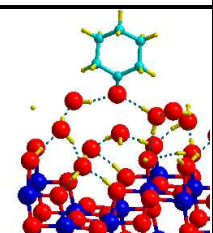
For low surface hydration (6.2  $\text{H}_2\text{O}$  molecules per  $\text{nm}^2$ ) three different physisorption sites are available, the basic-OH, acidic-OH and Ti- $\text{H}_2\text{O}$  sites, while chemisorption may occur in the presence of free Ti sites. At room temperature, physisorption on the basic-OH of higher adsorption enthalpy (-48.8 kJ/mol) will be energetically favored: the calculations show that 98.3 % of the physisorbed molecules have this configuration. The other adsorption configurations, due to their low probability can be neglected.

For 9.3 H<sub>2</sub>O molecules per nm<sup>2</sup>, three possible physisorption configurations can be considered, physisorption on Ti-H<sub>2</sub>O sites, basic-OH, and an adsorbed H<sub>2</sub>O molecule. In this case the preference is towards adsorption on a Ti-H<sub>2</sub>O site, with an extra H-bond to a neighboring adsorbed molecule (-89.4 kJ/mol) and the other adsorption configurations can be neglected. So the active sites of preferable adsorption depend on the hydration level. Cyclohexanone adsorption on the (100) TiO<sub>2</sub> plane is enhanced at intermediate hydration levels (9.3 H<sub>2</sub>O molecules per nm<sup>2</sup>), where the adsorption enthalpy of -89.4 kJ/mol is considerably larger than the H<sub>2</sub>O adsorption of -61.7 kJ/mol.

At higher hydration levels, direct physisorption of cyclohexanone on the (100) surface is not favored, with the molecule being pushed away from the surface towards to top of the H<sub>2</sub>O layer. Therefore only one physical adsorption configuration is possible, which is on the adsorbed H<sub>2</sub>O layer of -34 kJ/mol.

The occurrence of cyclohexanone chemisorption is negligible, because its enthalpy, which ranges from 15 to 50 kJ/mol, depending on the hydration level, is lower than the enthalpy for H<sub>2</sub>O chemisorption (-68.5 kJ/mol).

**Table 4.3.** Energies (kJ/mol) of cyclohexanone physisorption and chemisorption on the (100)  $\text{TiO}_2$  plane at increasing surface hydration, and the corresponding configurations. The probability of the physisorption configuration is determined based on the Boltzmann distribution equation at 25°C. The preferred configuration at each hydration level is highlighted with a box.

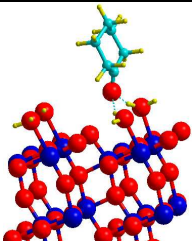
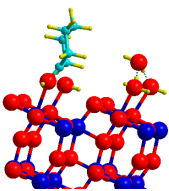
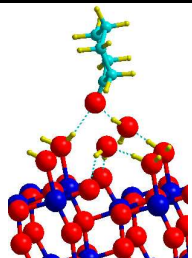
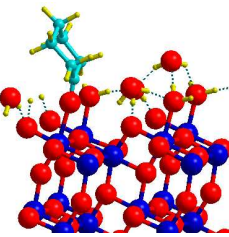
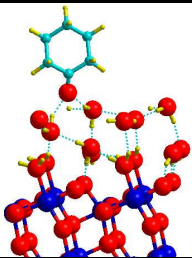
Hydration	Physisorption		Chemisorption	
	I	II	II	IV
6.2 $\text{H}_2\text{O}/\text{nm}^2$				
OH site	Basic OH	Acidic OH	Ti- $\text{H}_2\text{O}$	Free Ti
Energy	-48.8 kJ/mol	-39.2 kJ/mol	-29.3 kJ/mol	-15.2 kJ/mol
Distribution	98.3%	1.7%	0.0%	0.0%
9.3 $\text{H}_2\text{O}/\text{nm}^2$				
OH site	Ti- $\text{H}_2\text{O}$	Basic OH	$\text{H}_2\text{O}$ ads.	Free Ti
Energy	-89.4 kJ/mol	-70.9 kJ/mol	-34.6 kJ/mol	-51.4 kJ/mol
Distribution	99.9%	0.1%	0.0%	0.0%
18.5 $\text{H}_2\text{O}/\text{nm}^2$				
OH site	$\text{H}_2\text{O}$ ads.			
Energy	-34.0 kJ/mol			
Distribution	100.0%			



The calculated energies for cyclohexanone physisorption and chemisorption on the (101) TiO<sub>2</sub> plane are summarized in Table 4.4, for different extents of water adsorption. Cyclohexanone physisorption on the (101) plane with 4.8 H<sub>2</sub>O molecules per nm<sup>2</sup> occurs on the only available active site, Ti-H<sub>2</sub>O, with a relatively weak interaction (-23.5 kJ/mol). At a higher hydration level (9.6 H<sub>2</sub>O/nm<sup>2</sup>), the presence of neighboring adsorbed H<sub>2</sub>O molecules allows for further stabilization of cyclohexanone physisorption by H-bonding (-37.0 kJ/mol). Direct physisorption of cyclohexanone on a TiO<sub>2</sub> active site at 16.8 H<sub>2</sub>O molecules/nm<sup>2</sup> is not favorable, with the cyclohexanone molecules being pushed away to the top of the water layer, where its adsorption is most stable (-62.1 kJ/mol).

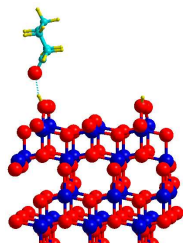
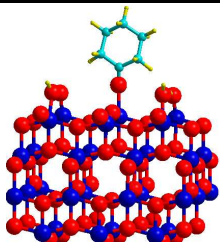
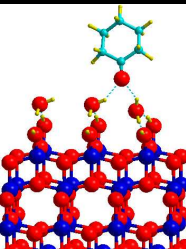
The energy for cyclohexanone chemisorption was determined for the lowest hydration levels only, at high hydration levels it was not favorable. Chemisorption of cyclohexanone shows enthalpies in the same range or even higher than physisorption configurations. However chemisorption is possible only in the presence of a Ti free site, or when the energy for cyclohexanone chemisorption is larger than water chemisorption in this plane (-65.7 kJ/mol). A free Ti site at such conditions will not be preferred due to the high hydration level and cyclohexanone chemisorption is not strong enough to displace H<sub>2</sub>O chemisorbed on the surface, so chemisorption configuration can be neglected at either hydration level.

**Table 4.4.** Energies (kJ/mol) of cyclohexanone physisorption and chemisorption on the (101)  $\text{TiO}_2$  plane at increasing surface hydration, and the corresponding configurations. The probability of each surface configuration is determined based on the Boltzmann distribution equation at 25°C. The preferred configuration at each hydration level is highlighted with a box.

Hydration	Physisorption	Chemisorption
4.8 $\text{H}_2\text{O}/\text{nm}^2$		
OH site	Ti-H <sub>2</sub> O	Free Ti
Energy	-23.5 kJ/mol	-48.9 kJ/mol
Distribution	100.0%	0.0%
9.3 $\text{H}_2\text{O}/\text{nm}^2$		
OH site	Ti-H <sub>2</sub> O	Free Ti
Energy	-37.0 kJ/mol	-31.2 kJ/mol
Distribution	100.0%	0.0%
16.8 $\text{H}_2\text{O}/\text{nm}^2$		
OH site	Ads. H <sub>2</sub> O	
Energy	-62.1 kJ/mol	
Distribution	100.0%	

The calculated energies for cyclohexanone physisorption and chemisorption on the (001) TiO<sub>2</sub> plane are summarized in Table 4.5, for different extents of water adsorption. For low surface hydrations (2.3 H<sub>2</sub>O/nm<sup>2</sup>), cyclohexanone can physisorb on a Ti-OH site or chemisorb on an existing free Ti site. Energy for physisorption is very weak, below -20 kJ/mol, but the chemisorption energy is considerably high (-78.8 kJ/mol). The (001) plane at low hydration level contains free Ti active sites, so chemisorption will be the preferred configuration. However such low hydration levels are not expected, as demonstrated by <sup>1</sup>H-MAS-NMR (Figure 4.1). At higher hydration level (7.0 H<sub>2</sub>O/nm<sup>2</sup>) no free Ti sites are in the surface, and strong adsorption of water (-184.7 kJ/mol, Table 4.2) is favorable. At these conditions, H-bridging of cyclohexanone to adsorbed H<sub>2</sub>O molecules is the preferred configuration, but the adsorption enthalpy is very low (-12.4 kJ/mol).

**Table 4.5.** Energies (kJ/mol) of cyclohexanone physisorption and chemisorption on the (001)  $\text{TiO}_2$  plane at increasing surface hydration, and the corresponding configurations. The probability of each surface configuration is determined based on the Boltzmann distribution equation at 25°C. The preferred configuration at each hydration level is highlighted with a box.

Hydration	Physisorption	Chemisorption
2.3 $\text{H}_2\text{O}/\text{nm}^2$		
OH site	Ti-OH	Free Ti
Energy	-19.6 kJ/mol	-78.8 kJ/mol
Distribution	0.0%	100.0%
7.0 $\text{H}_2\text{O}/\text{nm}^2$		
OH site	Ads. $\text{H}_2\text{O}$	
Energy	-12.4 kJ/mol	
Distribution	100.0%	

#### 4.4.4. ATR-FTIR vs. DFT calculations

The wavenumbers of the vibrations calculated by DFT are usually overestimated, so in order to compare with experimental IR spectra, it is common practice to apply a ‘scaling factor’. In Table 4.6, the scaling factors applied for the calculated carbonyl vibrations for each surface plane, are presented.

**Table 4.6.** Scaling factor determined by the ratio between the experimentally observed free carbonyl vibration (1722 cm<sup>-1</sup>) and the carbonyl vibration of an isolated cyclohexanone molecule calculated by DFT, for each unit cell.

	Frequency (cm <sup>-1</sup> )	Scaling Factor
(100)	1738	0.990
(101)	1728	0.997
(001)	1746	0.986

In Figure 4.3, the calculated spectra of the preferred adsorbed cyclohexanone configurations on the (100) plane with different surface hydrations, are compared with the spectra of cyclohexanone adsorbed on TiO<sub>2</sub>, as measured by ATR-FTIR spectroscopy. The spectra calculated for cyclohexanone physisorption, show carbonyl vibrations in the region of the experimentally observed vibration at 1681 cm<sup>-1</sup>. The redshift of the peaks is not proportional to the adsorption strength. The calculated spectra of physisorbed cyclohexanone on TiO<sub>2</sub> (100) with 9.3 H<sub>2</sub>O molecules per nm<sup>2</sup> matches best the experimental IR adsorption spectrum. This absorption occurring at higher wavenumbers (1685 cm<sup>-1</sup>), showed the strongest adsorption enthalpy, -89.4 kJ/mol. Cyclohexanone physisorption on (100) plane with low and high hydration level, occur redshifted in regard to the peaks of the experimental reference. The calculated spectra of chemisorbed cyclohexanone on (100) plane with low and intermediate hydration level occur at 1682 and 1591cm<sup>-1</sup> respectively, but are not shown due to the low probability of these configurations.

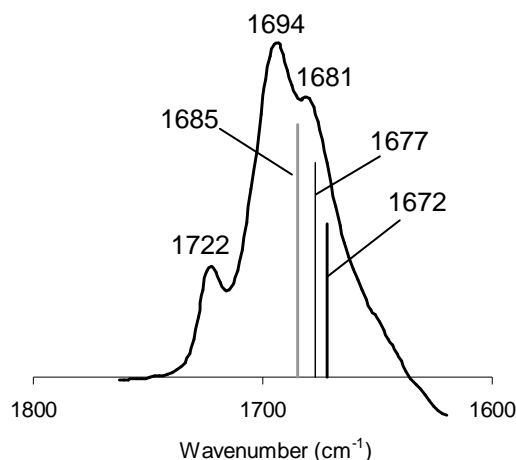


**Figure 4.3.** Adsorbed cyclohexanone reference spectrum, measured by ATR-FTIR spectroscopy (thick black spectrum), and the spectra of cyclohexanone physisorbed on a (100)  $\text{TiO}_2$  with 6.2  $\text{H}_2\text{O}$  molecules/ $\text{nm}^2$  (thick black line), with 9.3  $\text{H}_2\text{O}$  molecules/ $\text{nm}^2$  (thick grey line) and with 18.5  $\text{H}_2\text{O}$  molecules/ $\text{nm}^2$  (thin black line), as determined by DFT calculations.

The spectra of the most stable configurations of cyclohexanone adsorption on (101)  $\text{TiO}_2$ , for each hydration level are represented in Figure 4.4. The calculated carbonyl vibrations for cyclohexanone physisorption on low and intermediate hydration levels are centered at 1690 and 1679  $\text{cm}^{-1}$ , which gives a good correlation to experimentally observed peaks (1694 and 1681  $\text{cm}^{-1}$ ). The band of cyclohexanone physisorption on (101) with 16.8  $\text{H}_2\text{O}$  molecules/ $\text{nm}^2$  hydration level, absorbs at lower wavenumbers (1672  $\text{cm}^{-1}$ ) and does not describe the experimental spectra. Cyclohexanone chemisorption on (101) plane with low and intermediated hydration levels show absorption bands at 1679 and 1672  $\text{cm}^{-1}$ , respectively, but this kind of configuration is not expected to occur on the surface due to their low probability.

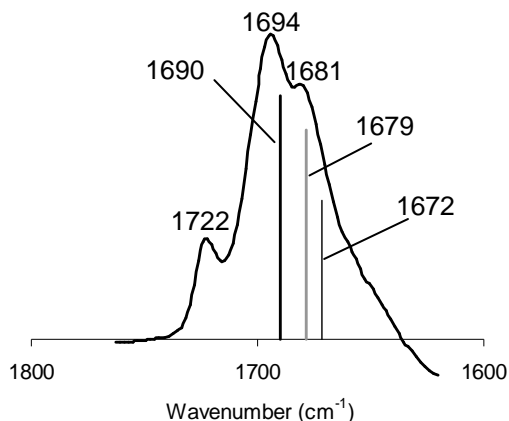


**Figure 4.4.** Comparison between an adsorbed cyclohexanone reference spectrum, measured by ATR-FTIR spectroscopy (thick black spectrum), and the spectra of cyclohexanone physisorbed on a (101) TiO<sub>2</sub> with 4.8 H<sub>2</sub>O molecules/nm<sup>2</sup> (thick black line), with 9.6 H<sub>2</sub>O molecules/nm<sup>2</sup> (thick grey line) and with 16.8 H<sub>2</sub>O molecules/nm<sup>2</sup> (thin black line), as determined by DFT calculations.

The calculated spectra of cyclohexanone physisorption on (001) TiO<sub>2</sub>, show carbonyl vibrations centered at 1698 and 1682 cm<sup>-1</sup>. The former band, of cyclohexanone physisorption on (001) plane with 7.0 H<sub>2</sub>O molecules/nm<sup>2</sup>, is blue shifted in respect to the experimental spectra. Though the band at 1682 cm<sup>-1</sup> occurs in the region of the experimental spectra, the adsorption enthalpies are too low (-19.6 kJ/mol) to consider this plane. Cyclohexanone chemisorption on (001) plane with 2.3 H<sub>2</sub>O molecules/nm<sup>2</sup> also absorbs at 1682 cm<sup>-1</sup>, but given the high chemisorption energy of water on the (001) surface (-184.7 kJ/mol), the presence of free Ti sites is unlikely and so is this configuration of cyclohexanone chemisorption.

## 4.5. DISCUSSION

### 4.5.1. Structure and level of hydration of the $\text{TiO}_2$ surface

Before discussing the conformational modes of adsorbed cyclohexanone, we will first address the selection of the surface planes that were taken into consideration. TEM imaging showed that the most common crystalline plane of the anatase catalyst under study (Hombikat UV100) is the (101) plane. However, TEM should be considered as a bulk technique and other less abundant crystal planes may not be clearly resolved. Based on literature data, the planes (100) and (001) were therefore also considered in the DFT calculations. Besides the nature of the surface exposed planes, also the respective degree of hydration of these planes is important in determining the interaction with cyclohexanone. The  $^1\text{H}$ -MAS-NMR study (Figure 4.2) suggests that the catalyst representative for photo-catalytic conversion of cyclohexane contains rigid water molecules on the surface. These can be assigned to physisorbed  $\text{H}_2\text{O}$  or isolated  $\text{Ti-H}_2\text{O}$  sites. Three levels of hydration were therefore taken into consideration in the DFT calculations, i.e. in the ranges of 2-6, 7-10, and 16-18  $\text{H}_2\text{O}$  molecules per  $\text{nm}^2$ , the exact value depending on the respective exposed crystal plane.

When evaluating subsequently by DFT the modes of interaction of cyclohexanone with the hydrated surfaces, several sites were taken into consideration (depending on the exposed surface planes these can range from acid to basic sites), of which usually one is highly preferred. This is further discussed in the following.

### 4.5.2. Spectral interpretation

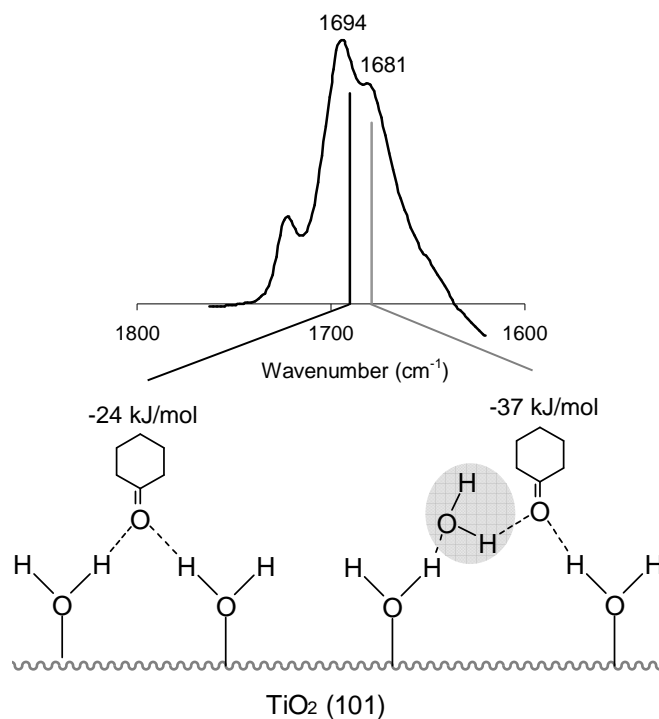
In scheme 4.1 the spectrum of cyclohexanone adsorbed on  $\text{TiO}_2$  is again shown. The presence of two bands assigned to adsorbed cyclohexanone (at 1694 and 1681  $\text{cm}^{-1}$ ) can originate from different phenomena. First, cyclohexanone might be chemisorbed in certain surface sites, and physisorbed in other surface sites of the same crystal plane. A very important conclusion is that the DFT calculations show that chemisorption of water on all evaluated Ti-sites is much more favorable than chemisorption of cyclohexanone. Therefore cyclohexanone chemisorption can be discarded, as well as this explanation for the presence of two IR bands of adsorbed cyclohexanone. Another possibility to



explain the presence of two absorption bands is that physisorption occurs on two different sites. As stated previously the strengths of cyclohexanone physisorption on different available active sites (of similar level of hydration) showed a strong preference towards a specific site with a probability of practically 100%, so also this explanation is not very likely. This leaves two additional explanations for two modes of cyclohexanone adsorption, i.e. i) the adsorption on different exposed planes, or ii) adsorption on the same plane, which consists of separate areas of different levels of hydration. The first option is not very likely, since the TiO<sub>2</sub> (001) plane interacting with physisorbed cyclohexanone yields very low enthalpies (10-20 kJ/mol, Table 4.5), which does not agree with the long desorption times observed experimentally [23,25]. So this plane, if present in the commercial TiO<sub>2</sub> surface, should hardly contribute to the experimentally observed spectra. The best correlation found for the experimentally observed spectra and the calculated values is obtained for the same plane, i.e. the (101) plane, taking into account two local levels of hydration. Although the hydration level is expected to be constant considering the TiO<sub>2</sub> surface globally, the local presence or absence of homogeneously spread physisorbed water, induce the two observed cyclohexanone configurations, as shown in Scheme 4.1. The calculated bands are within 4 cm<sup>-1</sup> of the experimental bands, which is a reasonable error for DFT. Cyclohexanone adsorption on a Ti-H<sub>2</sub>O active site is of lowest enthalpy (-23.5 kJ/mol), and also of lowest infrared redshift (1694 cm<sup>-1</sup>). When the TiO<sub>2</sub> hydration level is slightly higher, the adsorption of cyclohexanone on a Ti-H<sub>2</sub>O site is stabilized by a neighboring adsorbed H<sub>2</sub>O molecule inducing a higher adsorption enthalpy (-37.0 kJ/mol) and consequently a larger IR redshift (1681 cm<sup>-1</sup>). The latest configuration is preferred, but is limited by the presence of adsorbed H<sub>2</sub>O molecules. So, it can also be concluded that TiO<sub>2</sub> at experimental conditions exhibits a hydration level between 6 and 9 H<sub>2</sub>O/nm<sup>2</sup>, and the free sites available on the surface are probably Ti-H<sub>2</sub>O sites.

In previous work the desorption kinetics of photo-catalytically formed cyclohexanone was studied [25]. Besides reversible adsorption of cyclohexanone, also irreversibly adsorbed cyclohexanone was observed. This is not easy to explain based on the DFT data presented here. Irreversible cyclohexanone adsorption cannot be explained by chemisorption, which is not favorable in the presence of surface hydrated sites. At the same time, even though this surface plane is not experimentally observed, the (100) plane shows very strong physisorption energies of cyclohexanone (Table 4.3),

especially at hydration levels of 9 H<sub>2</sub>O molecules per nm<sup>2</sup> (-89.4 kJ/mol). Furthermore this mode of adsorption would lead to an absorption band 1685 cm<sup>-1</sup>, which is observed experimentally. Unfortunately, irreversibly adsorbed cyclohexanone also induces an absorption band at 1694 cm<sup>-1</sup>, which at present is not completely understood. Other effects may be influencing adsorption modes of cyclohexanone, like the existence of surface defects, common in TiO<sub>2</sub> catalysts or an increased surface hydrophilicity caused by UV illumination [27,28]. However, consideration of these phenomena would require additional advanced DFT calculations. We can conclude based on the presented results, that in order to improve cyclohexanone desorption during cyclohexane photo-oxidation, the TiO<sub>2</sub> catalyst should present preferentially the (101) exposed plane, and a low concentration of surface defects.



**Scheme 4.1.** Spectral interpretation of weak cyclohexanone adsorption on (101) TiO<sub>2</sub> plane with different local hydration.

## 4.6. CONCLUSIONS

To understand the IR features of cyclohexanone adsorption on anatase TiO<sub>2</sub>, different DFT calculations were made, namely related to physisorption and chemisorption of cyclohexanone on different adsorption sites of (100), (101) and (001) TiO<sub>2</sub> surfaces, with different levels of surface hydration. A good correlation was found between the adsorbed cyclohexanone infrared spectra, obtained by ATR-FTIR spectroscopy, and cyclohexanone physisorption configurations on the (101) surface with low and intermediate hydration levels. The adsorption energies of these configurations are -23.5 kJ/mol and -37.0 kJ/mol, which account for 60% and 40% of the TiO<sub>2</sub> surface, respectively. Stronger adsorption of cyclohexanone could to some extent be related to cyclohexanone physisorption on hydrated (100) planes with a calculated adsorption enthalpy of -89.4 kJ/mol. However, the influence of surface defects and surface sites modified by UV illumination, not considered in the present study, may also contribute to strong cyclohexanone adsorption.

## REFERENCES

- [1] J.M.Herrmann, *Top. Catal.* 34 (2005) 49.
- [2] A.R.Almeida, J.A.Moulijn, G.Mul, *J. Phys. Chem. C* 112 (2008) 1552.
- [3] S.Dzwigaj, C.Arrouvel, M.Breysse, C.Geantet, S.Inoue, H.Toulhoat, P.Raybaud, *J. Catal.* 236 (2005) 245.
- [4] C.B.Mendive, T.Bredow, A.Feldhoff, M.A.Blesa, D.Bahnmann, *Phys. Chem. Chem. Phys.* 11 (2009) 1794.
- [5] M.Lazzeri, A.Vittadini, A.Selloni, *Phys. Rev. B* 63 (2001) 155409.
- [6] A.Vittadini, M.Casarin, A.Selloni, *Theor. Chem. Acc.* 117 (2007) 663.
- [7] J.Soria, J.Sanz, I.Sobrados, J.M.Coronado, A.J.Maira, M.D.Hernandez-Alonso, F.Fresno, *J. Phys. Chem. C* 111 (2007) 10590.
- [8] A.Y.Nosaka, T.Fujiwara, H.Yagi, H.Akutsu, Y.Nosaka, *J. Phys. Chem. B* 108 (2004) 9121.

- [9] A.Vittadini, A.Selloni, F.P.Rotzinger, M.Gratzel, J. Phys. Chem. B 104 (2000) 1300.
- [10] P.Du, J.A.Moulijn, G.Mul, J. Catal. 238 (2006) 342.
- [11] G.Kresse, J.Hafner, Phys. Rev. B 48 (1993) 13115.
- [12] G.Kresse, J.Hafner, Phys. Rev. B 49 (1994) 14251.
- [13] J.P.Perdew, J.A.Chevary, S.H.Vosko, K.A.Jackson, M.R.Pederson, D.J.Singh, C.Fiolhais, Phys. Rev. B 46 (1992) 6671.
- [14] M.Calatayud, C.Minot, Surf. Sci. 552 (2004) 169.
- [15] C.Arrouvel, M.Digne, M.Breysse, H.Toulhoat, P.Raybaud, J. Catal. 222 (2004) 152.
- [16] P.E.Bloch, Phys. Rev. B 50 (1994) 17953.
- [17] F.Tielens, D.Costa, V.Humblot, C.M.Pradier, J. Phys. Chem. C 112 (2008) 182.
- [18] M.M.Islam, D.Costa, M.Calatayud, F.Tielens, J. Phys. Chem. C 113 (2009) 10740.
- [19] J.T.Carneiro, T.J.Savenije, J.A.Moulijn, G.Mul, J. Phys. Chem. C 114 (2010) 327.
- [20] A.Chemseddine, T.Moritz, Eur. J. Inorg. Chem. (1999) 235.
- [21] J.Soria, J.Sanz, I.Sobrados, J.M.Coronado, A.J.Maira, M.D.Hernandez-Alonso, F.Fresno, J. Phys. Chem. C 111 (2007) 10590.
- [22] A.Y.Nosaka, Y.Nosaka, Bull. Chem. Soc. Jpn. 78 (2005) 1595.
- [23] A.R.Almeida, J.T.Carneiro, J.A.Moulijn, G.Mul, J. Catal. 273 (2010) 116.
- [24] V.M.Mastikhin, I.L.Mudrakovsky, A.V.Nosov, Prog. Nucl. Magn. Reson. Spectrosc. 23 (1991) 259.
- [25] T.J.A.Renckens, A.R.Almeida, M.R.Damen, M.T.Kreutzer, G.Mul, Catal. Today 155 (2010) 302.
- [26] A.Vittadini, A.Selloni, F.P.Rotzinger, M.Gratzel, Phys. Rev. Lett. 81 (1998) 2954.
- [27] N.Sakai, A.Fujishima, T.Watanabe, K.Hashimoto, J. Phys. Chem. B 107 (2003) 1028.
- [28] A.Fujishima, X.T.Zhang, D.A.Tryk, Surf. Sci. Rep. 63 (2008) 515.

# Chapter 5

## Cyclohexane photo-catalytic oxidation over $\text{TiO}_2$ : a novel interpretation of temperature dependent performance

The rate of cyclohexane photo-catalytic oxidation to cyclohexanone over anatase  $\text{TiO}_2$  was studied at temperatures between 23 and 60°C by *in situ* ATR-FTIR spectroscopy, and the kinetic parameters were estimated using a microkinetic model. At low temperatures, surface cyclohexanone formation is limited by  $\text{H}_2\text{O}$  desorption, limiting cyclohexane adsorption, rather than previously assumed cyclohexanone desorption. Up to 50°C, the activation energy for photo-catalytic cyclohexanone formation is zero, while carboxylates are formed mainly by the direct oxidation of cyclohexane, with activation energy of  $18.4 \pm 3.3 \text{ kJ.mol}^{-1}$ . Above 50°C, significant (thermal) oxidation of cyclohexanone contributes to carboxylate formation. The irreversibly adsorbed carboxylates lead to deactivation of the catalyst, and are most likely the predominant cause of the non-Arrhenius behavior at relatively high reaction temperatures, rather than previously proposed cyclohexane adsorption limitations. The results imply that elevating the reaction temperature of photo-catalytic cyclohexane oxidation reduces selectivity, and is not a means to suppress catalyst deactivation.

This chapter is based on the following publication: A.R.Almeida, R.Berger, J.A.Moulijn, G.Mul (2010) submitted.

## 5.1. INTRODUCTION

The photo-catalytic oxidation of cyclohexane to cyclohexanone over  $\text{TiO}_2$  catalysts is a potential substitute for the commercially applied, but intrinsically inefficient cyclohexane oxidation process [1].  $\text{TiO}_2$  catalysts show a high selectivity towards the formation of cyclohexanone [2], but are also known to suffer from deactivation due to formation of strongly adsorbed carboxylate species [3-5]. Previously, we have analyzed the  $\text{TiO}_2$  surface by *in situ* techniques, and we proposed that slow desorption of cyclohexanone induces the formation of these deactivating species at room temperature [6].

Few studies have analyzed the effect of elevated temperature on the behavior of the photo-catalyst, which might be a means to stimulate cyclohexanone desorption, and thus prevent extensive over-oxidation to carboxylates and the accompanying deactivation. Herrmann et al. [7,8] concluded that the reaction was not limited by adsorption or desorption steps in the temperature interval of 23-55°C, where the activation energy was estimated at 10.5 kJ/mol. Product desorption and reactant adsorption were proposed to be limiting reaction rates at lower (< 23°C) and higher temperatures (>55°C), respectively. Unfortunately, their kinetic study was based on the analysis of bulk concentrations only, not considering details of surface chemistry and catalyst deactivation.

In this work, a diamond ATR-FTIR cell was used to run photo-catalytic cyclohexane oxidation at different temperatures, and to evaluate if enhancing temperature is a means to prevent carboxylate accumulation and catalyst deactivation. Furthermore, the activation energy of cyclohexanone formation and the desorption energy of cyclohexanone from the anatase  $\text{TiO}_2$  surface were evaluated on the basis of the data and a microkinetic model. This has led to a novel interpretation of the temperature dependent performance of  $\text{TiO}_2$  in cyclohexane photo-oxidation, which will be extensively discussed.

## 5.2. EXPERIMENTAL METHODS

A Specac Golden Gate ATR accessory with a diamond internal reflection element (IRE) was coupled to a Thermo Nicolet 8700 spectrometer. The diamond IRE has a 2x2 mm surface and exhibits three internal infrared reflections. The top plate of the Golden Gate ATR accessory can be heated and the temperature in the cell was measured by a thermocouple. The home-made ATR cell has a diameter of 1.2 cm, a height of 1 cm, and is sealed by a quartz window on top, which allows for UV-illumination. An extra pyrex window was placed over the quartz window in order to cut off low wavelengths ( $\lambda < 275$  nm), emitted by the UV source [2].

The photo-catalyst used was Hombikat UV100 TiO<sub>2</sub> (Sachtleben) of 100% anatase crystallinity. After drying the TiO<sub>2</sub> catalyst for 1 h at 120°C, a suspension of 2.7 mg/mL of TiO<sub>2</sub> in distilled water was prepared and sonicated for 30 min. The catalyst coating on the diamond ATR crystal was prepared by placing a 5  $\mu$ L droplet of the suspension on the crystal, followed by evacuation of the cell with an 82 mbar membrane pump, while slowly elevating the temperature to 40°C. The same procedure was repeated two more times, until a coating of TiO<sub>2</sub> covering the complete surface of the crystal was obtained. The coating was dried and evacuated at 120°C for 30 min and cooled down to the required temperature for the respective experiments. The experiments were run at 23, 30, 40, 50, 55 and 60°C. After each experiment the catalyst was removed from the Diamond crystal and a new TiO<sub>2</sub> coating was prepared. The photo-catalytic tests were performed with cyclohexane of 99.0% purity from Sigma Aldrich, dried over Molsieve (type 4A) overnight to remove traces of water. The cyclohexane was saturated with O<sub>2</sub> by bubbling dry air at 7.65 mL/min flow, and introduced in the ATR cell with a syringe filling almost the entire inner volume of the cell.

For the analysis a TRS N<sub>2</sub>-cooled detector was used applying a rapid scan mode at 8.8617 cm/s. The first step of the experiment consisted of recording 500 scans (1.2 min) in the dark followed by 850 scans (2 min) under illumination, and measurements in the dark for 20 min. The initial 500 scans in the dark were used to calculate the background spectrum, while spectra measured during illumination and in subsequent dark conditions were obtained by averaging 25 scans. These spectra represent a time interval of 3.5 seconds. A 150 W Xe illumination source was shielded by a Uniblitz Shutter (with a VCM-D1 controller), equipped with a diaphragm which opens or closes in

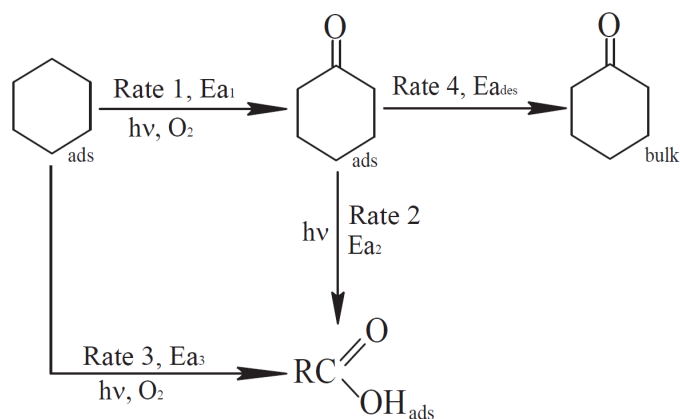
synchronization with the infrared measurement. The synchronization between the spectrometer and the shutter was achieved by a home-made Labview method.

A deconvolution method of the Omnic 7.3 software from Thermo Scientific was applied for all spectra between 4000-3010  $\text{cm}^{-1}$  and between 1880-1475  $\text{cm}^{-1}$ , with a fixed number of IR bands, for the integration of the spectral contributions of water, cyclohexanone and carboxylate, respectively.

### 5.3. THEORETICAL METHODS

A microkinetic model describing the kinetics of cyclohexane photo-oxidation was developed, and, together with a simple batch reactor model, implemented in the software package Athena Visual Studio. The diffusion time of cyclohexanone over 2  $\mu\text{m}$ , which is the penetration depth of the infrared radiation, considering a diffusion coefficient in the order of  $10^{-9} \text{ m}^2/\text{s}$ , was estimated to be a few milliseconds. Therefore all diffusion and mass transfer limitations can be neglected. The microkinetic model was developed based on the reaction mechanism of cyclohexane photo-oxidation proposed previously [6], which is presented in Scheme 5.1. The scheme contains cyclohexane photo-oxidation to cyclohexanone, and the consecutive paths of cyclohexanone desorption. The formation of strongly adsorbed carboxylate species is included as a consecutive oxidation of adsorbed cyclohexanone, as well as via a direct route from cyclohexane. While carbonates have also often been observed as a surface adsorbed species during photo-catalytic cyclohexane oxidation, we have not taken this into consideration because of the relatively small contribution of these species in the limited time of exposure to light. For simplicity and due to lack of spectroscopic evidence, intermediates for cyclohexanone formation were not considered in the model.





**Scheme 5.1.** Applied simplified reaction mechanism of the cyclohexane photo-oxidation.

Table 5.1 shows the reaction steps and the corresponding rate equations considered in the microkinetic model together with the continuity equations required for the reactor simulation and fitting of the experimental data. The rate of the cyclohexanone formation is described by a kinetic equation with a reaction constant  $k_1$ , the occupancy of cyclohexane on the surface ( $\theta_{\text{Cyh}}$ ) and the oxygen concentration  $[\text{O}_2]$ . Due to the low conversion, up to only about 0.6%, the oxygen concentration was assumed to be invariable and for simplicity the reaction order with respect to oxygen was set at unity. Since the time for desorption of cyclohexanone in dark conditions is known to be in the order of minutes [9,10], the cyclohexanone desorption rate was considered to be limiting, as shown in Table 5.1 by reaction 4. The net forward rate of reaction 4 equals the rate of cyclohexanone desorption minus the rate of cyclohexanone adsorption, and is a function of the cyclohexanone desorption constant,  $k_4$ , the cyclohexanone surface occupation,  $\theta_{\text{CyhO}}$ , the cyclohexanone Langmuir constant,  $K_{\text{CyhO}}$ , the cyclohexanone concentration in the bulk,  $C_{\text{CyhO}}$ , and the fraction of free sites,  $\theta^*$ . While still adsorbed, cyclohexanone can be further oxidized, especially in the presence of  $\cdot\text{OH}$  radicals (Reaction 2). This reaction results in a variety of products that have been identified by *in situ* ATR-FTIR spectroscopy as carboxylate species. For simplicity it is assumed that only the simplest carboxylate molecule ( $\text{C}_6\text{H}_{11}\text{O}_2$ ) is formed, which is irreversibly adsorbed on one active  $\text{TiO}_2$  site. Reaction 2 is described by its reaction constant,  $k_2$ , and the surface occupation with cyclohexanone,  $\theta_{\text{CyhO}}$ . Reaction 3 describes an

alternative path of carboxylate formation, which is the direct oxidation of adsorbed cyclohexane in the presence of  $O_2$  and  $\cdot OH$  radicals.

The temperature dependency of the reaction rate constants is described using a modified Arrhenius expression  $k_{i,T} = k_{i,T_{ref}} \exp\left\{\frac{-E_{a,i}}{R}\left(\frac{1}{T} - \frac{1}{T_{ref}}\right)\right\}$  [11], which avoids a strong correlation between the rate constants and the activation energies. In this equation,  $k_{i,T_{ref}}$  is the rate constant of any of the four reactions at the reference temperature,  $T_{ref}$  and  $E_{a,i}$  is the corresponding apparent activation energy of the reaction. The reference temperature  $T_{ref}$  is 296 K.

The total number of active sites ( $N_T$ ) was determined by  $NH_3$ -TPD [2] to be  $4.9 \times 10^{-8}$  mol per mass of catalyst used, and it is assumed that this number is constant. During the photo-catalytic oxidation the  $TiO_2$  catalyst is occupied by different products, as described in the site balance. The adsorption of cyclohexane and  $H_2O$  are assumed to be at equilibrium at all times. The initially adsorbed  $H_2O$  molecules are considered as spectators, occupying  $TiO_2$  active sites and reducing the surface occupation with cyclohexane.

The adsorption equilibria of cyclohexane and  $H_2O$  are assumed to follow the Langmuir isotherm with the adsorption constants  $K_{Cyh}$  and  $K_{H_2O}$ , respectively. Since the adsorption entropy and enthalpy are assumed to be constant in the temperature range covered in the experiments, the temperature dependency of the adsorption constants is expressed using  $K_{i,T} = K_{i,T_{ref}} \exp\left\{\frac{-\Delta H_{ads,i}}{R}\left(\frac{1}{T} - \frac{1}{T_{ref}}\right)\right\}$ , with the reference temperature  $T_{ref}$  set at 296 K.

The consumption rate of the reactant and the formation rates of the products follow directly from the reaction rates considering the total number of active sites ( $N_T$ ) and a reactor volume ( $V_R$ ) of  $1.1 \times 10^{-6} m^3$ . In order to fit the IR experimental results, two calibration factors had to be incorporated in the model, to relate the cyclohexanone and  $H_2O$  concentrations to their IR peak areas ( $cm^{-1}$ ). Unfortunately, it is not possible to obtain these calibration factors by a direct measurement since the total amount adsorbed, expressed in moles, is always negligibly small compared to the amount in the bulk. Therefore these calibration factors had to be included in the model as fitting factors. The adsorbed band of hexanoic acid was compared to the adsorbed band of

cyclohexanone (not shown) and the first was around two times larger than the second, so the calibration factor of carboxylates was set at two times the value for the cyclohexanone. The temperature dependency of the oxygen solubility in cyclohexane [12,13], has been taken into account.

The 14 kinetic parameters, consisting of 4 rate constants, 4 activation energies, 3 adsorption constants, 3 adsorption enthalpies, and 2 calibration factors, were obtained by minimization of the sum of the squared differences between the experimental and the simulated responses. The adsorption enthalpies of cyclohexanone and H<sub>2</sub>O on TiO<sub>2</sub> were previously estimated by Density Functional Theory (DFT) calculations [14]. The adsorption enthalpy of cyclohexanone on a dry TiO<sub>2</sub> surface was estimated to be -24 kJ/mol, while on hydrated surfaces a value of -37 kJ/mol was calculated [14]. The adsorption energy of water on TiO<sub>2</sub> varied between -57 and -67 kJ/mol, depending on the extent of hydration [6,14-17]. Initial guesses for cyclohexanone and H<sub>2</sub>O adsorption on TiO<sub>2</sub> of -37 and -65 kJ/mol were included in the model and these values were not allowed to vary more than 20 kJ/mol from the initial guess. The following weighing factors in the microkinetic model were applied to compensate for the differences in the orders of magnitude of the infrared responses: adsorbed cyclohexanone (cm<sup>-1</sup>): 1.0; bulk cyclohexanone (cm<sup>-1</sup>): 0.005; carboxylates (cm<sup>-1</sup>): 0.3; and H<sub>2</sub>O (cm<sup>-1</sup>): 0.05.

In the investigation two alternative models were considered, one involving the adsorption of cyclohexanone being at equilibrium at all times, and another assuming that the <sup>•</sup>OH radical concentration is proportional to the water coverage instead of a constant value. Although both models showed an almost equally good fit, they were disregarded based on physical grounds and available knowledge in literature [9,10].

**Table 5.1.** Microkinetic model

Reactions	Equations
1)	rate 1 = $k_1 \theta_{\text{Cyh}} [\text{O}_2]^n$
$\text{Cyh}^* + \text{O}_2^- \xrightarrow{\cdot\text{OH}} \text{CyhO}^* + \text{H}_2\text{O}^*$	$k_1 = k_{1\_296} \exp\left(-E_{a1} \frac{1.0 \times 10^3}{8.314}\right) \left(\frac{1}{T} - \frac{1}{296}\right)$
2)	rate 2 = $k_2 \theta_{\text{CyhO}}$
$\text{CyhO}^* + \cdot\text{OH} \longrightarrow \text{C}_6\text{H}_{11}\text{O}_2^*$	$k_2 = k_{2\_296} \exp\left(-E_{a2} \frac{1.0 \times 10^3}{8.314}\right) \left(\frac{1}{T} - \frac{1}{296}\right)$
3)	rate 3 = $k_3 \theta_{\text{Cyh}} [\text{O}_2]^n$
$\text{Cyh}^* + \text{O}_2^- + \cdot\text{OH} \longrightarrow \text{C}_6\text{H}_{11}\text{O}_2^* + \text{H}_2\text{O}^*$	$k_3 = k_{3\_296} \exp\left(-E_{a3} \frac{1.0 \times 10^3}{8.314}\right) \left(\frac{1}{T} - \frac{1}{296}\right)$
4)	rate 4 = $k_4 \theta_{\text{CyhO}} - k_4 K_{\text{CyhO}} C_{\text{CyhO}} \theta^*$
$\text{CyhO}^* \rightarrow \text{CyhO} + ^*$	$k_4 = k_{4\_296} \exp\left(-E_{a4} \frac{1.0 \times 10^3}{8.314}\right) \left(\frac{1}{T} - \frac{1}{296}\right)$
Adsorption equilibria	
$\text{Cyh} + ^* \rightleftharpoons \text{Cyh}^*$	$K_{\text{Cyh}} = K_{\text{Cyh\_296}} \exp\left(-\Delta H_{\text{Cyh,ads}} \frac{1.0 \times 10^3}{8.314}\right) \left(\frac{1}{T} - \frac{1}{296}\right)$ with $K_{\text{Cyh}} = \frac{\theta_{\text{Cyh}}}{[\text{Cyh}] \theta^*}$
$\text{H}_2\text{O}^* \rightleftharpoons \text{H}_2\text{O} + ^*$	$K_{\text{H}_2\text{O}} = K_{\text{H}_2\text{O\_296}} \exp\left(-\Delta H_{\text{H}_2\text{O,ads}} \frac{1.0 \times 10^3}{8.314}\right) \left(\frac{1}{T} - \frac{1}{296}\right)$ With $K_{\text{H}_2\text{O}} = \frac{\theta_{\text{H}_2\text{O}}}{[\text{H}_2\text{O}] \theta^*}$
Site balance	$1 = \theta^* + \theta_{\text{Cyh}} + \theta_{\text{CyhO}} + \theta_{\text{H}_2\text{O}} + \theta_{\text{Carbox}}$
Rates of product formation ( $\text{mol.m}^{-3}.\text{s}^{-1}$ )	Rate (Cyh) = $(-\text{rate1} - \text{rate3}) * N_T / V_R$ Rate (CyhO) = $(\text{rate1} - \text{rate2}) * N_T / V_R$ Rate ( $\text{H}_2\text{O}$ ) = $(\text{rate1} + \text{rate3}) * N_T / V_R$
Rate of formation of carboxylates species ( $\text{s}^{-1}$ )	rate (Carbox) = $\text{rate 2} + \text{rate3}$

## Notation

$k_1$ ( $\text{m}^3 \cdot \text{mol}^{-1} \cdot \text{s}^{-1}$ ), $k_2$ ( $\text{s}^{-1}$ ), $k_3$ ( $\text{m}^3 \cdot \text{mol}^{-1} \cdot \text{s}^{-1}$ ), $k_4$ ( $\text{s}^{-1}$ )	Rate constants of reaction 1, 2, 3 and 4
$k_{1\_296}$ ( $\text{m}^3 \cdot \text{mol}^{-1} \cdot \text{s}^{-1}$ ), $k_{2\_296}$ ( $\text{s}^{-1}$ ), $k_{3\_296}$ ( $\text{m}^3 \cdot \text{mol}^{-1} \cdot \text{s}^{-1}$ ) and $k_{4\_296}$ ( $\text{s}^{-1}$ )	Rate constants of reaction 1, 2, 3 and 4 at $T_{\text{ref}} = 296 \text{ K}$
$k_T$ ( $\text{m}^3 \cdot \text{mol}^{-1} \cdot \text{s}^{-1}$ )	Rate constants of reaction 1 at each temperature
$[\text{O}_2]$ ( $\text{mol} \cdot \text{m}^{-3}$ )	Oxygen concentration
$n$	Order of reaction 1 and 3 in oxygen concentration
$N_T$ (mol)	Total number of active sites (in the reactor)
$V_R$ ( $\text{m}^3$ )	Reactor volume
$\theta_{\text{Cyh}}$ , $\theta_{\text{CyhO}}$ , $\theta_{\text{H}_2\text{O}}$ , $\theta_{\text{Carbox}}$	Occupancy of the active sites with cyclohexane, cyclohexanone, carboxylates and water
$\theta^*$	Fraction of free active sites
$K_{\text{Cyh}}$ , $K_{\text{CyhO}}$ , $K_{\text{H}_2\text{O}}$ ( $\text{m}^3 \cdot \text{mol}^{-1}$ )	Adsorption constant of cyclohexane, cyclohexanone and water
$K_{\text{Cyh\_296}}$ , $K_{\text{CyhO\_296}}$ , $K_{\text{H}_2\text{O\_296}}$ ( $\text{m}^3 \cdot \text{mol}^{-1}$ )	Adsorption constant of cyclohexane, cyclohexanone and water at 296 K
$E_{a1}$ , $E_{a2}$ , $E_{a3}$ , $E_{a4}$ ( $\text{kJ} \cdot \text{mol}^{-1}$ )	Activation energy of reactions 1, 2, 3 and 4
$\Delta H_{\text{Cyh,ads}}$ , $\Delta H_{\text{CyhO,ads}}$ , $\Delta H_{\text{H}_2\text{O,ads}}$ ( $\text{kJ} \cdot \text{mol}^{-1}$ )	Adsorption enthalpy of cyclohexane, cyclohexanone and water
$k_{\text{Cyh,ads}}$ , $k_{\text{Cyh,des}}$ ( $\text{s}^{-1}$ )	Rate of cyclohexane adsorption and desorption
$k_{\text{H}_2\text{O,ads}}$ , $k_{\text{H}_2\text{O,des}}$ ( $\text{s}^{-1}$ )	Rate of water adsorption and desorption
$cf_{\text{CyhOads}}$ , $cf_{\text{H}_2\text{Oads}}$ ( $\text{m}^3 \cdot \text{mol}^{-1} \cdot \text{cm}^{-1}$ )	Coefficient that relates concentration with infrared peak area; for adsorbed cyclohexanone and water

## 5.4. RESULTS

The photo-catalytic reaction was performed at different temperatures, corresponding to different hydration levels of the  $\text{TiO}_2$  surface. This is illustrated in Figure 5.1(a). The broad band between  $3500$  and  $3000\text{ cm}^{-1}$  is characteristic of the OH stretching vibration of water adsorbed on the  $\text{TiO}_2$  surface. This water originates from the catalyst layer preparation, and the lab environment to which the layer was exposed before starting the experiment. The very large water band present at  $23^\circ\text{C}$  significantly decreases at higher temperatures. In Figure 5.1(b), the peak area of adsorbed  $\text{H}_2\text{O}$  is represented as a function of temperature, showing an exponential decrease with temperature. From  $23$  to  $40^\circ\text{C}$  a decrease of at least 60% in quantity of adsorbed water is observed, while above this temperature surface dehydration becomes less pronounced.

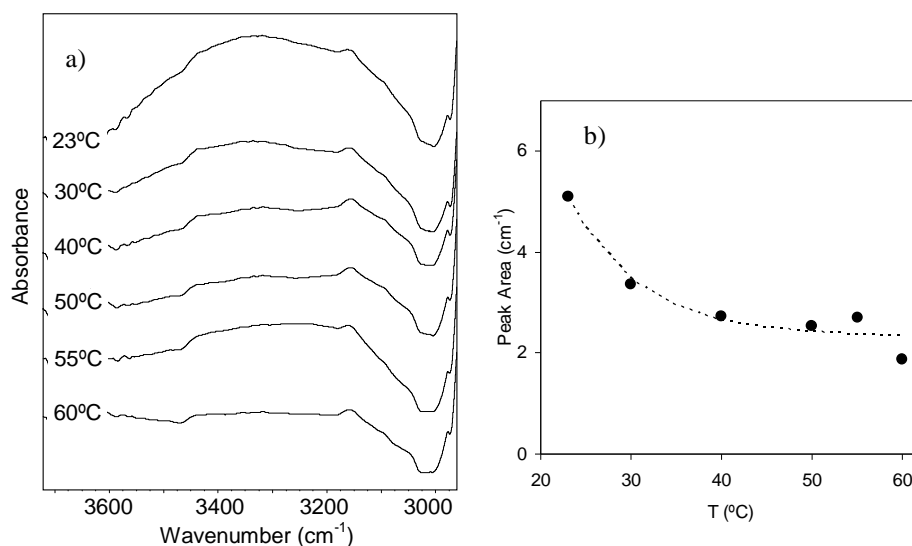


**Figure 5.1.** (a) Spectra of cyclohexane adsorbed on  $\text{TiO}_2$  at different temperatures, prior to the photo-catalytic reaction, at the region of the OH stretching vibration of adsorbed  $\text{H}_2\text{O}$  (Diamond ATR background). (b) Peak area of adsorbed  $\text{H}_2\text{O}$  as function of temperature, by integration between  $3590$  and  $3010\text{ cm}^{-1}$ .

#### 5.4.1. UV illumination conditions

At each temperature, cyclohexane photo-catalytic oxidation was performed for only two min with the purpose of analyzing the first steps of the reaction. In general, the first minutes of cyclohexane photo-oxidation at room temperature are characterized by the formation of cyclohexanone in parallel with adsorbed H<sub>2</sub>O, but also the formation of carboxylate species causing catalyst deactivation [6]. Figure 5.2 shows the spectrum and its deconvolution after 2 min of cyclohexane photo-oxidation at 23°C. In the higher frequency range (Figure 5.2a), a positive contribution of the OH stretching vibration of H<sub>2</sub>O with two characteristic bands can be seen. These peaks have been proposed to correspond to water adsorbed on the TiO<sub>2</sub> active sites (3238 cm<sup>-1</sup>) and to multilayer hydrogen-bonded water (3432 cm<sup>-1</sup>) [18]. A negative contribution for the OH stretching vibration of bridging active sites on TiO<sub>2</sub> is observed at 3642 cm<sup>-1</sup> [19]. This active site is of acidic character and occupies 77% of the TiO<sub>2</sub> catalyst, as determined by NH<sub>3</sub>-TPD and the Fe(acac)<sub>3</sub> titration method [2]. At the lower frequency range (Figure 5.2b), the contribution of the adsorbed reaction product cyclohexanone is visible by its carbonyl vibration at 1694 and 1682 cm<sup>-1</sup> [6]. DFT calculations on hydrated (101) TiO<sub>2</sub> surfaces showed that the former band corresponds to the direct adsorption of the carbonyl on TiO<sub>2</sub> adsorption sites, while the latter band is more redshifted because the cyclohexanone is also H-bridged to a neighboring adsorbed H<sub>2</sub>O molecule [14]. To improve the spectral deconvolution [10], the main contribution above 1700 cm<sup>-1</sup> was fitted with two peaks that are proposed to correspond to desorbed molecules of cyclohexanone under different environments. Water formation can be observed by its bending vibration at 1650 cm<sup>-1</sup>, which grows in parallel with the broad contribution between 3600-3000 cm<sup>-1</sup>. The contribution of the carboxylic acid vibrations is located at 1578 and 1523 cm<sup>-1</sup>. Table 5.2 resumes the bands used for spectral deconvolution with their applied assignments.

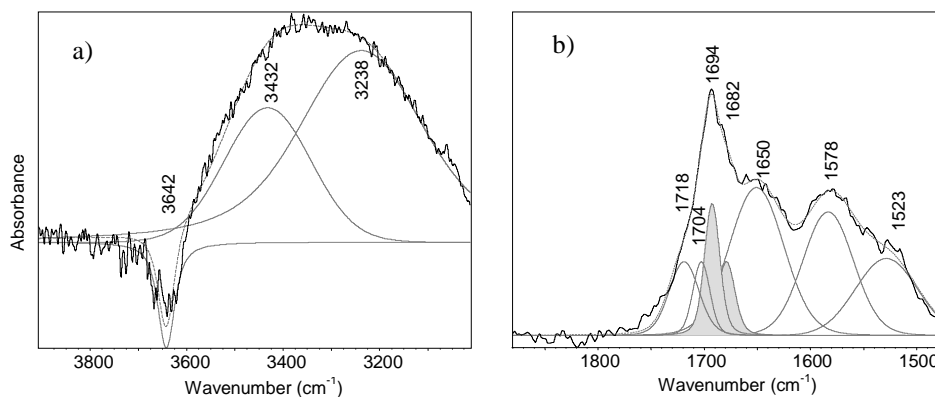


**Figure 5.2.** Spectral deconvolution after 2 min of cyclohexane photo-oxidation on  $\text{TiO}_2$  at  $23^\circ\text{C}$  in the a) high wavenumbers region and (b) low wavenumbers region. The black line represents the original spectra, the grey bands correspond to the deconvoluted peaks and the dashed grey line represents the sum of the deconvoluted peaks. The two grey-shaded peaks in (b) correspond to adsorbed cyclohexanone.

**Table 5.2.** Assignment of deconvolution peaks observed during cyclohexane photo-oxidation.

Peaks ( $\text{cm}^{-1}$ )	Vibration	Assignment [6,19-21]
3642	OH stretching	Bridging OH in $\text{TiO}_2$
3432, 3238	OH stretching	Adsorbed $\text{H}_2\text{O}$
1718, 1704	C=O stretching	Bulk cyclohexanone
1694, 1682	C=O stretching	Adsorbed cyclohexanone
1650	OH bending	Adsorbed water
1578, 1523	Asymmetric C=O stretching	Adsorbed carboxylates

The same deconvolution method was applied at all temperatures and the spectral results can be found in the Appendix. Figure 5.3 shows the trends and as expected, the conversion rate of cyclohexane into cyclohexanone increases with temperature up to  $50^\circ\text{C}$ . At  $55^\circ\text{C}$  only the contribution of adsorbed cyclohexanone decreases and at  $60^\circ\text{C}$ , a considerable decrease in both adsorbed and bulk cyclohexanone can be seen. The



experimental results also show that the formation rate of carboxylates increases with temperature, up to 50°C.

It appeared that only the experimental data in the temperature range 23-50°C could be fitted properly with a single microkinetic model. Above this temperature the production rate of cyclohexanone decreases much faster than the model predicts and therefore it is concluded that the reaction kinetics change significantly above 50°C. This is probably due to the onset of thermally induced reactions causing additional deactivation, as will be discussed later. An alternative explanation is total oxidation of cyclohexane into CO<sub>2</sub> and H<sub>2</sub>O. The experimental results obtained at 55°C and 60°C were therefore not used in the model.

Although most product formation profiles are well predicted by the microkinetic model, the carboxylate species show a significant deviation at 23°C and 30°C. At 23°C, the experimental data for formation of carboxylates shows a clear delay, not predicted by the microkinetic model, which indicates that carboxylates at low temperatures may be a product of a consecutive reaction. At 40 and 50°C this delay in carboxylate formation is not observed. The peak area of water includes the initial surface adsorbed water shown in Figure 5.1, and for higher temperatures it shows a slight decrease at longer UV-illumination times.

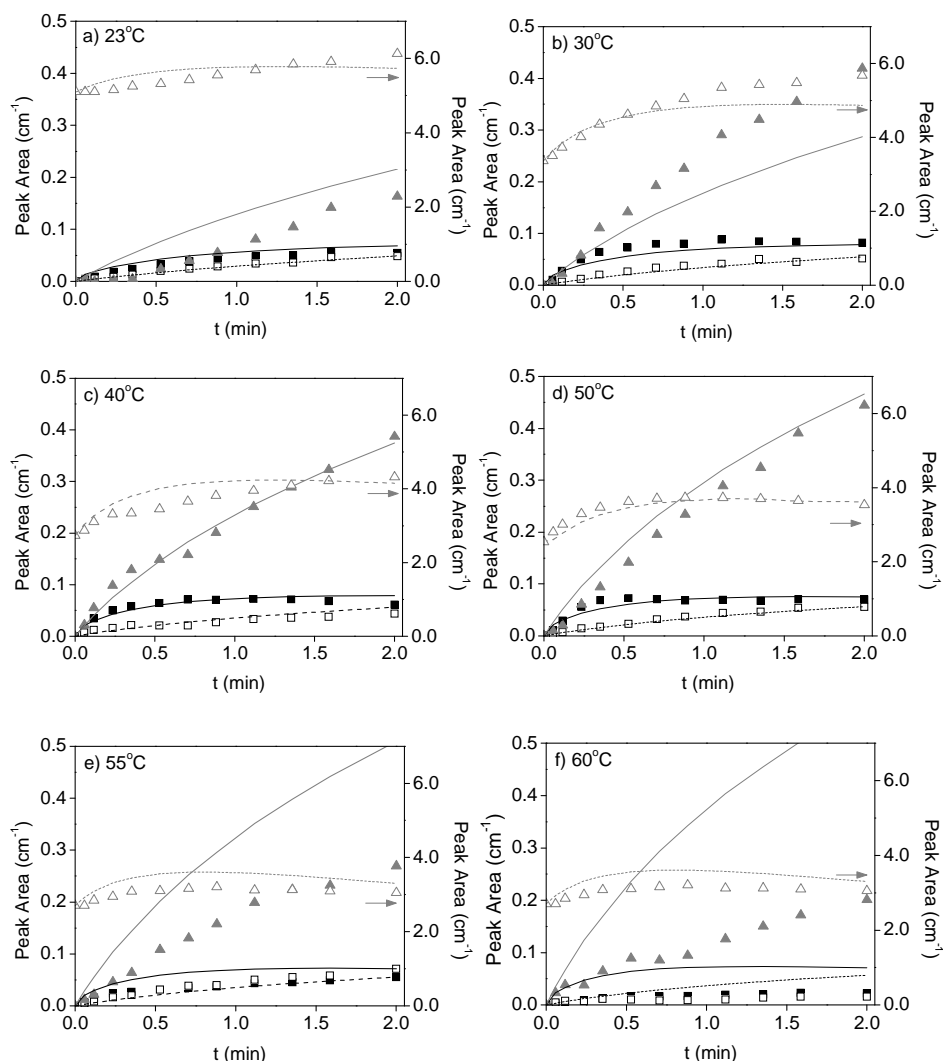


**Figure 5.3.** Product profiles and simulation results obtained with the fitted kinetic model for adsorbed cyclohexanone (solid squares: 1694 + 1682 cm<sup>-1</sup>; model fit: black curve), bulk cyclohexanone divided by 1000 (empty squares: 1718 + 1704 cm<sup>-1</sup>; model fit: black dashed curve), carboxylates (solid grey triangles: 1578 + 1523 cm<sup>-1</sup>; model fit: grey curve) and water (empty grey triangles: 3432, 3238 cm<sup>-1</sup>; model fit: grey dashed curve) formed during photo-oxidation in time at (a) 23°C, (b) 30°C, (c) 40°C, (d) 50°C, (e) 55°C and (f) 60°C. The right y-axis represents the peak area of water.

Table 5.3 resumes the kinetic parameters obtained from the parameter estimation using the microkinetic model for cyclohexane photo-oxidation. The obtained value of -36.9 kJ/mol for the adsorption energy of cyclohexanone,  $\Delta H_{\text{ads}_{\text{C}_{6}\text{H}_{10}\text{O}}}$ , is in excellent agreement with the adsorption energy on a hydrated (101) TiO<sub>2</sub> surface of -37 kJ/mol, estimated using DFT [14]. The model fit shows an adsorption enthalpy of H<sub>2</sub>O on TiO<sub>2</sub> of  $-47.1 \pm 3.2$  kJ/mol, which is smaller than the energy of water adsorption on the (101) crystal phase estimated from DFT calculations [14], ranging between -57 and -67 kJ/mol. Although the calculated adsorption enthalpy was lower than expected, the determined  $K_{\text{H}_2\text{O}_{296}}$  confirms the high hydrophilicity of the TiO<sub>2</sub> catalyst. The microkinetic model fit shows no thermal enhancement of the formation of adsorbed cyclohexanone ( $E_{a1} = 0$  kJ/mol). The rate constant of cyclohexanone formation ( $k_1$ ) is considerably higher than the rate constants of carboxylate formation ( $k_2$  and  $k_3$ ). Furthermore, according to the optimal fit, the contribution of the reaction of cyclohexanone to carboxylates is negligible (i.e.  $k_{2_{296}} = 0 \text{ s}^{-1}$ ). This is probably due to the very high cyclohexanone desorption rate calculated by the model. Contrary to what was presumed, under illumination cyclohexanone desorption is not rate limiting, confirmed by the 0 kJ/mol activation energy determined for cyclohexanone desorption. However this may not be true at 23°C since at that temperature carboxylate formation shows a clear delay, implying that at low temperatures, the oxidation of cyclohexanone to carboxylates seems to be an important deactivation step. Contrarily to cyclohexane photo-oxidation to cyclohexanone, the model fit shows that cyclohexane photo-oxidation to carboxylate species is thermally enhanced with apparent activation energy of  $18.4 \pm 3.3$  kJ/mol. The correlation matrix of the estimated microkinetic model parameters, calculated under UV illumination conditions, can be found in the Appendix. The quite high correlation coefficient between  $k_{1_{296}}$  and  $K_{\text{H}_2\text{O}_{296}}$  may have contributed to the relatively large uncertainty in the calculated  $K_{\text{H}_2\text{O}_{296}}$ . The parameter  $k_{4_{296}}$  is associated with an even larger uncertainty, which results from the low sensitivity of the model to this parameter.

**Table 5.3.** Kinetic parameters determined from the microkinetic model fitting to experimental data obtained during cyclohexane photo-oxidation.

Parameter	Prediction	95% confidence range	Units
$cf_{\text{CyhOads}}$	0.68	$\pm 0.04$	a. u.
$cf_{\text{H}_2\text{Oads}}$	1.29	$\pm 0.06$	a. u.
$K_{\text{Cyh}_{296}}$	0.31	$\pm 0.03$	$\text{m}^3.\text{mol}^{-1}$
$\Delta H_{\text{adsCyh}}$	-34.4	$\pm 3.7$	$\text{kJ}.\text{mol}^{-1}$
$K_{\text{CyhO}_{296}}$	$26.9^{1)}$	$\pm 2.6$	$\text{m}^3.\text{mol}^{-1}$
$\Delta H_{\text{adsCyhO}}$	-36.9	$\pm 3.9$	$\text{kJ}.\text{mol}^{-1}$
$K_{\text{H}_2\text{O}_{296}}$	766	$\pm 84$	$\text{m}^3.\text{mol}^{-1}$
$\Delta H_{\text{adsH}_2\text{O}}$	$-47.1^{1)}$	$\pm 3.2$	$\text{kJ}.\text{mol}^{-1}$
$k_{1_{296}}$	10.84	$\pm 0.25$	$\text{m}^3.\text{mol}^{-1}.\text{s}^{-1}$
$E_{a1}$	$0.00^{2)}$	--	$\text{kJ}.\text{mol}^{-1}$
$k_{2_{296}}$	$0.00^{2)}$	--	$\text{s}^{-1}$
$E_{a2}$	n.a. <sup>3)</sup>	--	$\text{kJ}.\text{mol}^{-1}$
$k_{3_{296}}$	$1.74 \times 10^{-3}$	$\pm 0.16 \times 10^{-3}$	$\text{m}^3.\text{mol}^{-1}.\text{s}^{-1}$
$E_{a3}$	18.4	$\pm 3.3$	$\text{kJ}.\text{mol}^{-1}$
$k_{4_{296}}$	1286	$\pm 878$	$\text{s}^{-1}$
$E_{a4}$	$0.00^{2)}$	--	$\text{kJ}.\text{mol}^{-1}$

<sup>1)</sup> Value limited within a narrow range around the value estimated from DFT calculations (see text).

<sup>2)</sup> Value limited by its lower boundary.

<sup>3)</sup> Not applicable: insignificant parameter.

The corresponding surface occupancies of cyclohexane, cyclohexanone, H<sub>2</sub>O and carboxylates obtained with the kinetic model are shown in Figure 5.4. As mentioned above, the kinetic model is only able to describe the results properly at temperatures up to 50°C, with the exception of the formation of carboxylates at 23 and 30°C, which shows some deviation. Above 50°C the model seems to overestimate the occupancies of cyclohexanone and carboxylates. At room temperature, half of the available adsorption

sites are occupied with adsorbed water. At increasing temperatures the water occupancy decreases whereas those of the other components increase. The enhanced product formation is most considerable for the carboxylates species, which is also due to its thermal activation ( $E_{a3} > 0$  kJ/mol). The fraction of free active sites is always very small, in the order of  $10^{-4}$ , although its fraction increases with temperature (not shown).

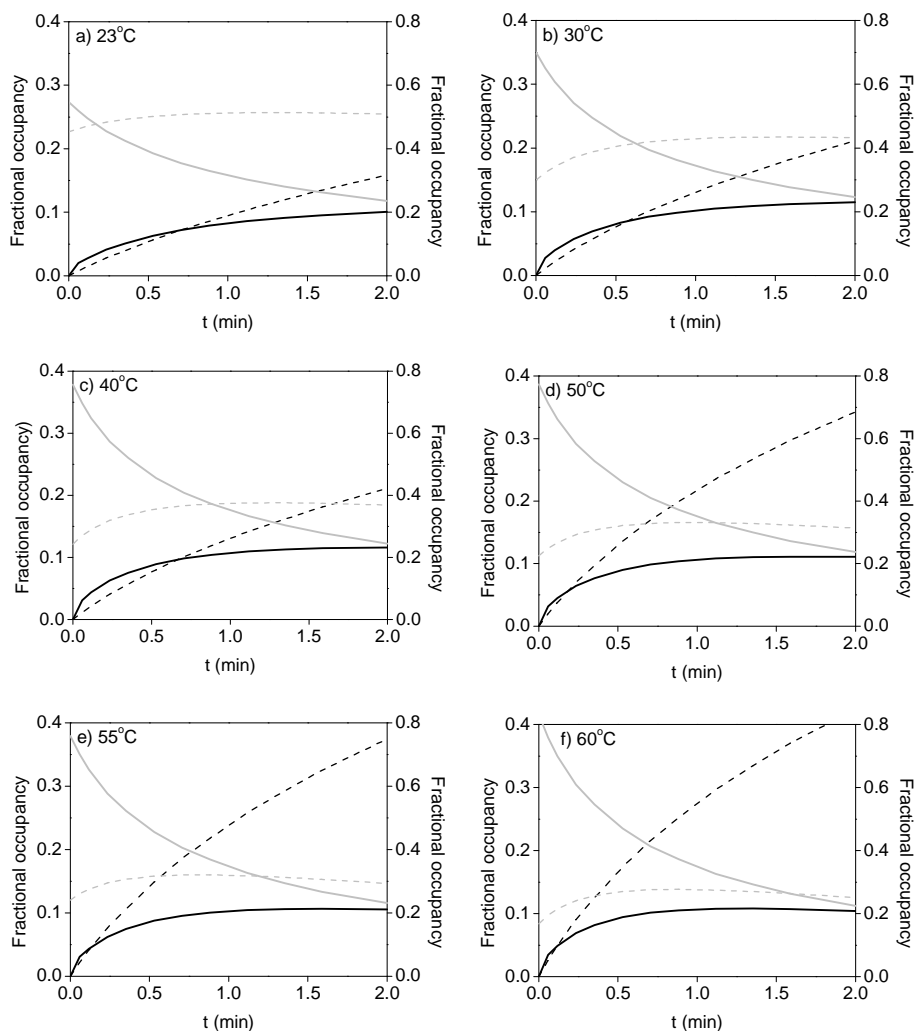


**Figure 5.4.** Surface occupation with cyclohexanone (black curve), carboxylates (black dashed curve), cyclohexane (grey curve), and water (grey dashed curve) as a function of time at (a) 23°C, (b) 30°C, (c) 40°C, (d) 50°C, (e) 55°C and (f) 60°C. The right y-axis represents the occupancy of cyclohexane and water.

Fitting the experimental data up to 50°C resulted in an apparent activation energy approaching zero for cyclohexanone formation. In order to get more insight whether this result is really acceptable, the parameter estimation has also been carried out separately at all temperatures. In these estimations the rate constants  $k_1$ ,  $k_2$ ,  $k_3$  and  $k_4$  were allowed to vary whereas the two calibration factors and the six parameters related to the adsorption constants were kept at the values presented in Table 5.3. The resulting rate constants of the formation of cyclohexanone at the different temperatures ( $k_T$ ) are plotted in an Arrhenius plot in Figure 5.5, with the straight line corresponding to the microkinetic model fit at all temperatures, i.e.  $E_a = 0$  kJ/mol. It appears that the individual results for the cyclohexanone formation constant also correspond, with a small experimental error, to zero activation energy up to 55°C. Above this temperature the rate decreases significantly, probably due to the onset of one or more reactions not accounted for in the kinetic model, such as the thermally activated oxidation of cyclohexanone to carboxylates, as will be discussed later.

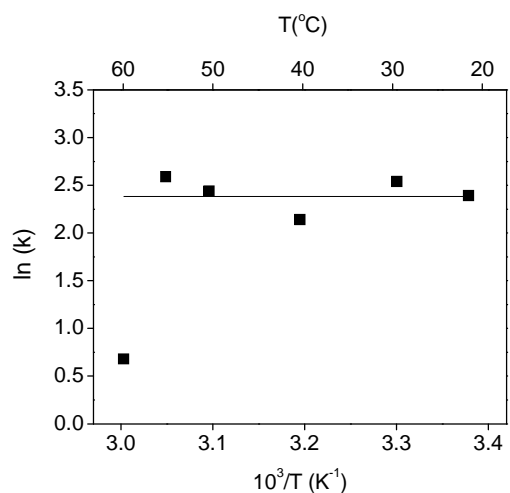


**Figure 5.5.** Arrhenius plot of the dependency of the constant of cyclohexanone formation with the inverse of reaction temperature. The horizontal line corresponds to the  $k_1$  (m<sup>3</sup>.mol<sup>-1</sup>.s<sup>-1</sup>) value in Table 5.3 and the squares correspond to the  $k_T$  (m<sup>3</sup>.mol<sup>-1</sup>.s<sup>-1</sup>) values, determined at a single temperature using the microkinetic model.

The selectivity of the cyclohexane photo-oxidation reaction to cyclohexanone, shown in Figure 5.6, is calculated dividing the rate of cyclohexanone formation by the sum of the rates of formation of cyclohexanone and carboxylates, which corresponds to  $k_1/(k_1 + k_3)$ . The values of the rate constants  $k_1$  and  $k_3$  were calculated using  $k_{1\_296}$ ,  $k_{3\_296}$ ,  $E_{a1}$ , and  $E_{a3}$  in Table 5.3, and the modified Arrhenius equation. The selectivity to the desired product is very high and slowly decreasing with temperature. The non-selective carboxylate product is very detrimental to performance, since it is strongly adsorbed causing irreversible deactivation. Figure 5.6 shows the selectivity at all temperatures however above 50°C the microkinetic model does not apply (Figure 5.3e and 5.3f). It is noted that the real selectivity to cyclohexanone is probably lower than calculated here since the cyclohexane photo-oxidation reaction on TiO<sub>2</sub> is known to produce up to 5% of cyclohexanol [22,23]. The small cyclohexanol contribution was not included in the microkinetic model since the amount cannot be estimated reliably due to a large overlap of its IR features with the other bands.

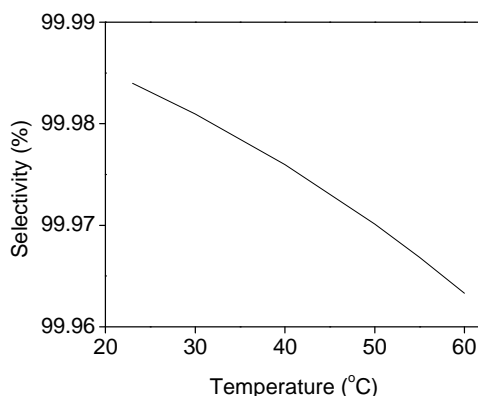


**Figure 5.6.** Selectivity of cyclohexane photo-oxidation to cyclohexanone, calculated by  $k_1/(k_1 + k_3)$ .

#### 5.4.2. Dark conditions

When the UV-illumination is turned off, the cyclohexanone formation stops and photon-independent phenomena, like desorption, can be isolated. The decrease of the adsorbed cyclohexanone peak under dark conditions was recorded and fitted using the

microkinetic model. The results are shown in Figure 5.7 for all temperatures studied and these show that the desorption of cyclohexanone in dark conditions is a slow process, in the order of minutes, in agreement with previous studies [9,10]. At higher temperatures the rate of desorption increases, but complete desorption was not reached up to 60°C. The results show that the relative concentration of irreversibly adsorbed cyclohexanone vs the initial concentration increases with reaction temperature.

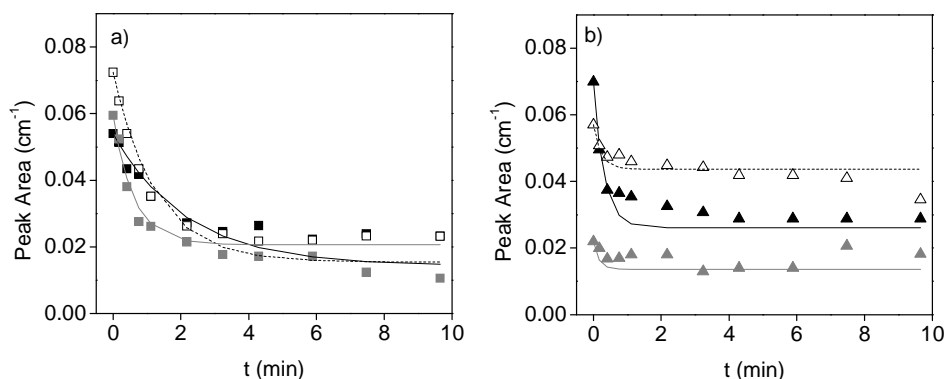


**Figure 5.7.** Desorption of cyclohexanone from the  $\text{TiO}_2$  catalyst in dark conditions at a) 23°C (black squares), 30°C (empty squares) and 40°C (grey squares); and b) 50°C (black triangles), 55°C (empty triangles) and 60°C (grey triangles). The curves are the fits obtained with the adapted parameters in Table 5.4.

The four kinetic parameters obtained for the microkinetic fitting under dark conditions are compared with the values obtained under UV illumination, in Table 5.4. The results show a very large value of  $K_{\text{CyhO}}$  ( $2663 \pm 210$ ) compared to the value found under UV illumination ( $26.9 \pm 2.6$ ). The large cyclohexanone adsorption constant calculated under dark conditions is affected by the significant extent of irreversible adsorption visible in Figure 5.7. The cyclohexanone adsorption constant under UV illumination suggests that this irreversible adsorption does not occur under UV light, which apparently causes a modification of the  $\text{TiO}_2$  surface [24]. The results also show that in dark conditions the activation energy for cyclohexanone desorption from the  $\text{TiO}_2$  surface amounts to  $58.5 \pm 5.3$  kJ/mol, while a value of zero was found under photo-catalytic conditions. Apparently the rate of desorption is much lower under dark



conditions than in the presence of UV light. It is therefore concluded that the adsorption characteristics of cyclohexanone on TiO<sub>2</sub> under UV illumination and dark conditions are not comparable; under UV illumination the cyclohexanone adsorption appears to be in equilibrium, whereas in dark conditions the cyclohexanone desorption is slow. The correlation matrix of the microkinetic model parameters, calculated under dark conditions, can be found in the Appendix. No strong dependency between any of the estimated parameters was found.

**Table 5.4.** Comparison between the kinetic parameters determined from the microkinetic model fitting to experimental data obtained under UV illumination and under dark conditions.

Parameter	UV illumination			Dark		
	Prediction	95% confidence range	Units	Prediction	95% confidence range	Units
$K_{\text{CyhO}_{296}}$	26.9	$\pm 2.6$	$\text{m}^3 \cdot \text{mol}^{-1}$	2663	$\pm 210$	$\text{m}^3 \cdot \text{mol}^{-1}$
$\Delta H_{\text{adsCyhO}}$	-36.9	$\pm 3.9$	$\text{kJ} \cdot \text{mol}^{-1}$	-14.7	$\pm 3.1$	$\text{kJ} \cdot \text{mol}^{-1}$
$k_{4_{296}}$	1286	$\pm 878$	$\text{s}^{-1}$	$7.27 \times 10^{-3}$	$\pm 0.68 \times 10^{-3}$	$\text{s}^{-1}$
$E_{a4}$	0.00	--	$\text{kJ} \cdot \text{mol}^{-1}$	58.5	$\pm 5.3$	$\text{kJ} \cdot \text{mol}^{-1}$

The development of the carboxylate peak area as a function of time at all temperatures studied is shown in Figure 5.8. Below 50°C the carboxylates peak grows under illumination, but starts to decrease when switching to dark conditions (Figure 5.8a). This decrease is relatively small and could therefore also be caused by inaccuracy in the deconvolution procedure. Above 50°C the carboxylates peak clearly continues growing after switching to dark conditions (Figure 5.8b), although the formation rates are lower than under illumination conditions. This shows that the formation of carboxylates occurs almost exclusively photo-catalytically below 50°C, but above 50°C both f-catalytically and thermally. Above 50°C, the increase of the carboxylate peaks is opposed by a decrease in the peaks of adsorbed cyclohexanone (compare Figures 5.8b and 5.7b). This suggests that a serial reaction scheme is operative: cyclohexanone is thermally oxidized to carboxylates.

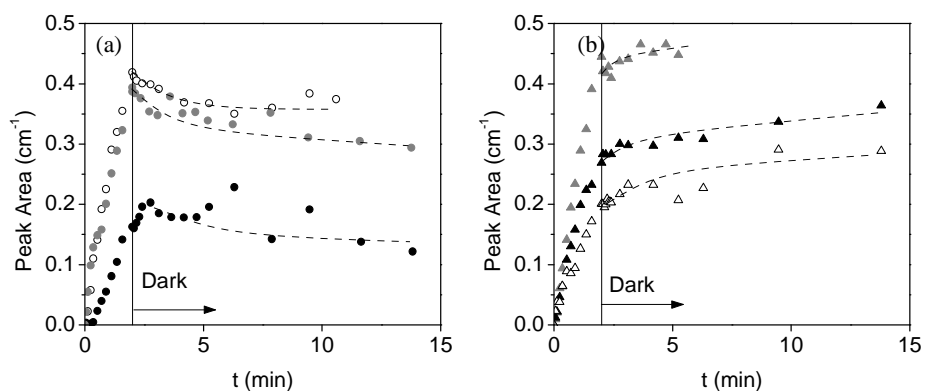


**Figure 5.8.** Profiles of adsorbed carboxylates ( $1578, 1523\text{ cm}^{-1}$ ) at a)  $23^{\circ}\text{C}$  (black dots),  $30^{\circ}\text{C}$  (empty dots),  $40^{\circ}\text{C}$  (grey dots) and b)  $50^{\circ}\text{C}$  (black triangles),  $55^{\circ}\text{C}$  (empty triangles) and  $60^{\circ}\text{C}$  (grey triangles). The first 2 min represent the illumination conditions and the remainder dark conditions. The curves were drawn to guide the eye.

## 5.5. DISCUSSION

### 5.5.1. Activation energy for cyclohexanone formation

Photo-catalytic reactions are activated by photon absorption, and an energy of 300-350 kJ/mol is required to initiate the process of electron-hole separation [25]. Nevertheless, the activation energy of a photo-catalytic reaction, like the selective oxidation of cyclohexane is expected to be small. From pulse radiolysis it was found that for the reaction of organic molecules with  $\cdot\text{OH}$  radicals the typical activation energy is in the range of 5-13 kJ/mol [26]; similarly, an activation energy for the formation of the superoxide anion was estimated as 11 kJ/mol [27].

It is striking that our study, based on activity measurements using ATR-FTIR analysis, provided an estimate of 0 kJ/mol for the apparent activation energy for the selective cyclohexane photo-oxidation to cyclohexanone (Table 5.3), implying that this reaction is not thermally activated. Hermann et al. estimated an apparent activation energy of 10.5 kJ/mol between  $23\text{--}55^{\circ}\text{C}$  for the same reaction [7]. While the apparent activation energy determined in our work is based on the formation rate constant of adsorbed cyclohexanone, previous studies only evaluated the formation rate of desorbed

cyclohexanone [7,8]. This may explain the difference in apparent activation energies found, since the latter is influenced by sorption effects. The *in situ* ATR-FTIR technique appeared very suitable for distinguishing these effects.

Herrmann et al. reported the highest activation energy (58 kJ/mol) at temperatures below 23°C [7,8], which was ascribed to cyclohexanone desorption limitations. Although we did not study the reactivity below 23°C, the results in Table 5.3 indicate that cyclohexanone desorption is not limiting under photo-catalytic conditions. Our data suggest that the high apparent activation energy reported by Herrmann et al. is related to a variation of the degree of surface adsorbed water. The results in Figure 5.1 clearly show that the number of adsorption sites available for cyclohexane adsorption is not constant but dependent on the extent of surface hydration. This is particularly significant at low temperatures, at 23°C more than 50% of the surface is occupied by adsorbed H<sub>2</sub>O, resulting in a lower quantity of adsorbed cyclohexanone (Figure 5.4a) and a lower product formation rate (Figure 5.3a). Below 23°C the effect of surface hydration is likely to be even stronger. Therefore at low temperatures the apparent activation energy of the cyclohexanone formation is more accurately predicted from:  $E_{app} = E_a + (1 - \theta_{Cyh})\Delta H_{Cyh} - \theta_{H_2O}\Delta H_{H_2O}$  [28]. In our study a water adsorption enthalpy of -47.1 kJ/mol was estimated, indicating that the apparent activation energy calculated below 23°C by Herrmann et al. may partly correspond to the desorption of H<sub>2</sub>O from a considerably hydrated TiO<sub>2</sub> surface. The other part of the difference in the value of the activation energy might be due to the decrease in number of active sites by the formation of carboxylates, maybe in combination with irreversibly adsorbed cyclohexanone, as shown in Figure 5.7.

At temperatures above 55°C the microkinetic model is not applicable since other reactions not considered in the model interfere with the kinetics of cyclohexane photo-oxidation, resulting in lower rates than predicted by the model. Herrmann et al. observed a similar effect, reported as a negative value of the apparent activation energy at higher temperature, which they, however, explained by cyclohexane adsorption limitation instead of deactivation. Our model does not predict cyclohexane adsorption limitations (Figure 5.4) under UV illumination up to 50°C. The results at 55 and particularly 60°C (Figures 5.3e and 5.3f), showing a significantly lower reaction rate than at lower temperature, however, might be related to adsorption limitations.

The results in Figure 5.8 indicate that above 50°C, besides the photo-catalytic route, a thermal route must be taken into account in the carboxylate formation. The contribution of the thermal deactivation is the largest at 60°C, which is accompanied by a decreased product formation. Based on these results, the apparent activation energy at temperatures above 55°C can be estimated with  $E_{app} = E_a + (1 - \theta_{Cyh})\Delta H_{Cyh} - E_{deact}$  [28]. The activation energy for the thermal deactivation route was not estimated since it was only significant in the 60°C experiment of which the results were not used in the microkinetic model.

From our findings it has become evident that apparent activation energies estimated using a simple Arrhenius method based on liquid phase concentrations, must be interpreted with care since the values are influenced significantly by competitive adsorption and deactivation phenomena. More mechanistic insight is obtained using *in situ* techniques, which are able to analyze these phenomena. This is particularly important for the highly hydrophilic and easily deactivated TiO<sub>2</sub> photo-catalysts for organic transformation, as demonstrated herein.

### 5.5.2. Temperature effect on selectivity

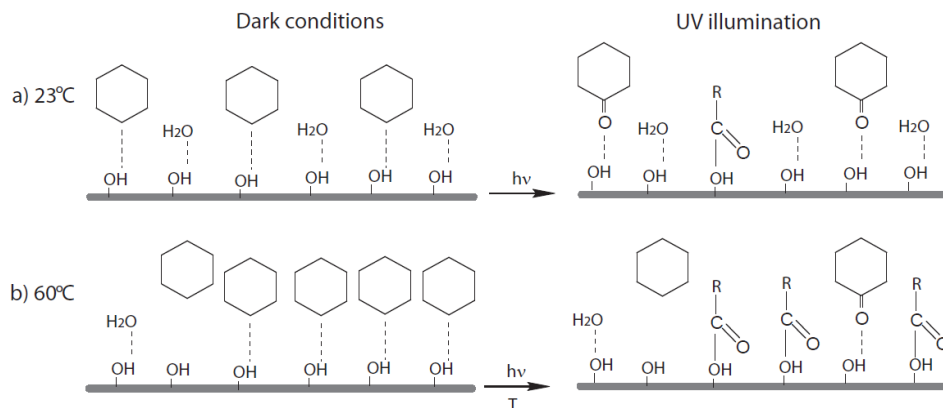
The kinetic model contains two routes to carboxylate formation: (i) an indirect route via oxidation of cyclohexanone to carboxylates, and (ii) a direct route via formation of carboxylates from cyclohexane. The results of the kinetic parameter estimation show that the direct route is clearly the predominant one; only at 23°C this seems not true since then the formation of carboxylates shows a clear delay. This indicates that the oxidation of cyclohexanone to carboxylates is an important deactivation route at low temperatures. The fact that this reaction is negligible according to our modeling might be due to the high cyclohexanone desorption rate constant under illumination, resulting in a low cyclohexanone occupancy within the error of the calculations.

The results show that selectivity towards cyclohexanone formation decreases with reaction temperature (Figure 5.4). Scheme 5.2 resumes by a simplified illustration, the surface occupation according to our model at different temperatures, under dark conditions as well as under illumination conditions. At 23°C, competitive water adsorption hinders the cyclohexane adsorption, resulting in a low reaction rate.

Although H<sub>2</sub>O is included in the microkinetic model as a spectator only, it may in reality also intervene in the reaction, e.g. in the formation of <sup>•</sup>OH radicals or by inducing a lower product selectivity. The carboxylates are represented with chemical bonds to the active sites to stress that these species are irreversibly adsorbed, causing deactivation. At temperatures up to 50°C, the surface hydration decreases and cyclohexane adsorption increases, increasing the yield under UV illumination conditions. At 60°C the yield decreases significantly, probably due to the thermal formation of carboxylates, (Figure 5.8b), although also a limitation in the cyclohexane adsorption may play a role.

The kinetics of cyclohexanone desorption under dark conditions, not shown in Scheme 5.2, proved to be unrelated to the desorption of cyclohexanone under UV illumination. According to our results the TiO<sub>2</sub> catalyst under photon absorption conditions shows a much “cleaner” surface, while in dark conditions, cyclohexanone is much more strongly or even irreversibly adsorbed on the surface.

**Scheme 5.2.** Schematic representation of the expected species covering the surface of the TiO<sub>2</sub> catalyst under dark conditions (prior to reaction) and during photo-catalytic oxidation of cyclohexane (UV illumination), at a) low temperatures and b) high temperatures. The –OH site represented in the scheme is a simplification of the multiplicity of sites present in the TiO<sub>2</sub> surface. The solid lines represent irreversible adsorption while the dotted lines represent weak H-bonded adsorption.



## 5.6. CONCLUSIONS

The temperature dependence of the photo-catalytic cyclohexane oxidation on  $\text{TiO}_2$  was evaluated using *in situ* ATR-FTIR spectroscopy, allowing the analysis of surface adsorbed species. The experimental data were fitted using a microkinetic model, which predicts the absence of a temperature effect on the rate of selective formation of cyclohexanone ( $E_{a1} = 0 \text{ kJ/mol}$ ). The cyclohexane photo-catalytic oxidation is significantly limited by both competitive water adsorption and catalyst deactivation. The formation of carboxylates, which according to the model fit are mainly formed from direct cyclohexane oxidation under UV illumination, showed an activation energy of  $18.4 \pm 3.3 \text{ kJ.mol}^{-1}$ . Above  $50^\circ\text{C}$  carboxylates are also formed by consecutive oxidation of cyclohexanone, as demonstrated by spectral changes in dark conditions. The results imply that elevating the reaction temperature of photo-catalytic cyclohexane oxidation reduces selectivity, and is not a means to suppress catalyst deactivation.

## REFERENCES

- [1] G.Franz and R.A.Sheldon, in: (Eds.), Ullmann's Encyclopedia of Industrial Chemistry, Oxidation, Wiley Interscience, New York (2005).
- [2] P.Du, J.A.Moulijn, G.Mul, J. Catal. 238 (2006) 342.
- [3] J.Peral, X.Domenech, D.F.Ollis, J. Chem. Technol. Biotechnol. 70 (1997) 117.
- [4] H.Einaga, S.Futamura, T.Ibusuki, Appl. Catal. , B 38 (2002) 215.
- [5] S.A.Larson, J.L.Falconer, Catal. Lett. 44 (1997) 57.
- [6] A.R.Almeida, J.A.Moulijn, G.Mul, J. Phys. Chem. C 112 (2008) 1552.
- [7] W.Mu, J.M.Herrmann, P.Pichat, Catal. Lett. 3 (1989) 73.
- [8] J.M.Herrmann, Top. Catal. 34 (2005) 49.
- [9] A.R.Almeida, J.T.Carneiro, J.A.Moulijn, G.Mul, J. Catal. 273 (2010) 116.
- [10] T.J.A.Renckens, A.R.Almeida, M.R.Damen, M.T.Kreutzer, G.Mul, Catal. Today 155 (2010) 302.
- [11] R.J.Berger, E.H.Stitt, G.B.Marin, F.Kapteijn, J.A.Moulijn, Cattech 5 (2001) 30.
- [12] A.K.Suresh, T.Sridhar, O.E.Potter, Aiche J. 34 (1988) 55.

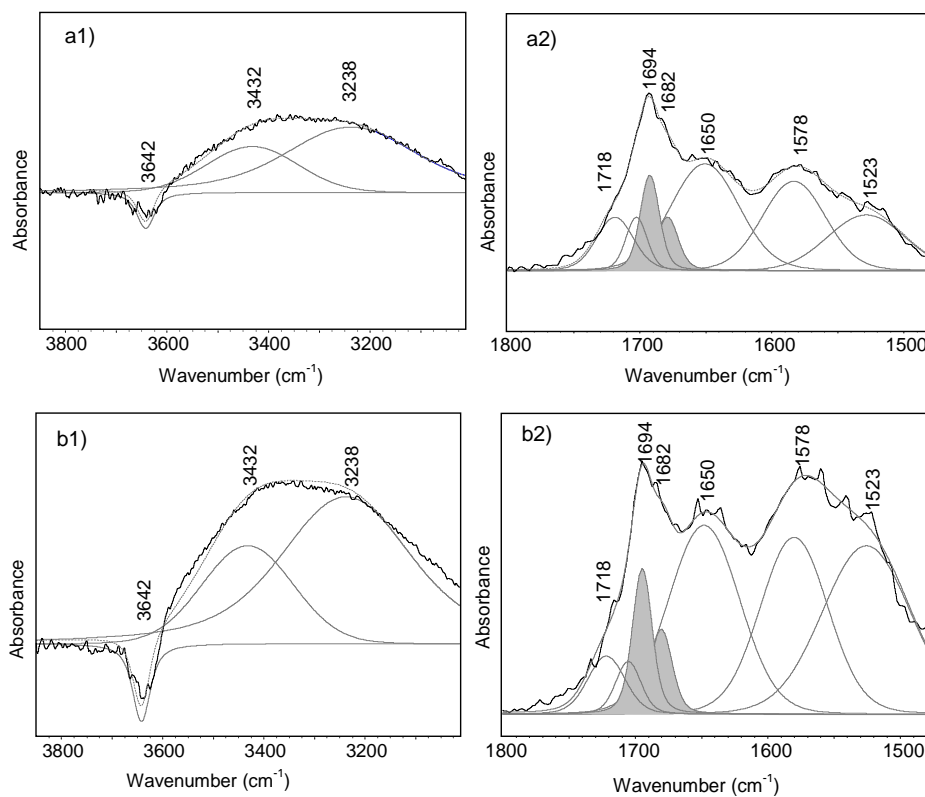
- [13] J.D.Wild, T.Sridhar, O.E.Potter, Chem. Eng. J. 15 (1978) 209.
- [14] A.R.Almeida, M.Calatayud, F.Tielens, J.A.Moulijn, G.Mul (2010) submitted.
- [15] M.Egashira, S.Kawasumi, S.Kagawa, T.Seiyama, Bull. Chem. Soc. Jpn. 51 (1978) 3144.
- [16] A.A.Levchenko, G.S.Li, J.Boerio-Goates, B.F.Woodfield, A.Navrotsky, Chem. Mat. 18 (2006) 6324.
- [17] C.Arrouvel, M.Digne, M.Breyse, H.Toulhoat, P.Raybaud, J. Catal. 222 (2004) 152.
- [18] J.Soria, J.Sanz, I.Sobrados, J.M.Coronado, A.J.Maira, M.D.Hernandez-Alonso, F.Fresno, J. Phys. Chem. C 111 (2007) 10590.
- [19] S.H.Szczepankiewicz, A.J.Colussi, M.R.Hoffmann, J. Phys. Chem. B 104 (2000) 9842.
- [20] D.J.Yates, J. Phys. Chem. 65 (1961) 746.
- [21] P.Z.Araujo, C.B.Mendive, L.A.G.Rodenas, P.J.Morando, A.E.Regazzoni, M.A.Blesa, D.Bahnemann, Coll. Surf. A 265 (2005) 73.
- [22] P.Du, J.A.Moulijn, G.Mul, J. Catal. 238 (2006) 342.
- [23] P.Du, J.T.Cameiro, J.A.Moulijn, G.Mul, Appl. Catal. A 334 (2008) 119.
- [24] N.Sakai, A.Fujishima, T.Watanabe, K.Hashimoto, J. Phys. Chem. B 107 (2003) 1028.
- [25] X.Fu, L.A.Clark, W.A.Zeltner, M.A.Anderson, J. Photochem. Photobiol. , A 97 (1996) 181.
- [26] A.J.Elliot, A.S.Simons, Rad. Phys. Chem. 24 (1984) 229.
- [27] A.J.Elliot, D.R.Mccracken, G.V.Buxton, N.D.Wood, J. Chem. Soc. Faraday Trans. 86 (1990) 1539.
- [28] J.A.Moulijn, F.Kapteijn, G.Mul, in Heterogeneous Catalysis for Chemical Engineers (2004).

## 5.7. APPENDIX

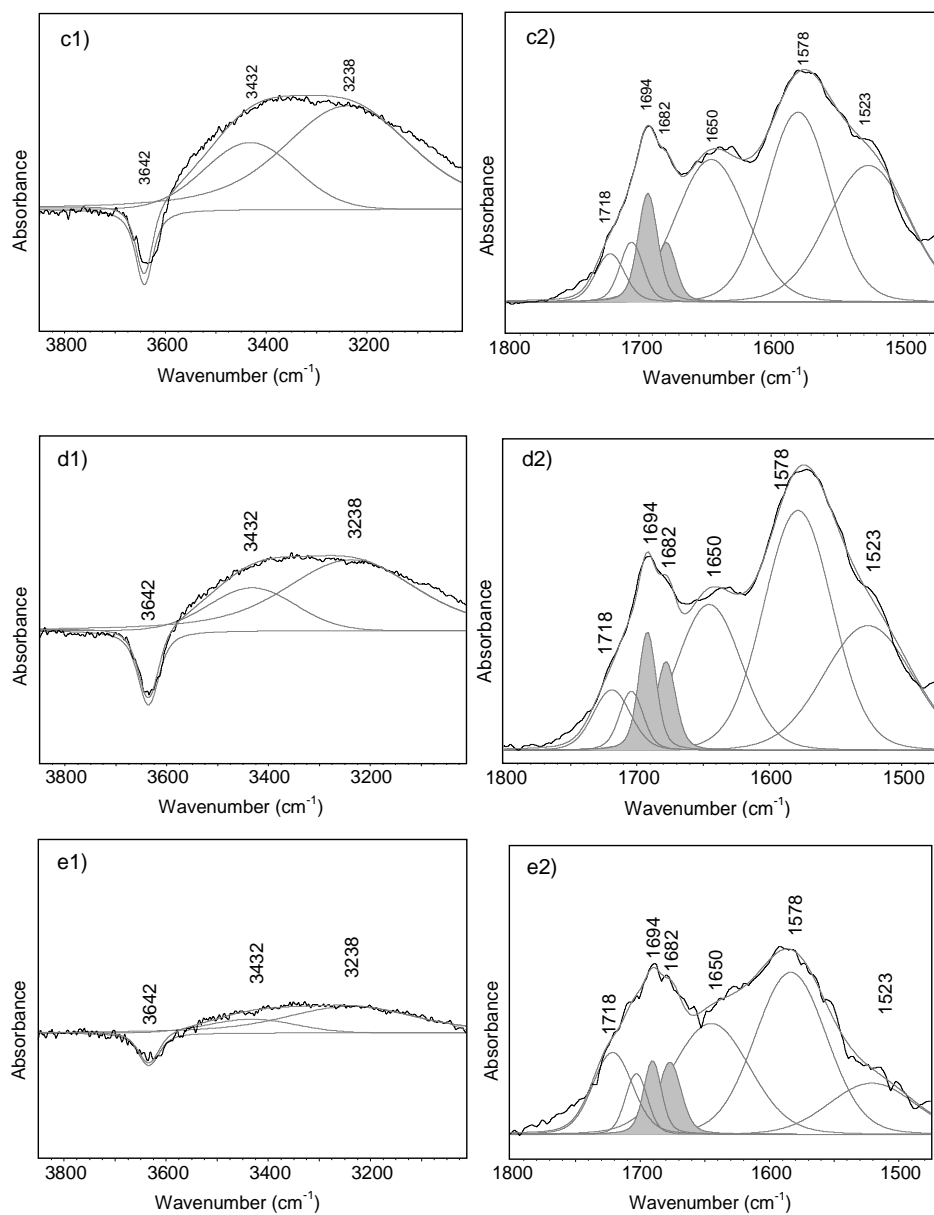
This Appendix includes supporting information for Chapter 5, containing extra spectroscopic and microkinetic model results.

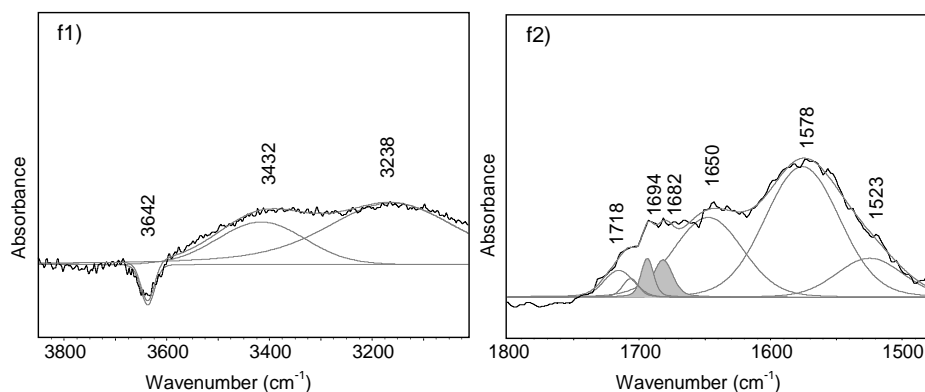
### 5.7.1. UV illumination conditions

Figure 5.9 shows the spectrum and its deconvolution after two min of cyclohexane photo-oxidation at several temperatures, both in the high and low wavenumber range.









**Figure 5.9.** Spectral deconvolution after two min of cyclohexane photo-oxidation on  $\text{TiO}_2$  at (a) 23°C, (b) 30°C, (c) 40°C, (d) 50°C, (e) 55°C and (f) 60°C for the 1) high wavenumbers region and 2) low wavenumbers region. The spectra are represented in common scale of absorbance among the same wavenumber region. The black line represents the original spectra, the grey bands correspond to the deconvoluted peaks and the dashed grey line represents the sum of the deconvoluted peaks. The two grey-shaded peaks correspond to adsorbed cyclohexanone.

Table 5.5 shows the correlation matrix of the 11 parameters that could be fitted, without becoming limited by the boundaries that were set to avoid the values moving into physically unacceptable ranges. None of the absolute values of the correlation coefficients between different parameters exceeds the value of 0.99 indicating the absence of a strong correlation between any of the estimated parameters [1]. The quite high correlation coefficient of 0.97 between  $k_{1\_296}$  and  $K_{\text{H}_2\text{O}_2\_296}$  may have contributed to the relatively large uncertainty in the calculated  $K_{\text{H}_2\text{O}_2\_296}$ . The parameter  $k_{4\_296}$  is associated with an even larger uncertainty, which results from the low sensitivity of the model to this parameter.

**Table 5.5.** Correlation matrix of the estimated microkinetic model parameters, calculated under UV illumination conditions.

Parameter	cf <sub>CyH<sub>2</sub>O<sub>ads</sub></sub>	cf <sub>H<sub>2</sub>O<sub>ads</sub></sub>	$\Delta H_{ads}$ <sub>CyH</sub>	K <sub>CyH<sub>2</sub>O<sub>296</sub></sub>	$\Delta H_{ads}$ <sub>CyHO</sub>	K <sub>H<sub>2</sub>O<sub>296</sub></sub>	$\Delta H_{ads}$ <sub>H<sub>2</sub>O</sub>	k <sub>1_296</sub>	k <sub>3_296</sub>	E <sub>a3</sub>	k <sub>4_296</sub>
cf <sub>CyH<sub>2</sub>O<sub>ads</sub></sub>	1										
cf <sub>H<sub>2</sub>O<sub>ads</sub></sub>	-0.82	1									
$\Delta H_{ads}$ <sub>CyH</sub>	-0.77	0.90	1								
K <sub>CyH<sub>2</sub>O<sub>296</sub></sub>	-0.24	-0.20	-0.24	1							
$\Delta H_{ads}$ <sub>CyHO</sub>	-0.59	0.70	0.76	-0.46	1						
K <sub>H<sub>2</sub>O<sub>296</sub></sub>	0.64	-0.92	-0.90	0.49	-0.77	1					
$\Delta H_{ads}$ <sub>H<sub>2</sub>O</sub>	-0.66	0.80	0.88	-0.35	0.84	-0.89	1				
k <sub>1_296</sub>	0.66	-0.94	-0.93	0.43	-0.72	0.97	-0.83	1			
k <sub>3_296</sub>	-0.32	-0.11	-0.21	0.74	-0.22	0.40	-0.30	0.37	1		
E <sub>a3</sub>	0.12	-0.17	-0.08	-0.07	0.09	0.05	0.12	0.12	-0.47	1	
k <sub>4_296</sub>	0.15	-0.27	-0.26	0.52	-0.24	0.36	-0.25	0.36	0.23	0.04	1

### 5.7.2. Dark conditions

Table 5.6 shows the correlation matrix of the 4 parameters that were fitted to the ATR-FTIR results under dark conditions. Since the absolute values of all the correlation coefficients between different parameters are significantly lower than 0.99, it can be concluded that there is no strong dependency between any of the estimated parameters.

**Table 5.6.** Correlation matrix of the microkinetic model parameters, calculated under dark conditions.

Parameter	$K_{\text{CyhO}_{296}}$	$\Delta H_{\text{ads}_{\text{CyhO}}}$	$k_{4_{296}}$	$E_{a4}$
$K_{\text{CyhO}_{296}}$	1			
$\Delta H_{\text{ads}_{\text{CyhO}}}$	-0.89	1		
$k_{4_{296}}$	0.60	-0.56	1	
$E_{a4}$	-0.42	0.54	-0.77	1

## REFERENCES

- [1] Caracotsios, M., Personal Communication (1997).

# Chapter 6

## Cyclohexane photo-catalytic oxidation on $\text{TiO}_2$ : evidence for a Mars-van Krevelen mechanism

Cyclohexane photo-catalytic oxidation with  $^{18}\text{O}_2$  over anatase  $\text{TiO}_2$  was analyzed by *in situ* Attenuated Total Reflection Fourier Transform Infrared (ATR-FTIR) spectroscopy, to gain insight in the mechanistic steps of formation of cyclohexanone and of deactivating carboxylate species, respectively. Cyclohexane photo-oxidation on  $\text{TiO}_2$  with increasing concentration of labeled  $\text{Ti-}^{18}\text{OH}$  sites, yielded cyclohexanone and surface deactivating species with an isotopic distribution reflecting the concentration of  $\text{Ti-}^{18}\text{OH}$  sites on the surface. This finding suggests that oxygen incorporated in cyclohexanone, as well as in deactivating carboxylates, originates from the catalyst surface, rather than from dissolved  $\text{O}_2$ . This suggests that cyclohexyl hydroperoxide observed spectroscopically, is a spectator species, rather than the commonly assumed reaction intermediate. The proposed Mars-van Krevelen cycle is completed by regeneration of surface sites by reaction with  $^{18}\text{O}_2$ . In contrast to cyclohexanone formation, the formation of carboxylate species shows a kinetic isotopic effect, suggesting that consecutive oxidation reactions involve C-O bond formation as a rate limiting step.

This chapter is based on the following publication: A.R.Almeida, J.A.Moulijn, G.Mul (2010) submitted.

## 6.1. INTRODUCTION

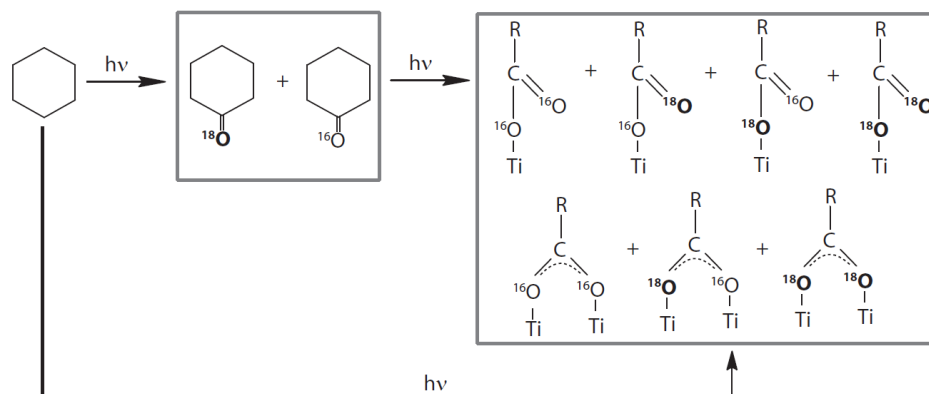
Cyclohexane photo-catalytic oxidation on anatase  $\text{TiO}_2$  is a promising alternative to the commercially applied and intrinsically inefficient cyclohexanone production process [1]. The high selectivity towards cyclohexanone formation [2] is unfortunately associated with extensive catalyst deactivation due to formation of strongly adsorbed carboxylate and carbonate species [3]. Cyclohexanone desorption from  $\text{TiO}_2$  in dark conditions is a slow process, with a time scale in the order of minutes [4,5], and the congruent formation of carboxylates suggests that consecutive oxidation of cyclohexanone is a major contributor to the formation of these species.

To further improve on photo-oxidation selectivity, it is important to understand the origin of oxygen yielding cyclohexanone and carboxylates, respectively. It is often proposed in the literature that photo-catalytic cyclohexanone formation occurs through a cyclohexyl hydroperoxide intermediate [2,3,6-8], suggesting that oxygen dissolved in cyclohexane is the primary oxygen source yielding cyclohexanone. Besides cyclohexyl hydroperoxide, also cyclohexanol has been proposed as an intermediate [7-9], which might be formed by recombination of cyclohexyl and OH radicals, the latter originating from the catalyst surface.

Isotopic labeling is a powerful approach for obtaining information on the origin of oxygen incorporated in oxidation products. Scheme 6.1 represents the most abundant products of cyclohexane photo-oxidation with  $^{18}\text{O}_2$ , with carboxylates being formed either through direct unselective oxidation of cyclohexane, or through consecutive oxidation of the product cyclohexanone. Both monodentate and bidentate carboxylates are shown.

The present study will discuss the validity of these various light induced reaction steps occurring over  $\text{TiO}_2$  surfaces, also addressing the role of (surface) peroxide intermediates. To this end, cyclohexane photo-catalytic oxidation was performed using  $^{18}\text{O}_2$  in combination with *in situ* ATR-FTIR spectroscopy.

**Scheme 6.1.** Expected products of cyclohexane photo-oxidation with <sup>18</sup>O<sub>2</sub>, including the selective formation of cyclohexanone, and two possible routes towards carboxylates, with monodentate and bridging conformations.



## 6.2. EXPERIMENTAL

### 6.2.1. Photo-catalytic reactions

A Nicolet 8700 spectrometer with a ZnSe ATR accessory, described elsewhere [3], was used for the *in situ* study. The ATR cell of 4 mL inner volume was sealed by a quartz window and covered by a pyrex glass, to shield UV light wavelengths below 275 nm. A 75 W Xe illumination source was equipped with a shutter that opens or closes in synchronization with the measuring spectrometer, and was controlled by a home-made Labview method.

The photo-catalyst used in this study was Hombikat UV100 TiO<sub>2</sub> (Sachtleben) of 100% anatase crystallinity (determined by XRD), a  $S_{\text{BET}}$  of 337 m<sup>2</sup>/g and a primary particle size of approximately 5 nm [2]. The catalyst was dried at 120 °C for 1 h in static air and suspended in water at a concentration of 1.5 g/L. The suspension was treated for 30 min in a 35 kHz Elmasonic ultrasonic bath; 2 mL of this suspension was spread on a ZnSe crystal (50x10x2 mm) and dried in vacuum overnight. The obtained TiO<sub>2</sub> coating was dried for 1 h in air at 120°C, prior to catalytic testing.

Cyclohexane (99.0% from Sigma-Aldrich) was saturated with two different oxygen gas mixtures: 1) 5% <sup>16</sup>O<sub>2</sub>, as obtained by diluting air in He and 2) 5% <sup>18</sup>O<sub>2</sub>/He (Isotec).

Pre-illumination of the  $\text{TiO}_2$  catalysts under  $^{18}\text{O}_2$  environment (gas mixture 2) was continued for 15, 30, 60 min in order to induce Oxygen Isotopic Exchange (OIE) of surface active sites. Pre-illumination of the  $\text{TiO}_2$  catalysts under  $^{16}\text{O}_2$  environment (gas mixture 1) was continued for 30 min, for comparison. Cyclohexane pre-dried with molsieve 4A, was saturated with either 5%  $^{16}\text{O}_2/\text{He}$  or 5%  $^{18}\text{O}_2/\text{He}$ , in a separated vessel. After saturation the liquid was directed to the ATR cell by a syringe and illumination was continued for 10 min. A reference experiment with 30 min pre-illumination of the  $\text{TiO}_2$  coating in He, followed by 10 min UV illumination of cyclohexane adsorbed on  $\text{TiO}_2$  containing dissolved He, was also performed. After each experiment the  $\text{TiO}_2$  catalyst coating was removed from the ZnSe crystal and a fresh  $\text{TiO}_2$  coating was prepared.

A TRS  $\text{N}_2$ -cooled detector was used for the rapid scan measurements, applying a scan rate of  $8.8617 \text{ cm.s}^{-1}$  and a spectral resolution of  $4 \text{ cm}^{-1}$ . The first steps in the experiment consisted of recording 500 scans (1.2 min) in dark conditions, which were averaged and used as background in the experiment. 4250 scans (10 min) were measured under illumination, which were averaged in time-slices of 100 scans, resulting in spectra representing a period of 14 s. A deconvolution method was developed in the Omnic 7.3 software from Thermo Scientific, and applied between  $1880\text{--}1475 \text{ cm}^{-1}$  wavenumbers. The wavelengths of the infrared bands were allowed to vary  $\pm 3 \text{ cm}^{-1}$  from the original guess, in order to reduce residuals in the fitting.

### 6.2.2. Spectra of reference compounds

Cyclohexane and a solution of 0.05 M of cyclohexanone in cyclohexane were dried over Molsieve type 4A overnight before use. A volume of 50 mL of cyclohexane was flown through the  $\text{TiO}_2$  coated ATR cell for 1 h by means of a series II high performance liquid chromatography pump. After surface stabilization a spectrum was taken as background. For the measurement of the spectrum of cyclohexanone adsorbed on  $\text{TiO}_2$ , the inlet of the ATR cell was switched from pure cyclohexane to the solution of 0.05 M of cyclohexanone in cyclohexane. The spectrum obtained after 2 h of cyclohexanone exposure to the  $\text{TiO}_2$  catalyst was subsequently recorded.

A similar reference spectrum was recorded by exposing a fresh  $\text{TiO}_2$  coating to a



mixture containing 5.5% cyclohexyl hydroperoxide, 0.73% cyclohexanol, 0.69% cyclohexanone and 0.09% adipic acid in cyclohexane. This was done for only a few minutes because of the potential instability of the peroxide.

A Nicolet 8700 spectrometer equipped with a TRS N<sub>2</sub>-cooled detector was used for spectral recording. The measurements were done with a mirror velocity of 1.8988 cm.s<sup>-1</sup> and a resolution of 4 cm<sup>-1</sup>. The background and the sample spectra were averaged from 64 and 32 spectra, respectively.

### 6.3. RESULTS

#### 6.3.1. Cyclohexane photo-oxidation with <sup>16</sup>O<sub>2</sub>

Prior to reaction, the TiO<sub>2</sub> coating was pre-illuminated in an environment of 5% <sup>16</sup>O<sub>2</sub>/He for 30 min. After this pre-treatment, cyclohexane photo-oxidation with <sup>16</sup>O<sub>2</sub> was performed; the products after 2 and 10 min of UV illumination can be seen in Figure 6.1. These results are compared with reference spectra of cyclohexanone and cyclohexyl hydroperoxide adsorbed on TiO<sub>2</sub> (in dark conditions). The broad feature with two main contributions at 3350 and 3230 cm<sup>-1</sup> corresponds to the OH stretching vibrations of adsorbed water. The O-H stretching vibration of the bridging Ti-(<sup>16</sup>OH)-Ti active sites is observed at 3630 cm<sup>-1</sup> wavelength. While the amount of adsorbed water increases with time, the Ti-(<sup>16</sup>OH)-Ti group decreases, as a result of either deprotonation, or H-bonding with an adsorbate. The basic-<sup>16</sup>OH group which is expected to absorb around 3415 cm<sup>-1</sup>, is overlapped by strong water contributions [10]. Cyclohexanone does not show characteristic infrared bands in this spectral range, but adsorption on TiO<sub>2</sub> also leads to a negative intensity at 3630 cm<sup>-1</sup>. Cyclohexyl hydroperoxide adsorption on TiO<sub>2</sub>, also shows the negative contribution of Ti-(<sup>16</sup>OH)-Ti site, as well as the characteristic bands of water adsorption on TiO<sub>2</sub>, at 3230, and 3350 cm<sup>-1</sup>. The only characteristic peak of the peroxide in this region is the OH stretching vibration, which is expected at 3512 cm<sup>-1</sup> [11], but is again overlapped by the large water contributions of the TiO<sub>2</sub> surface.

The spectra in the 1900-1200 cm<sup>-1</sup> infrared region are also shown. Direct comparison between the reaction spectrum after 2 min of illumination, and the reference spectra

shows that cyclohexanone is the main product of cyclohexane photo-oxidation. The cyclohexanone bands can be observed in the  $1700\text{ cm}^{-1}$  region, with three obvious contributions: 1) a shoulder at  $1720\text{ cm}^{-1}$  corresponding to the  $\text{C}=\text{}^{16}\text{O}$  stretching vibration of bulk/desorbed cyclohexanone, 2)  $1690\text{ cm}^{-1}$  and 3)  $1679\text{ cm}^{-1}$ , both corresponding to the  $\text{C}=\text{}^{16}\text{O}$  stretching vibration of cyclohexanone, adsorbed on the  $\text{TiO}_2$  surface. Cyclohexanone adsorption on hydrated (101)  $\text{TiO}_2$  surfaces was studied by DFT calculations. The band at  $1690\text{ cm}^{-1}$  was assigned to cyclohexanone adsorption on a relatively dry surface, while the  $1679\text{ cm}^{-1}$  band was assigned to the interaction of cyclohexanone with neighboring adsorbed  $\text{H}_2\text{O}$  molecules [12]. The small  $1313$  and  $1278\text{ cm}^{-1}$  bands are related to the  $\text{CH}_2$  bending and twisting vibrations of the cyclohexyl ring in cyclohexanone.

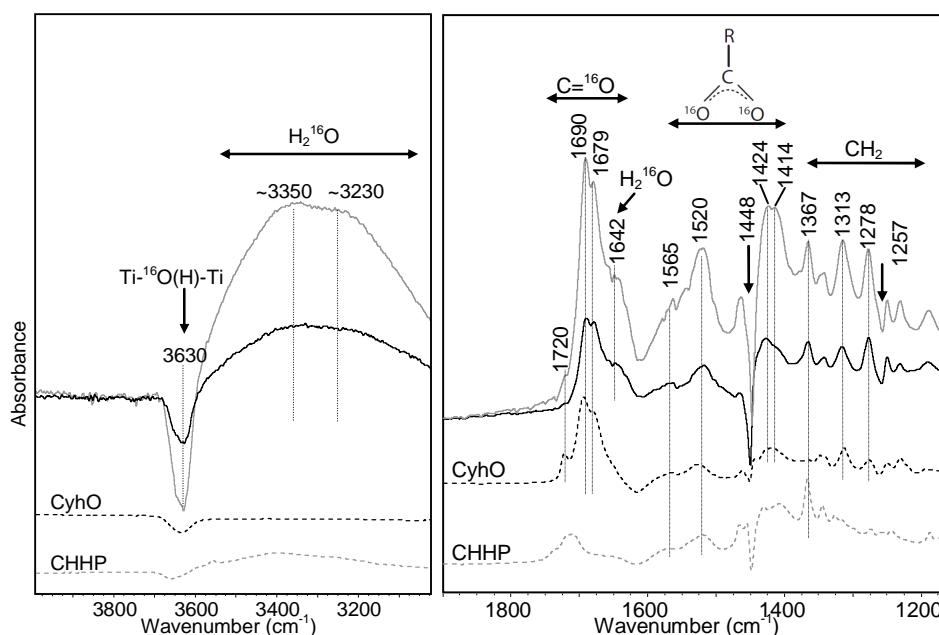


**Figure 6.1.** Infrared spectra in the  $4000\text{--}3000\text{ cm}^{-1}$  and  $1900\text{--}1200\text{ cm}^{-1}$  regions, after 2 min (black spectrum) and 10 min (grey spectrum) of cyclohexane photo-oxidation with 5%  $^{16}\text{O}_2/\text{He}$ , on a  $\text{TiO}_2$  catalyst which has been pretreated by submitting it to UV illumination for 30 min under 5%  $^{16}\text{O}_2/\text{He}$  environment. The black dashed spectrum corresponds to cyclohexanone adsorbed on  $\text{TiO}_2$ , and the grey dashed spectrum to cyclohexyl hydroperoxide adsorbed on  $\text{TiO}_2$ , both measured in dark conditions.

The spectrum obtained after 2 min of reaction is not completely identical to the cyclohexanone adsorption spectra. Bands of cyclohexyl hydroperoxide can also be seen, of which the most prominent one is located at  $1367\text{ cm}^{-1}$ , corresponding to the  $\text{CH}_2$  bending mode of the cyclohexyl ring. This shows that cyclohexyl hydroperoxide is a product of cyclohexane oxidation, as proposed previously [2,3,9,13], but not necessarily an intermediate to cyclohexanone. Rather, the apparent accumulation of the peroxide on the surface implies that the (thermal) rearrangement of the peroxide intermediate to the products cyclohexanone and  $\text{H}_2\text{O}$  is slow, if any. While spectral contributions at  $1713\text{ cm}^{-1}$  are observed in the reference spectrum of adsorbed cyclohexyl hydroperoxide, these are likely the result of the presence of small amounts of cyclohexanone and caproic acid in the reference mixture (see above under Experimental).

The spectrum after 10 min of illumination shows a strong contribution at 1565, 1520, 1424 and  $1414\text{ cm}^{-1}$ , assigned to carboxylates and carbonates, which cause catalyst deactivation [14]. We propose that the  $1565/1424\text{ cm}^{-1}$  and  $1520/1414\text{ cm}^{-1}$  doublets correspond to the stretching vibrations of monodentate carboxylate [15] and bidentate carboxylate [16], respectively, but other contributions of carbonates and bicarbonates may also exist in this region of the IR spectrum. At room temperature, these species are observed only after 2 min of photo-oxidation, suggesting that they are a product of consecutive reactions.

The bending vibration of the water formed during reaction can be seen at  $1642\text{ cm}^{-1}$  wavenumbers. The consumption of cyclohexane in time can be followed by the decreasing bands at 1448 and  $1257\text{ cm}^{-1}$  corresponding to the  $\text{CH}_2$  bending and twisting vibrations of the cyclohexane ring.

A blank experiment, done with He gas instead of  $^{16}\text{O}_2/\text{He}$  (not shown), induced no reaction products. Under anaerobic conditions only a small decrease in water and cyclohexane band intensities was observed, probably related to a slight increase in temperature under UV illumination.

### 6.3.2. Cyclohexane photo-oxidation with $^{18}\text{O}_2$

Prior to the cyclohexane oxidation experiments, the  $\text{TiO}_2$  catalyst coatings were pre-illuminated in 5%  $^{18}\text{O}_2/\text{He}$  gas phase environment for 0, 15, 30 and 60 min, respectively, to prepare surfaces with variable amounts of  $\text{Ti-}^{18}\text{OH}$  active sites. During pre-treatment in  $^{18}\text{O}_2/\text{He}$ , spectral changes were minor, except for a decrease in the intensity of water bands. IR shifts of OH groups were unfortunately difficult to identify. The spectra after 2 and 10 min of cyclohexane photo-oxidation with  $^{18}\text{O}_2$ , over  $\text{TiO}_2$  coatings of variable  $\text{Ti-}^{18}\text{OH}$  content, are shown in Figure 6.2. The use of isotopically labeled oxygen is expected to induce a red shift in the infrared vibrations of the oxygen containing reaction products. However, the observed bands in the  $4000\text{-}3000\text{ cm}^{-1}$  region are similar for all the experiments, and also similar to the ones observed in Figure 6.1, with the bridging  $\text{Ti-(}^{16}\text{OH)-Ti}$  stretching vibration at  $3630\text{ cm}^{-1}$ , and the H-bridged water contributions centered at  $3350$  and  $3230\text{ cm}^{-1}$ , respectively. This suggests that  $\text{H}_2^{16}\text{O}$  is the predominant product of photo-oxidation. The extent of reduction in intensity of  $\text{Ti-(}^{16}\text{OH)-Ti}$  sites is comparable in all experiments, showing the reproducibility in rates of oxidation.

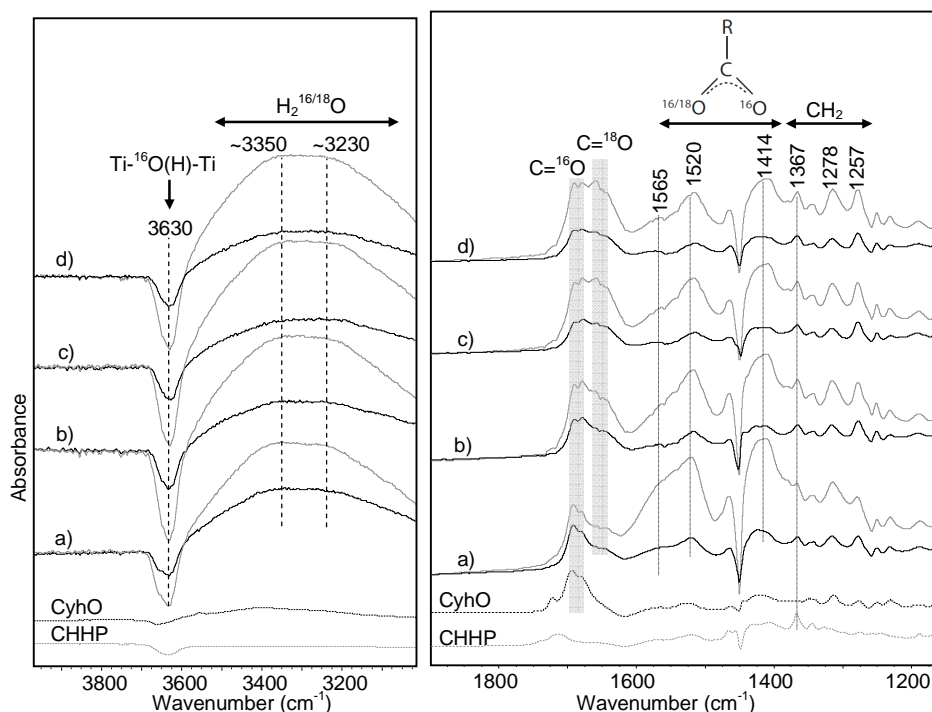
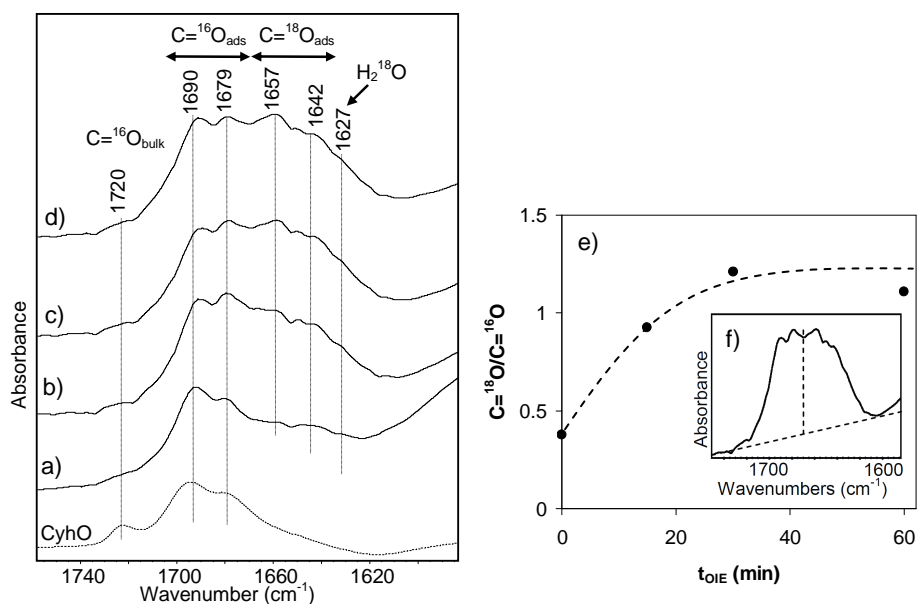


**Figure 6.2.** Infrared spectra in the  $4000\text{--}3000\text{ cm}^{-1}$  and  $1900\text{--}1200\text{ cm}^{-1}$  region, after 2 min (black spectra) and 10 min (grey spectra) of cyclohexane photo-oxidation with 5%  $^{18}\text{O}_2/\text{He}$  on a  $\text{TiO}_2$  catalyst which has been submitted to  $^{18}\text{O}$  exchange for a) 0 min, b) 15 min, c) 30 min and d) 60 min. The black dashed spectrum corresponds to the cyclohexanone (CyhO) adsorption, and the grey dashed spectrum to cyclohexyl hydroperoxide (CHHP) adsorption on  $\text{TiO}_2$ , both measured in dark conditions.

The region below  $1800\text{ cm}^{-1}$  is also shown in Figure 6.2 and the carbonyl bands, between  $1800$  and  $1600\text{ cm}^{-1}$  are depicted in more detail in Figure 6.3. Without OIE, the spectrum is similar to the one shown in Figure 6.1, where  $^{16}\text{O}_2$  was used as oxidant. It is striking that while  $^{18}\text{O}_2$  is fed, mostly cyclohexanone with  $\text{C}=\text{C}^{16}\text{O}$  carbonyl signature is predominant, in particular for the catalyst not pretreated by  $^{18}\text{O}_2$  exchange. Small contributions of labeled cyclohexanone can be observed at longer illumination times, but the analysis is ambiguous due to the strong absorption of water bending modes in the same spectral region. When the photo-catalytic reaction is preceded by OIE in  $^{18}\text{O}_2/\text{He}$  gas phase conditions, contributions of cyclohexanone with a red shifted

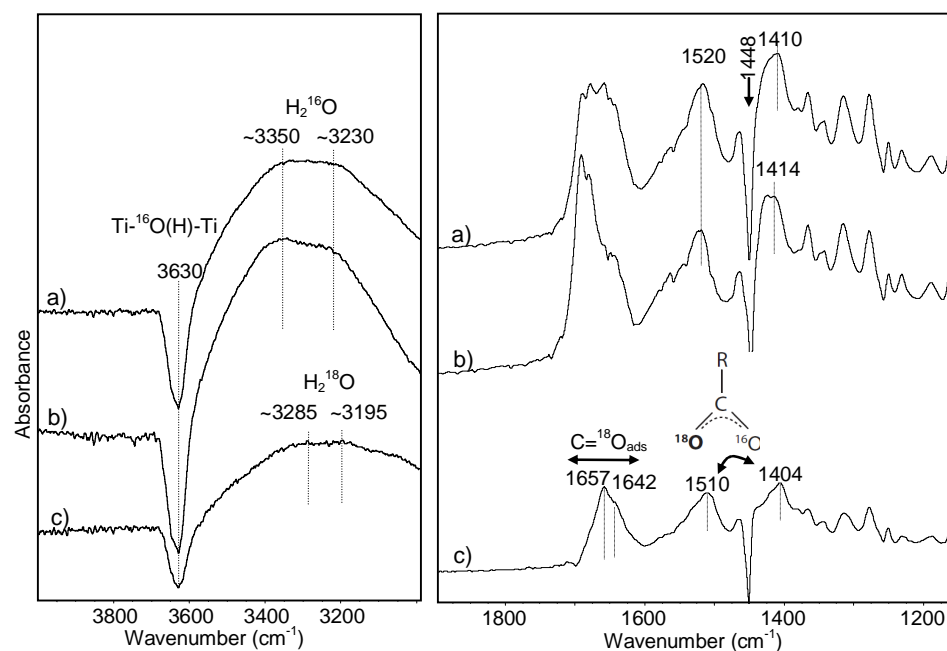
carbonyl vibration can be observed, as shown in more detail in Figure 6.3. Four contributions of adsorbed cyclohexanone are apparent, at 1690 and 1679  $\text{cm}^{-1}$ , corresponding to adsorbed cyclohexanone containing a  $\text{C}=\text{}^{16}\text{O}$  carbonyl group, and at 1657  $\text{cm}^{-1}$  and 1642  $\text{cm}^{-1}$  corresponding to adsorbed cyclohexanone with a  $\text{C}=\text{}^{18}\text{O}$  carbonyl group. A rough assessment of the contribution of labeled versus unlabeled cyclohexanone on the  $\text{TiO}_2$  surface after 10 min of cyclohexane photo-oxidation, as a function of the time of pre-OIE, is shown in Figure 6.3e). The contribution of the  $\text{C}=\text{}^{18}\text{O}$  carbonyl peaks increases with time of OIE up to 30 min. At longer  $t_{\text{OIE}}$  no further increase is observed, indicating that a maximum exists in the number of surface sites containing  $^{18}\text{O}$ , (under the applied OIE conditions). A maximum of around 50% of isotopically labeled cyclohexanone is produced. This rough assessment is however affected by the level of surface adsorbed water, absorbing in the same region, which probably results in an overestimation of the contribution of labeled cyclohexanone. It is therefore expected that the contribution of labeled cyclohexanone is smaller than represented in Figure 6.3e), especially for  $t_{\text{OIE}}=0$ .

Figure 6.2a) shows carboxylate bands at 1520 and 1414  $\text{cm}^{-1}$ , similarly to Figure 6.1, suggesting that these products are not  $^{18}\text{O}$ -labeled. Small infrared redshifts can be seen with increasing OIE time, associated with the isotope labeling of these products. It should be noted that the rate of formation of the deactivating species decreases as a function of the time of OIE. Spectra c) and d) in Figure 6.2 are very similar although the pre-OIE step was performed for 30 min and 1 h, respectively. This again demonstrates the reproducibility of the experiments, and that a maximum level of surface exchanged sites is reached after 30 min of exchange.



**Figure 6.3.** Infrared spectra after 10 min of cyclohexane photo-oxidation with 5%  $^{18}\text{O}_2/\text{He}$  on a  $\text{TiO}_2$  catalyst which has been submitted to OIE for a) 0 min, b) 15 min, c) 30 min and d) 60 min. The black dashed spectrum corresponds to the cyclohexanone (CyhO) adsorption. e) represents the ratio between the peak area of cyclohexanone with  $\text{C}=\text{O}^{18}$  (1618-1600  $\text{cm}^{-1}$ ) and cyclohexanone with  $\text{C}=\text{O}^{16}$  (1730-1668  $\text{cm}^{-1}$ ), as shown in f), as a function of OIE time.

In order to observe the spectral contributions of isotopically exchanged products more clearly, the spectrum of cyclohexane photo-oxidation with  $^{18}\text{O}_2$  (Figure 6.4a) was subtracted from the spectrum when using  $^{16}\text{O}_2$  as oxidant (Figure 6.4b); both spectra correspond to 30 min pre-illumination, for (a) in 5%  $^{18}\text{O}_2/\text{He}$  and (b) in 5%  $^{16}\text{O}_2/\text{He}$ . The result is shown in Figure 6.4c). The  $\text{C}=\text{O}^{16}$  carbonyl peak area in spectrum (b) was 0.6 times that of the intensity in spectrum (a). Therefore, in the subtraction procedure, a weighing factor of 0.6 for the contribution of spectrum (b) was applied.



**Figure 6.4.** Infrared spectra in the 4000-3000  $\text{cm}^{-1}$  and 1900-1200  $\text{cm}^{-1}$  region, a) after 10 min of cyclohexane photo-oxidation with 5%  $^{18}\text{O}_2/\text{He}$  on a  $\text{TiO}_2$  catalyst which has been submitted to 30 min of OIE in 5%  $^{18}\text{O}_2/\text{He}$ ; b) after 10 min of cyclohexane photo-oxidation with 5%  $^{16}\text{O}_2/\text{He}$  on a  $\text{TiO}_2$  catalyst which has been submitted to 30 min of pre-illumination in 5%  $^{16}\text{O}_2/\text{He}$ ; and c) Subtraction: (Spectrum a) - 0.6\*(Spectrum b).

Table 6.2 summarizes the interpretation of isotopically unlabeled and labeled bands seen in Figure 6.4, and their product assignments. The expected redshifts were calculated with the harmonic oscillator equation [17] and compared with the experimental data.

The main OH stretching bands of adsorbed  $\text{H}_2\text{O}$  ( $\sim 3350$  and  $\sim 3230 \text{ cm}^{-1}$ ), shift to 3285 and  $3195 \text{ cm}^{-1}$  in Figure 6.4c), which is a larger shift than expected on the basis of the harmonic oscillator equation. The large shift may be tentatively explained by the formation of a hydrogen bonded network involving  $\text{Ti}-^{18}\text{OH}$  and  $\text{H}_2^{18}\text{O}$ . The bridging  $\text{Ti}-\text{OH}$  active site does not show a clear shift, indicating that this active site, which occupies 75% of the catalyst surface [2], is not exchanged with labeled oxygen. The calculated and experimentally observed values for cyclohexanone containing  $\text{C}=\text{}^{18}\text{O}$



groups, are in reasonable agreement. The carboxylate peaks at 1520 and 1414 cm<sup>-1</sup> in Figure 6.4b), shift to 1510 and 1404 cm<sup>-1</sup> in spectra 6.4c). These bands correspond to the symmetric and asymmetric stretching vibration of the carbonyl group in the carboxylate molecule. Isotopically labeling the carbonyl group in the carboxylate molecule would induce, according to the harmonic oscillator equation, shifts in the order of 30 cm<sup>-1</sup>. Since much lower redshifts were observed, we conclude that only partial isotopic labeling occurred. The monodentate carboxylates and carbonate vibrations, being of lower intensity are difficult to analyze. The isotopic labeling of these deactivating species is therefore unresolved.

**Table 6.2.** Peak redshift caused by OIE, estimated by the harmonic oscillator equation.

Observed peak (cm <sup>-1</sup> ) <sup>16</sup> O	Observed peak (cm <sup>-1</sup> ) <sup>18</sup> O	Predicted peak (cm <sup>-1</sup> ) <sup>18</sup> O	Observed shift (cm <sup>-1</sup> ) <sup>1)</sup>	Predicted shift (cm <sup>-1</sup> ) <sup>2)</sup>	Vibration [3,18-21]	Species
3630	3630	3618	0	12	<sup>16</sup> O-H str.	Ti- <sup>16</sup> OH
3350	3285	3329	65	21	<sup>18</sup> O-H str.	H <sub>2</sub> <sup>18</sup> O
3230	3195	3210	35	20	<sup>18</sup> O-H str.	H <sub>2</sub> <sup>18</sup> O
1720	1681	1678	39	42	C= <sup>18</sup> O	Bulk cyclohexanone
1690	1657	1648	33	42	C= <sup>18</sup> O	Ads. cyclohexanone
1679	1642	1640	37	39	C= <sup>18</sup> O	Ads. cyclohexanone
1642	1627	1632	15	10	H- <sup>18</sup> O-H bend	H <sub>2</sub> <sup>18</sup> O
1520	1510	1489 <sup>3)</sup>	10	31	C( <sup>18</sup> OH)= <sup>16</sup> O str.	Carboxylates
1414	1404	1385 <sup>3)</sup>	10	28	C( <sup>18</sup> OH)= <sup>16</sup> O str.	Carboxylates

<sup>1)</sup> Subtraction between the observed peak of the oxidation with <sup>16</sup>O<sub>2</sub> with the observed peak of the oxidation with <sup>18</sup>O<sub>2</sub>.

<sup>2)</sup> Subtraction between the observed peak of the oxidation with <sup>16</sup>O<sub>2</sub> with the predicted peak of the oxidation with <sup>18</sup>O<sub>2</sub> (by the harmonic oscillator equation).

<sup>3)</sup> Harmonic oscillator equation applied for a tri-atomic vibration:

$$\left(\frac{\nu_i}{\nu}\right)^2 = \frac{m_c * m_{^{16}\text{O}} (m_c + 2 * m_{^{18}\text{O}} * \sin(\alpha)^2)}{m_c * m_{^{18}\text{O}} (m_c + 2 * m_{^{16}\text{O}} * \sin(\alpha)^2)}, \text{ with } \nu \text{ and } \nu_i \text{ corresponding to the frequencies of labeled}$$

and unlabeled vibration,  $m_c$ ,  $m_{^{16}\text{O}}$  and  $m_{^{18}\text{O}}$  to the atomic weights of C, <sup>16</sup>O and <sup>18</sup>O and  $\alpha$  the angle of the O-C-O bonds [22].

### 6.3.3. Kinetic Isotope Effect

Figure 6.5a) shows the deconvolution of the spectrum obtained after 10 min of photocatalytic cyclohexane oxidation with  $^{16}\text{O}_2$ , on a catalyst submitted to 30 min of pre-illumination in  $^{16}\text{O}_2/\text{He}$ . Figure 6.5b) shows the deconvolution of the spectrum shown in Figure 6.4c), i.e. the spectrum after 10 min of cyclohexane photo-oxidation with  $^{18}\text{O}_2$  on a  $\text{TiO}_2$  catalysts submitted to 30 min of OIE, after subtracting the contributions of unlabeled cyclohexanone. The vibrations used for the deconvolution are assigned according to Table 6.1. The deconvolution procedure of Figure 6.5b) was done assuming that the contribution of unlabeled products is negligible, except for the band at  $1568\text{ cm}^{-1}$ .

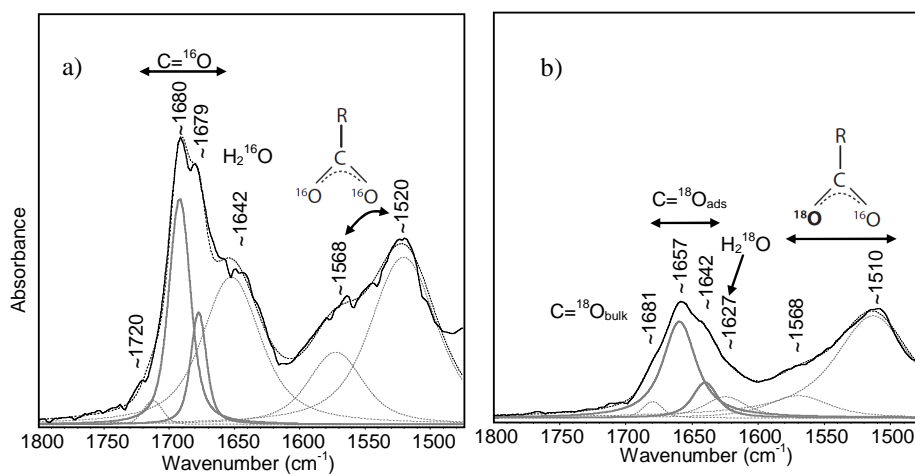


**Figure 6.5.** Spectral deconvolution of the cyclohexane photo-oxidation spectrum after 10 min of illumination using a) 5%  $^{16}\text{O}_2/\text{He}$  as oxidant; b) 5%  $^{18}\text{O}_2/\text{He}$  as oxidant after subtraction of unlabeled contributions. The catalyst coatings were submitted to 30 min of pre-illumination in  $^{16}\text{O}_2/\text{He}$  and  $^{18}\text{O}_2/\text{He}$ , respectively. The black line represents the original spectra, the grey bands correspond to the deconvoluted peaks and the dashed black line represents the sum of the deconvoluted peaks. The two bands represented by a full grey line correspond to adsorbed cyclohexanone.

The peak area profiles of the adsorbed cyclohexanone bands during illumination, can be fitted to an exponential curve,  $C(t)$ , according to the following equation:  $C(t)=C_0*[1-\exp(-k*t)]$ , in which,  $C_0$  corresponds to the cyclohexanone plateau and  $k$  to the formation constant of adsorbed cyclohexanone in time ( $t$ , min). The results can be seen in Figure 6.6a). The constant of unlabelled cyclohexanone formation,  $k_{\text{CyhO},^{16}\text{O}}$ , is  $0.22 \text{ min}^{-1}$ , while the constant of labeled cyclohexanone formation,  $k_{\text{CyhO},^{18}\text{O}}$ , is  $0.19 \text{ min}^{-1}$ . The effect of isotopic substitution on the kinetics can be assessed by calculating the kinetic isotope effect, the ratio of the two constants. The value of 1.17 is too close to unity to suggest a significant kinetic isotope effect in the formation of cyclohexanone, in view of the error related to the subtraction and the deconvolution methods.

A similar analysis can be made for the formation of carboxylates species, which is shown in Figure 6.6b). The formation of labeled carboxylates shows a delay in the first minute. The constant of unlabelled carboxylates formation,  $k_{\text{Carbox},^{16}\text{O}}$ , is  $0.09 \text{ min}^{-1}$ , while the constant of labeled cyclohexanone formation,  $k_{\text{Carbox},^{18}\text{O}}$ , is  $0.02 \text{ min}^{-1}$ . A kinetic isotope effect of 4.15 was determined, indicating that the rate of carboxylates formation is limited by a step involving an oxygen atom.

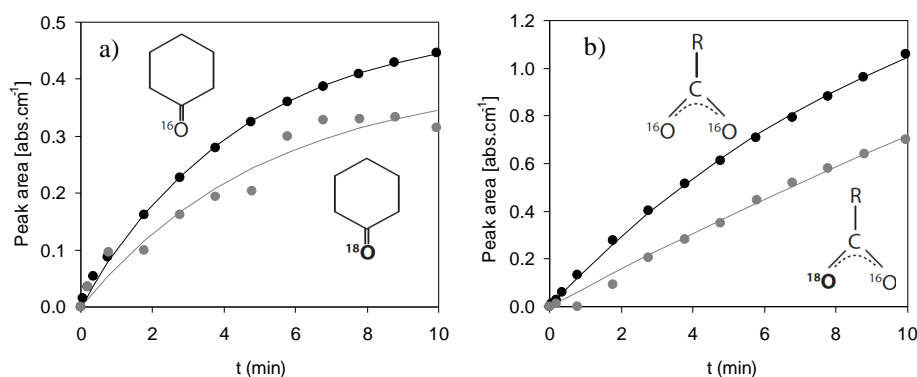


**Figure 6.6.** Peak area of a) adsorbed cyclohexanone and b) adsorbed carboxylates bands formed during 10 min of cyclohexane photo-oxidation with  $^{16}\text{O}_2$  (black circles) and  $^{18}\text{O}_2$  (grey circles). The lines correspond to the exponential fittings.

## 6.4. DISCUSSION

### 6.4.1. Selective photo-oxidation mechanism

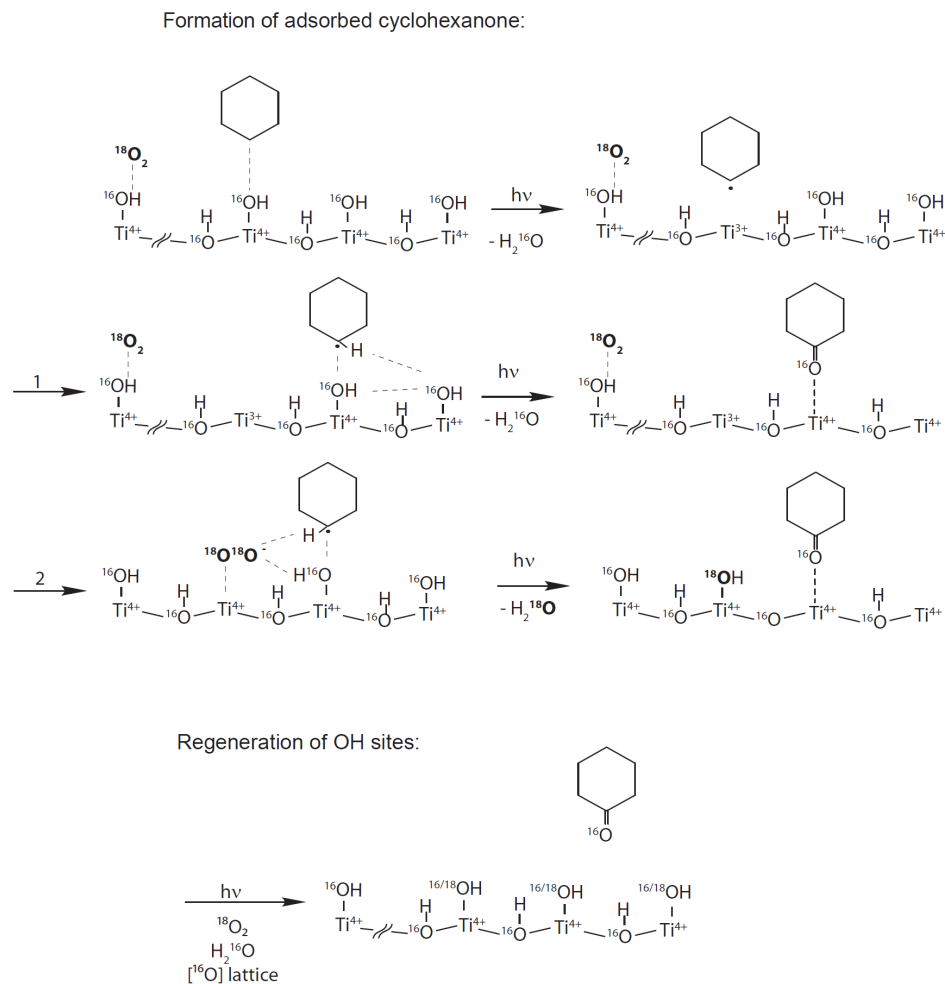
The spectroscopic data presented in Figures 6.1 to 6.5 provide important information on the mechanism of photo-oxidation of cyclohexane over  $\text{TiO}_2$  surfaces. Usually, it is postulated that cyclohexyl hydroperoxide is a key-intermediate in the oxidation process. Indeed, besides the strong features of adsorbed cyclohexanone, also bands of cyclohexyl hydroperoxide were observed in the process of photo-catalytic reaction with  $\text{O}_2$ . However, no real indication of the peroxide being an intermediate in cyclohexanone formation was obtained. Furthermore, cyclohexane photo-catalytic oxidation with  $^{18}\text{O}_2$ , without pre-isotopic exchange of the  $\text{TiO}_2$  surface, produces mainly unlabeled products and shows similar infrared spectra to those obtained when unlabeled  $^{16}\text{O}_2$  is used as oxidant. The rate of formation of labeled cyclohexanone increases with the time of OIE up to 30 min (Figure 6.3e). From these results, we conclude that the labeling of cyclohexanone product reflects the extent of isotopically labeled species on the  $\text{TiO}_2$  surface, suggesting that the oxygen in cyclohexanone originates from  $\text{TiO}_2$  associated active sites. The present isotopic study thus suggests a mechanistic route, where dissolved  $\text{O}_2$  is not directly involved in the formation of products, and in which peroxides play a minor role.

The mechanism proposed for cyclohexane photo-catalytic oxidation with  $^{18}\text{O}_2$ , (without pre-isotopic exchange), is shown in Scheme 6.2. Electron hole separation takes place in the  $\text{TiO}_2$  catalysts upon UV illumination, the electron being trapped on Titanium(IV) and the hole trapped on an OH site. The activation of the cyclohexane molecule occurs via the formation of a cyclohexyl radical and a water molecule, after which the reaction is proposed to follow two possible pathways. In the first pathway, instead of the previously proposed cyclohexyl hydroperoxide intermediate, cyclohexanone formation proceeds via cyclohexyl radical adsorption on a neighboring Ti-OH site. In this first pathway the dissolved oxygen molecule does not directly intervene in the formation of cyclohexanone, but acts as an electron scavenger inducing efficient electron-hole separation and re-oxidation of the  $\text{Ti}^{3+}$  site (not shown in Scheme 6.2). These steps are a prerequisite for cyclohexanone formation, as demonstrated by an experiment in which UV illumination of cyclohexane in the absence of  $\text{O}_2$  did not give

rise to any product. In the second pathway, besides the mentioned roles,  $\text{O}_2$  removes the second proton of the cyclohexyl radical, mediating the formation of cyclohexanone.

After the desorption of cyclohexanone, either formed by route 1, or route 2, the free  $\text{Ti}^{4+}$  sites are regenerated by different oxygen sources:  $\text{H}_2^{16}\text{O}$ ,  $\text{H}_2^{18}\text{O}$ ,  $^{18}\text{O}_2$  or oxygen originating from the  $\text{Ti}^{16}\text{O}_2$  lattice.

**Scheme 6.2.** Proposed mechanisms of cyclohexanone formation.



When  $t_{\text{OIE}} \geq 30$  min, the higher percentage of  $\text{Ti-}^{18}\text{OH}$  sites leads to a higher concentration of labeled cyclohexanone. The ratio of labeled/unlabeled cyclohexanone is close to 50% (Figure 6.3) meaning that only half of the surface could be isotopically exchanged under  $^{18}\text{O}_2/\text{He}$  illumination conditions. Three pathways of OIE are possible [23], and over  $\text{TiO}_2$  catalysts UV induced oxygen isotopic exchange occurs through a  $\text{R}_1$  type exchange, as represented by the following equations [23-26]:



This exchange mechanism (in gas phase conditions) has been proposed to occur through an  $\text{O}^{3-}$  intermediate [27,28]. The observed fraction of approximately 50% of exchange suggests that  $\text{O}_2$  adsorption and  $\text{O}^{3-}$  formation occurs over coordinatively unsaturated titanium sites [26,29,30].

OH-sites which are not active for OIE, are apparently active for cyclohexane photo-oxidation, leading to the formation of unlabeled cyclohexanone. This is in agreement with previous publications which have reported a faster rate of organic conversion than OIE [24,29], also in agreement with the high efficiency of adsorbed organics in scavenging holes [31,32].

The proposed mechanism is an example of a (surface) Mars-van Krevelen mechanism [33] in which the active OH sites on the surface of the metal oxide catalyst are consumed in the oxidation and are subsequently regenerated by dissolved oxygen. According to literature, exchange of oxygen atoms between the bulk structure and the  $\text{TiO}_2$  surface does not occur [30,34]. Therefore the main source of  $^{16}\text{O}$  are the  $\text{Ti-}^{16}\text{OH}$  sites in the surface. The reaction was carried out for only 10 min to highlight the initial steps of cyclohexanone formation and surface deactivation. At longer illumination times, the formation of unlabeled products is expected to decrease, while the formation of labeled cyclohexanone would become predominant.

The detailed structure of the cyclohexyl radical coordinated to a  $\text{Ti-OH}$  site in Scheme 6.2 is not fully clear yet. Occasionally cyclohexanol has been proposed as key intermediate in this reaction [7-9], but we do not believe that the intermediate complex proposed in Scheme 6.2, is identical to adsorbed cyclohexanol. Earlier results showed

that adding cyclohexanol to cyclohexane reduced, rather than increased, the rate of photo-catalytic formation of cyclohexanone [35].

Results do not show a clear kinetic isotope effect in the formation of cyclohexanone (Figure 6.6a), so the rate of photo-catalytic formation of this molecule is not determined by formation of carbon-oxygen bonds (Scheme 6.2), suggesting the catalyst re-oxidation step to be rate determining.

#### 6.4.2. Contribution of cyclohexyl hydroperoxide

As stated, the mechanism proposed in Scheme 6.2 disregards cyclohexyl hydroperoxide as a reaction intermediate. If cyclohexyl hydroperoxide would be an intermediate, common sense predicts that the primary reaction products should be labeled. Only if the rate of isotope exchange would be significantly faster than the rate of cyclohexane photo-oxidation with  $^{18}\text{O}_2$  ( $r_{\text{OIE}} \gg r_{\text{PO}}$ ), the involvement of the peroxide would be justified. Scrambled  $^{16}\text{O}^{18}\text{O}$  and  $^{16}\text{O}_2$ , according to equations (1) and (2), would lead to the formation of unlabeled or scrambled peroxide and a mixture of labeled and unlabeled cyclohexanone. However previous publications have shown that the rate of OIE is lower than the organic conversion [24,29]. A rate of OIE on TiO<sub>2</sub> catalysts of  $0.01 \text{ min}^{-1}$  has been determined [34], which is indeed at least an order of magnitude lower than the rate of cyclohexanone formation ( $0.22 \text{ min}^{-1}$ ). Although the isotopic study shows that cyclohexyl hydroperoxide is not the main intermediate product, it is observed spectroscopically (Figure 6.1), suggesting that this is a spectator species, i.e. a byproduct or an intermediate to a less favorable oxidation route.

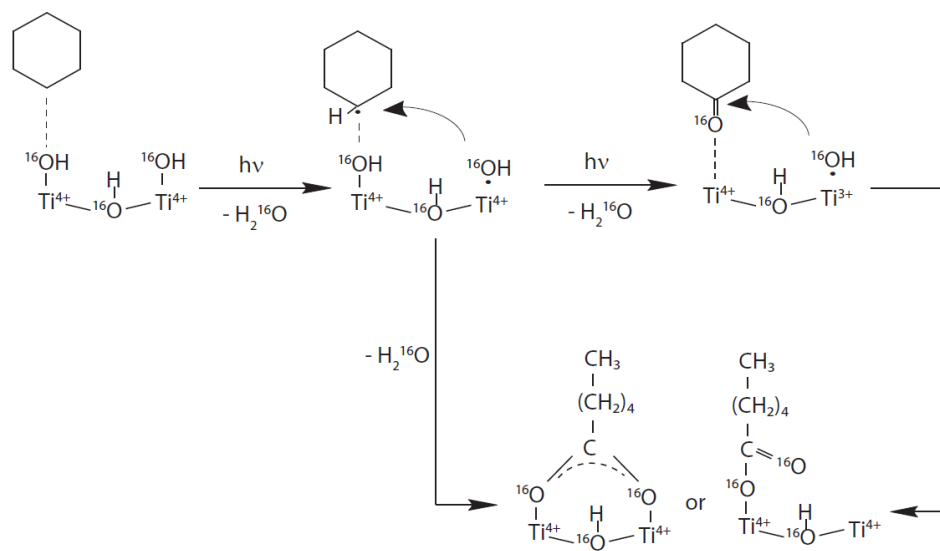
#### 6.4.3. Deactivation mechanism

A mechanism for carboxylates formation from cyclohexane photo-oxidation is proposed in scheme 6.3, as a product of direct oxidation of cyclohexane, or as a product of consecutive oxidation of cyclohexanone. Either a cyclohexyl radical or adsorbed cyclohexanone is attacked by an  $\bullet\text{OH}$  radical, inducing the opening of the ring with the formation of either monodentate or bidentate carboxylates. The  $\bullet\text{OH}$  radicals which induce the opening of the ring, may also originate from adsorbed H<sub>2</sub>O molecules, by

reaction with a hole. This adsorbed water can be  $\text{H}_2^{16}\text{O}$  and  $\text{H}_2^{18}\text{O}$  formed in the reaction (Scheme 6.2), or  $\text{H}_2^{16}\text{O}$  originally present on the catalyst surface. Similarly to cyclohexanone, increasing the concentration of  $\text{Ti}^{18}\text{OH}$  sites increased the partial labeling of carboxylates, indicating that the oxygen which is incorporated in this species originates from the surface.

It is striking that a considerable kinetic isotope effect was determined for carboxylate formation (Figure 6.6b), suggesting C-O bond formation to be limiting, as shown in Scheme 6.3. This is in agreement with a significant activation energy for carboxylate formation, reported elsewhere [5].

**Scheme 6.3.** Proposed mechanism for bidentate and monodentate carboxylates formation.



## 6.5. CONCLUSIONS

The extent of isotopic labeling in the selective oxidation of cyclohexane reflects the concentration of  $^{18}\text{O}$  of the  $\text{TiO}_2$  surface. This finding shows that the oxygen incorporated in cyclohexanone originates from the surface, rather than from dissolved  $\text{O}_2$ . A Mars-van Krevelen mechanism is thus very likely to be operative, with oxygen



being the electron scavenger and needed for regeneration of the catalytic surface. Cyclohexyl hydroperoxide, although being observed in the infrared spectra, is considered a byproduct or intermediate to a less favorable oxidation route. No kinetic isotope effect could be identified for cyclohexanone formation, while the rate of carboxylate formation is proposed to be limited by C-O bond formation.

## ACKNOWLEDGEMENTS

We acknowledge Rudi Parton, from DSM Research, for providing the mixture containing cyclohexyl hydroperoxide in cyclohexane.

## REFERENCES

- [1] G.Franz and R.A.Sheldon, in Ullmann's Encyclopedia of Industrial Chemistry, Oxidation, Wiley Interscience, New York (2005).
- [2] P.Du, J.A.Moulijn, G.Mul, J. Catal. 238 (2006) 342.
- [3] A.R.Almeida, J.A.Moulijn, G.Mul, J. Phys. Chem. C 112 (2008) 1552.
- [4] T.J.A.Renckens, A.R.Almeida, M.R.Damen, M.T.Kreutzer, G.Mul, Catal. Today 155 (2010) 302.
- [5] A.R.Almeida, R.Berger, J.A.Moulijn, G.Mul (2010) submitted.
- [6] M.A.Brusa, Y.Di Iorio, M.S.Churio, M.A.Grela, J. Mol. Catal. A 268 (2007) 29.
- [7] G.Palmisano, V.Augugliaro, M.Pagliaro, L.Palmisano, Chem. Commun. (2007) 3425.
- [8] P.Boarini, V.Carassiti, A.Maldotti, R.Amadelli, Langmuir 14 (1998) 2080.
- [9] C.B.Almquist, P.Biswas, Appl. Catal. , A 214 (2001) 259.
- [10] G.Martra, Appl. Catal. , A 200 (2000) 275.
- [11] G.Socrates, in: John Wiley & Sons Ltd., Infrared Characteristic Group Frequencies Tables and Charts, New York (1994).
- [12] A.R.Almeida, M.Calatayud, F.Tielens, J.A.Moulijn, G.Mul (2010) submitted.
- [13] M.A.Brusa, M.A.Grela, J. Phys. Chem. B 109 (2005) 1914.

- [14] I. Dolamic, T. Burgi, *J. Catal.* 248 (2007) 268.
- [15] J. M. Pettibone, D. M. Cwiertny, M. Scherer, V. H. Grassian, *Langmuir* 24 (2008) 6659.
- [16] K. D. Dobson, A. J. McQuillan, *Spectroc. Acta Pt. A-Molec. Biomolec. Spectr.* 55 (1999) 1395.
- [17] J. W. Niemantsverdriet, in: *Spectroscopy in Catalysis*, Wiley-VCH (2000).
- [18] S. H. Szczepankiewicz, A. J. Colussi, M. R. Hoffmann, *J. Phys. Chem. B* 104 (2000) 9842.
- [19] D. J. Yates, *J. Phys. Chem.* 65 (1961) 746.
- [20] P. Z. Araujo, C. B. Mendive, L. A. G. Rodenas, P. J. Morando, A. E. Regazzoni, M. A. Blesa, D. Bahnemann, *Coll. Surf. A* 265 (2005) 73.
- [21] H. Sun, F. Blatter, H. Frei, *J. Am. Chem. Soc.* 118 (1996) 6873.
- [22] S. Pinchas and I. Laulicht, in *Infrared spectra of labelled compounds*, Academic Press Inc., London (1971).
- [23] J. Novakova, *Catal. Rev.* 4 (1970) 77.
- [24] H. Courbon, M. Formenti, P. Pichat, *J. Phys. Chem.* 81 (1977) 550.
- [25] J. M. Herrmann, *Helv. Chim. Acta* 84 (2001) 2731.
- [26] J. Cunningham, E. L. Goold, J. L. G. Fierro, *J. Chem. Soc. Faraday Trans. I* 78 (1982) 785.
- [27] K. Tanaka, *J. Phys. Chem.* 78 (1974) 555.
- [28] L. F. Liao, C. F. Lien, D. L. Shieh, M. T. Chen, J. L. Lin, *J. Phys. Chem. B* 106 (2002) 11240.
- [29] P. Pichat, J. M. Herrmann, H. Courbon, J. Disdier, M. N. Mozzanega, *Can. J. Chem. Eng.* 60 (1982) 27.
- [30] P. Pichat, H. Courbon, R. Enriquez, T. T. Y. Tan, R. Amal, *Res. Chem. Intermed.* 33 (2007) 239.
- [31] Y. K. Krisnandi, R. F. Howe, *Appl. Catal. A* 307 (2006) 62.
- [32] R. F. Howe, M. Gratzel, *J. Phys. Chem.* 91 (1987) 3906.
- [33] P. Mars, D. W. van Krevelen, *Chem. Eng. Sci. Spec. Suppl.* 3 (1954) 41.
- [34] S. Sato, *J. Phys. Chem.* 91 (1987) 2895.
- [35] P. Du, *Catalysis Engineering of Light Induced Dye Degradation and Cyclohexane Photo-oxidation*, Thesis/Dissertation, Technical University of Delft (2009).

# Chapter 7

## Summary and outlook

This thesis is based on the premise that the cyclohexane photo-catalytic oxidation to cyclohexanone process, operated at room temperature and ambient pressure, is a potential alternative to the commercially applied but intrinsically inefficient process of cyclohexane oxidation. The low reaction yields and surface deactivation observed in the photo-catalytic alternative, motivated the use of *in situ* spectroscopy techniques in order to understand the mechanistic and kinetic limitations of this reaction. The combination of ATR-FTIR spectroscopy with isotope labeling, kinetic modeling and molecular modeling, provided a deeper understanding of the surface mechanism and allowed to unravel previously unknown mechanistic steps, to determine kinetic and equilibrium constants and to visualize the products adsorption configurations. The knowledge obtained is intended to aid to the performance enhancement of TiO<sub>2</sub> catalysts in the photo-catalytic cyclohexane oxidation and bring it closer to possible industrial applications.

## 7.1. SUMMARY

Since it was first found in 1921 that  $\text{TiO}_2$  is reduced in the presence of organics and sunlight, much interest has been given to the possibility of using sunlight to activate a photo-catalytic reaction, inducing the synthesis of bulk chemicals of commercial interest. Successful industrial application of photo-catalysis on the total oxidation of contaminants in water and air has already been achieved, but to selectively stop the oxidation process in a partially oxidized product, is a process which is still far from industrial applications. The reasons hereof are the low photonic efficiencies and strong catalyst deactivation of  $\text{TiO}_2$ , the most common catalyst for these reactions. The low efficiencies can be improved by reactor intensification and improving the electronic properties of the semiconductor i.e. reducing the rate of electron hole recombination. Besides the thermodynamic properties, the kinetic properties of the photo-catalyst in organic conditions must also be understood, which is the main focus of the work described in this thesis.

We chose to study the selective photo-catalytic oxidation of cyclohexane to cyclohexanone over  $\text{TiO}_2$  catalysts. A reason for the choice was the fact that cyclohexane is a simple probe molecule, suitable for infrared analysis. Furthermore cyclohexane oxidation has been previously proven to be selective, and the reaction of cyclohexane oxidation to cyclohexanone is of industrial relevance.

This thesis describes in detail the application of *in situ* ATR-FTIR spectroscopy to analyze the solid-liquid interface of real-time photo-catalytic oxidation of cyclohexane. Different reaction steps could be followed including the consumption of cyclohexane, the formation of cyclohexyl hydroperoxide, and cyclohexanone (adsorbed and desorbed), the formation and consumption of water, the formation of surface deactivating species and the deactivation or deprotonation of  $\text{Ti}(\text{OH})\text{-Ti}$  sites. Insight thus obtained allowed proposing the reaction mechanism illustrated in Chapter 2. Cyclohexyl hydroperoxide was proposed as the intermediate for cyclohexanone formation, but besides the observed features of this peroxide in the spectral results, no real proof for this route was obtained. This motivated the  $^{18}\text{O}$ -isotopic study described in Chapter 6, which led to a new mechanism. In contrast with the generally accepted mechanism, cyclohexyl hydroperoxide was concluded not to be the key intermediate,

but either a byproduct of the reaction, or an intermediate in a less favorable oxidation route. This conclusion is based on the observation that the labeling of cyclohexanone and of deactivating species formed, reflected the concentration of isotope on the  $\text{TiO}_2$  surface, through a Mars-van Krevelen mechanism. A new and more consistent mechanism is proposed considering the incorporation on  $^{16}\text{O}$  from the surface on the products and the surface regeneration by reaction with  $^{18}\text{O}_2$ .

The surface deactivating species, identified as carboxylates, carbonates and bicarbonates, are probably intermediates to the total oxidation route to  $\text{CO}_2$  and water. At room temperature, the formation of these species shows a delay suggesting that they are a consecutive step of cyclohexane oxidation products. It was proposed that this deactivation route involved the further oxidation of cyclohexanone. The slow cyclohexanone desorption, which under dark conditions occurred in the scale of minutes seemed to support this interpretation. However, the possibility of formation of deactivating species directly from cyclohexane was also considered, for no specific proof for either deactivating path had been obtained. Chapter 5 shows that operating the reaction at temperatures higher than  $23^\circ\text{C}$ , considerably enhances the initial rates of carboxylate formation, decreasing the selectivity of the reaction. Results suggest, that at room temperature, carboxylate formation is dominated by cyclohexanone over oxidation, but at elevated temperatures the direct cyclohexane oxidation dominates with an activation energy of  $18.4\text{ kJ/mol}$ .

In order to test if at room temperature, the consecutive cyclohexanone oxidation was leading to the deactivation of the surface, a strategy was developed to increase the rate of desorption of cyclohexanone. The strategies considered were: 1) the use of solvents, 2) operate the reaction at slightly elevated temperatures and 3) the modification of the  $\text{TiO}_2$  surface. The first option was thoroughly reported in literature, with cyclohexane photo-oxidation in dichloromethane providing the highest reaction rates, but also a decrease in the cyclohexanone to cyclohexanol ratio. The temperature effect on the rates of cyclohexanone desorption, in dark conditions, was positive but unfortunately temperature also enhanced deactivation leading to a decrease in selectivity (Chapter 5). Modifying the  $\text{TiO}_2$  surface by anchoring hydrophobic trimethylsilyl groups, increased the desorption rates of cyclohexanone and water and reduced the deactivation of the surface (Chapter 3). However, by anchoring silane groups to the surface, the number of available active sites is reduced. Two classes of catalysts could be identified: (1)

containing less than 1.0 wt% Si where the cyclohexanone formation rate is decreased by silylation due to a decrease in OH availability, and (2) containing more than 1.0 wt% Si where the improved desorption rate becomes dominant over the decreasing OH availability, and the cyclohexanone formation rate is increased. Besides the still necessary improvements in stability of surface silane groups, this strategy provided the best results in terms of product selectivities. Furthermore, the results showed that, at room temperature, cyclohexanone desorption is indeed limiting and its over oxidation is a considerable contributor to the formation of deactivating species.

Besides the mechanistic insight, isotope substitution also provides kinetic information on the rate determining step. The results obtained in Chapters 2 and 6 indicate that the kinetics of the photo-catalytic cyclohexanone formation are not determined by the breaking or formation of bonds involving hydrogen or oxygen atoms. A considerable kinetic isotope effect was determined for carboxylate formation, which is most likely related to C-O bond formation, yielding a carboxylate group and deactivating a  $\text{TiO}_2$  active site.

After obtaining mechanistic and kinetic information, we took a closer look into the interaction of the product cyclohexanone with the  $\text{TiO}_2$  surface and the effect of adsorbed water.  $\text{TiO}_2$  is known to be very hydrophilic, and DFT calculations showed that adsorbed water greatly affected the adsorption enthalpy of cyclohexanone and the resulting infrared absorption frequencies. A good correlation was found between the two ATR-FTIR bands of cyclohexanone adsorbed on  $\text{TiO}_2$ , and the frequencies calculated for configurations of cyclohexanone interacting with the (101) surface with low and intermediate levels of hydration. The corresponding adsorption enthalpies of these adsorbed configurations were calculated as -23.5 kJ/mol and -37.0 kJ/mol, respectively.

The microkinetic model in Chapter 5, predicts well the experimental results between 30 and 50 °C, although showing low sensitivity for determining the cyclohexanone adsorption equilibrium constants, providing some unexpected results. This model suggests that under UV illumination, much faster desorption rates take place than under dark conditions. This result indicates that, while looking closely to the organic conversions at the surface by ATR-FTIR spectroscopy, it is very important to also take into account the UV-induced electronic changes in the catalyst, for they affect the adsorption equilibrium constants.

## 7.2. OUTLOOK

The results presented in this thesis show that *in situ* spectroscopic techniques can be very insightful on the chemistry occurring at the catalyst surface during photo-catalytic reactions. However, the high sensitivity of ATR-FTIR can also be a limitation, because the unspecific character of this technique may induce very complicated spectral analysis. The combination of ATR-FTIR spectroscopy with isotope labeling and molecular modeling is therefore very useful to assign specific vibrations. Also an improved time resolution, which would allow the analysis of earlier stages of the reaction, could both simplify the spectral results and allow the analysis of labile intermediates. This could be obtained with Rapid Scan infrared spectroscopy, for analysis in the millisecond scale, or with Step Scan infrared spectroscopy for the analysis of steps in the microsecond and nanosecond time scale. However, Step Scan analysis requires averaging between repeatable experiments, which is difficult to achieve in room temperature catalysis, where strong product adsorption occurs. The use of infrared spectroscopy limits the analysis to an organic point of view, while the electronic process occurring during the reaction, which is also extremely important, is not studied. For example, the combination of Step Scan with Electron Paramagnetic Resonance (EPR) could extend the mechanistic knowledge from an organic viewpoint, to the preliminary steps of UV induced surface activated states and radical species.

Besides the improvements on the analytical techniques, also improvements on the illumination methods can be made, with the final objective being the use of sunlight as the illumination source for an efficient photo-catalytic reaction.  $\text{TiO}_2$  only absorbs light in the range of the UV, which corresponds to only 8% of the sunlight emission spectrum. To improve the light absorption of  $\text{TiO}_2$  catalyst, different strategies could be used. The first one is to modify the  $\text{TiO}_2$  catalyst to induce visible light absorption, which corresponds to 45% of the sunlight emission spectra. Different options have been considered in literature like doping the  $\text{TiO}_2$  catalyst with transition metals; synthesize composite semiconductor-semiconductor materials; and sensitize the  $\text{TiO}_2$  catalyst with a dye. A second option would be to maintain the absorption properties of  $\text{TiO}_2$  while using concentrated UV light to activate the catalyst in an optimized photo-reactor. To prevent excessive heating of the system, filters could be used to remove the visible and IR emission of the sun. A third option would be to use the efficient and well established

photovoltaic technology to absorb the solar light, transform it into electricity that could feed a UV lamp emitting in the range absorbed by the  $\text{TiO}_2$  catalyst. In this case a good illumination sources would be the Light Emitting Diodes (LED), which are small size lamps, with narrow emission spectrums and high energy efficiencies. The last two options are represented in Figure 7.1.

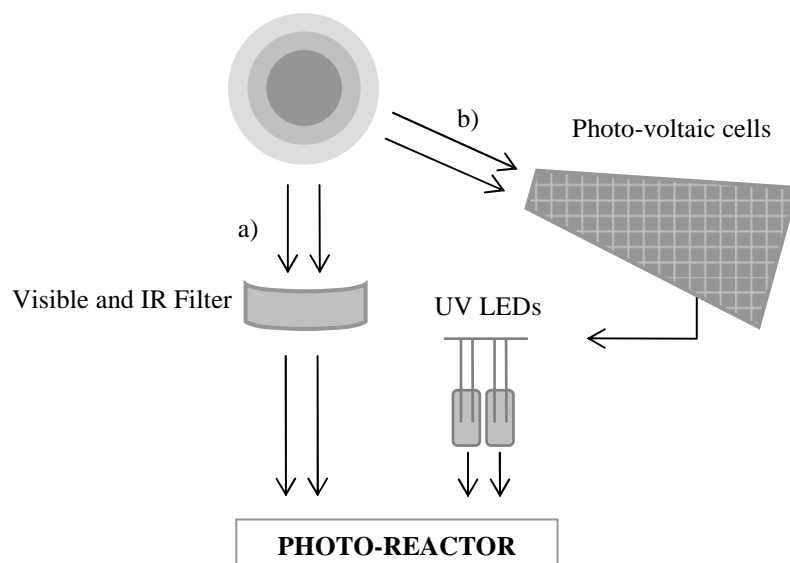


**Figure 7.1.** Schematic representations of the use of solar light on a photo-reactor by a) filtering the UV spectral contributions and b) by using photo-voltaic cells to transform solar light into electricity, to feed UV-LEDs incorporated in the photo-reactor design.



# SAMENVATTING

Sinds in 1921 gevonden werd dat  $\text{TiO}_2$  halfgeleiders reduceren in de aanwezigheid van organische verbindingen en zonlicht, is er veel aandacht geweest voor de mogelijkheid om zonlicht te gebruiken om fotokatalytische reacties in te zetten voor de synthese van economisch belangrijke bulkchemicaliën. Succesvolle industriële applicatie van fotokatalyse voor de volledige oxidatie van organische verontreinigingen in water en lucht is al bereikt maar het selectief stoppen van het oxidatieproces bij een partieel geoxideerd product is een proces dat nog ver verwijderd is van industriële toepassing. De redenen hiervoor zijn de lage foto-efficiënties en de sterke katalysatordeactivatie van  $\text{TiO}_2$ , de meest gebruikte katalysator voor deze reacties. De lage efficiënties kunnen verbeterd worden door reactorintensificatie en het verbeteren van de elektronische eigenschappen van de halfgeleider, zoals het reduceren van het aantal elektron gat recombinaties. Naast de elektronische eigenschappen, dienen de kinetische eigenschappen van de fotokatalysator in organische condities begrepen te worden, hetgeen het hoofddoel is van het werk beschreven in dit proefschrift.

We hebben ervoor gekozen om de selectieve fotokatalytische oxidatie van cyclohexaan naar cyclohexanon op  $\text{TiO}_2$  katalysatoren te bestuderen. De redenen voor deze keuze waren de volgende. Cyclohexaan is een eenvoudig molecuul, is niet erg reactief, en eerder is bewezen dat de oxidatie van dit molecuul selectief is. Het product cyclohexanon is zeer geschikt voor infrarood analyse, en bovendien is de oxidatie van cyclohexaan naar cyclohexanon een reactie van industriële relevantie.

Dit proefschrift beschrijft in detail de toepassing van AT-FTIR spectroscopie voor de analyse van het vast-vloeistof grensvlak tijdens real-time fotokatalytische oxidatie van cyclohexaan. Verschillende reagentia konden gevolgd worden, zoals de consumptie van cyclohexaan, de vorming van cyclohexyl hydroperoxide en cyclohexanon (geadsorbeerd en gedesorbeerd), de vorming en consumptie van water, de vorming van oppervlakdeactiverende moleculen en de deactivatie of deprotonatie van  $\text{Ti}(\text{OH})\text{-Ti}$  sites. Het gedetailleerde inzicht leidde tot het in Hoofdstuk 2 voorgestelde

reactiemechanisme. Cyclohexyl hydroperoxide wordt gepostuleerd als het intermediair in de vorming van cyclohexanon, maar buiten de geobserveerde spectrale resultaten is er geen overtuigend bewijs gevonden voor deze route. Dit was de motivatie voor de  $^{18}\text{O}$ -isotopen studie zoals uitgevoerd in hoofdstuk 6, die aanleiding gaf voor een voorstel van een alternatief mechanisme. In tegenstelling tot het algemeen geaccepteerde peroxide mechanisme, werd geconcludeerd dat cyclohexyl hydroperoxide niet het hoofdintermediair is, maar ofwel een bijproduct van de reactie, ofwel een intermediair van een minder gunstige oxidatie route. Deze conclusie is gebaseerd op de observatie dat de  $^{16}\text{O}/^{18}\text{O}$  verhouding van het geproduceerde cyclohexanon alsook gevormde deactiverende moleculen, overeenkomen met de verhouding van isotopen aangebracht op het  $\text{TiO}_2$  oppervlak. Een nieuw en meer consistent mechanisme wordt daarom voorgesteld, namelijk die van de incorporatie van 'O' van het oppervlak in de producten, gevolgd door oppervlak regeneratie door reactie met  $\text{O}_2$ , in feite een Mars en van Krevelen mechanisme.

De oppervlak deactiverende moleculen, geïdentificeerd als carboxylaten en bicarbonaten, zijn waarschijnlijk intermediairen in de totale oxidatieroute naar  $\text{CO}_2$  en water. Bij kamertemperatuur toont de vorming van deze moleculen een vertraging, wat een indicatie geeft dat deze in een opvolgende stap worden gevormd, en oxidatieproducten van cyclohexanon zijn. De trage cyclohexanon desorptie, die in het donker op de schaal van minuten plaats vindt lijkt deze interpretatie te ondersteunen. Desalniettemin is de mogelijkheid van de vorming van deactiverende moleculen direct uit cyclohexaan niet uit te sluiten, aangezien er voor geen van beide routes specifiek bewijs is gevonden.

Hoofdstuk 5 laat zien dat door het uitvoeren van de reactie bij temperaturen hoger dan  $23^\circ\text{C}$  de initiële reactiesnelheden van carboxylaatvorming vanuit cyclohexaan aanzienlijk worden verhoogd, wat de selectiviteit van de reactie verlaagt. Resultaten lijken aan te tonen dat carboxylaatvorming bij kamertemperatuur voornamelijk geschiedt door verdere oxidatie van cyclohexanon, maar dat bij verhoogde temperatuur (thermische) directe cyclohexaan oxidatie steeds belangrijker wordt. Hiervoor is een activeringsenergie van  $18.4 \text{ kJ/mol}$  bepaald.

Om te testen of bij kamertemperatuur de verdere oxidatie van cyclohexanon leidt tot deactivatie van het oppervlak zijn diverse strategieën ontwikkeld om de snelheid van cyclohexanon desorptie te verhogen. De beschouwde strategieën waren: 1) gebruik van

oplosmiddelen, 2) uitvoering van the reactie bij licht verhoogde temperatuur en 3) de modificatie van het  $\text{TiO}_2$ -oppervlak. De eerste optie is grondig gerapporteerd in bestaande literatuur, waaruit blijkt dat cyclohexaan foto-oxidatie in dichloromethaan de hoogste reactiesnelheden geeft, maar ook leidt tot een verlaging van de cyclohexanon/cyclohexanol verhouding. Verhoging van de temperatuur heeft een positief effect op de snelheid van cyclohexanon desorptie (in afwezigheid van licht) maar de door temperatuurverhoging verhoogde deactivatie leidt ook tot een afname in selectiviteit. Het modifieren van het  $\text{TiO}_2$  oppervlak door middel van het verankeren van hydrofobe trimethylsilyl groepen verhoogt de desorptiesnelheden van cyclohexanon en water. Echter, door het verankeren van silylgroepen aan het oppervlak wordt het aantal actieve sites verminderd. Twee katalysatorklassen konden worden onderscheiden: (1) minder dan 1.0 gewichtsprocent Si bevattend, waarbij de cyclohexanon vormingssnelheid verminderd wordt door silylatie wegens een verminderde beschikbaarheid van OH en (2) meer dan 1.0 gewichtsprocent Si bevattend, waarbij het positieve effect van de verhoogde desorptiesnelheid sterker is dan het negatieve effect van de verminderde OH beschikbaarheid en de vormingssnelheid van cyclohexanon dus bevordert wordt. Silylatie blokkeerde de meest reactieve sites en resulteerde, wegens de versnelde productdesorptie, in een verlaging van de deactivatiesnelheid. Ondanks de nog benodigde verbeteringen in de stabiliteit van de silaangroepen aan het oppervlak leidde deze strategie tot het beste resultaat op het gebied van selectiviteit. Verder tonen de resultaten aan dat, bij kamertemperatuur, de cyclohexanondesorptie inderdaad limiterend is en de verdere oxidatie een aanzienlijke bijdrage levert aan de vorming van deactiverende moleculen.

Naast het mechanistische inzicht levert isotoopuitwisseling ook kinetische informatie op betreffende de snelheidslimiterende stap. De in hoofdstuk 2 en 6 beschreven resultaten suggereren dat de kinetiek van de fotokatalytische cyclohexanon vorming niet bepaald wordt door het breken of creëren van bindingen waarbij waterstof- of zuurstofatomen betrokken zijn. Een aanzienlijk kinetisch isotoopeffect is bepaald voor carboxylaatforming, die waarschijnlijk gerelateerd is aan de vorming van een C-O binding, resulterend in een carboxylaatgroep en een gedeactiveerde  $\text{TiO}_2$  site.

Na het verkrijgen van kinetische informatie is in meer detail gekeken naar de interactie tussen het geproduceerde cyclohexanon en het  $\text{TiO}_2$  oppervlak alsmede het effect van geadsorbeerd water. Het is bekend dat  $\text{TiO}_2$  sterk hydrofiel is en DFT

berekeningen toonden aan dat geadsorbeerd water een sterk effect heeft op de adsorptie-enthalpie van cyclohexanon en de resulterende infrarood absorptie frequenties. Een goede correlatie werd gevonden tussen de twee ATR-FTIR banden van cyclohexanon geadsorbeerd op  $\text{TiO}_2$  en de frequenties berekend voor configuraties van cyclohexanon die interactie vertonen met een (101) anataas kristal vlak met lage en middelhoge niveaus van hydratatie. De corresponderende adsorptie enthalpieën van deze geadsorbeerde conformaties werden uitgerekend op -23.5 kJ/mol en -37.0 kJ/mol.

Het microkinetische model in hoofdstuk 5, dat de experimentele resultaten tussen 30 en 50°C goed voorspelt, levert een aantal onverwachte resultaten, hoewel de onzekerheid in de waarden van de evenwichtsconstanten voor cyclohexanonadsorptie aanzienlijk is. Het model suggereert dat in aanwezigheid van UV licht een veel snellere desorptie plaatsvindt dan in het donker. Dit geeft aan dat bij het in detail bestuderen van de organische conversies aan het oppervlak met ATR-FTIR het erg belangrijk is om de UV-geïnduceerde elektronische veranderingen in de katalysator in beschouwing te nemen, omdat deze de waarden van de evenwichtsconstanten voor adsorptie sterk kunnen beïnvloeden.

De resultaten in dit proefschrift tonen aan dat *in situ* spectroscopische technieken zeer inzichtelijk kunnen zijn betreffende de chemie die op het katalysatoroppervlak plaatsvinden tijdens fotokatalytische reacties. Een grondige mechanistische en kinetische studie is gemaakt voor de fotokatalytische cyclohexaan oxidatie op  $\text{TiO}_2$ . De twee belangrijkste valkuilen van de reactie waren de hoge deactivatiesnelheid van  $\text{TiO}_2$  en de lage fotonefficiëntie. Veel nadruk is gelegd op het verlagen van de katalysatordeactivatie, wat bereikt werd door het gebruik van een kristallijne  $\text{TiO}_2$  katalysator met verhoogde oppervlakhydrofobiciteit. Hoewel de nadruk van het werk gepresenteerd in dit proefschrift niet lag op het verhogen van de fotonefficiëntie van cyclohexaan foto-oxidatie, worden de volgende drie proposities betreffende het verhogen van de lichtabsorptie-efficiëntie door  $\text{TiO}_2$  katalysatoren voorgesteld:

(i) De  $\text{TiO}_2$  katalysator kan worden gemodificeerd om zichtbaar licht van de zon op te vangen, door transitimetalen aan de  $\text{TiO}_2$  katalysator toe te voegen, composiet semiconductor-semiconductor materialen te synthetiseren, of de  $\text{TiO}_2$  gevoeliger te maken met behulp van verfstoffen.

(ii) De  $\text{TiO}_2$  absorptie eigenschappen hebben geen nadelige invloed bij gebruik van geconcentreerd UV-licht door het gebruik van een geoptimaliseerde fotoreactor configuratie.

(iii) De gevestigde fotonvoltaïsche technologie kan worden toegepast om zonlicht te absorberen, deze te transformeren in elektriciteit om UV LEDs te voeden die licht uitzenden binnen het absorptiebereik van de katalysator.



# LIST OF ACRONYMS

ATR	Attenuated Total Reflection
FTIR	Fourier Transform Infrared
IRE	Internal Reflection Element
UV	Ultraviolet
LED	Light Emitting Diodes
LHHW	Langmuir-Hinshelwood-Hougen-Watson
MAS	Magical Angle Spinning
NMR	Nuclear Magnetic Resonance
DRIFTS	Diffuse Reflectance Infrared Spectroscopy
XRD	X-Ray Diffraction
$S_{\text{BET}}$	BET surface area
DTGS	Deuterated Triglycine Sulfate
TRS	Time-Resolved Spectroscopy
HMDS	Hexamethyldisilazane
TGA	Thermogravimetric Analysis
XRF	X-ray Fluorescence
GC	Gas Chromatography
HPLC	High-Performance Liquid Chromatography
MS	Mass Spectroscopy
TPD	Temperature-Programmed Desorption
TEM	Transmission Electron Microscopy
EPR	Electron Paramagnetic Resonance
FFT	Fast Fourier Transform
DFT	Density Functional Theory
VASP	Vienna Ab-Initio Simulation Package
GGA	Generalized Gradient Approximation
PW91	Perdew and Wang 91

PAW	Projector Augmented Wave
MD	Molecular Dynamics
Cyh	Cyclohexane
CyhO	Cyclohexanone
Carbox	Carboxylates
CHHP	Cyclohexyl Hydroperoxide
OIE	Oxygen Isotope Exchange
PO	Photo-oxidation



# LIST OF PUBLICATIONS AND PRESENTATIONS

## PUBLICATIONS

A.R. Almeida, J.A. Moulijn, G. Mul, Cyclohexane photo-catalytic oxidation on TiO<sub>2</sub>: evidence for a Mars-van Krevelen mechanism (2010) submitted.

A.R. Almeida, R. Berger, J.A. Moulijn, G. Mul, Cyclohexane photo-catalytic oxidation over TiO<sub>2</sub>: a novel interpretation of temperature dependent performance (2010) submitted.

A.R. Almeida, M. Calatayud, F. Tielens, J.A. Moulijn, G. Mul, Combined ATR-FTIR and DFT study of cyclohexanone adsorption on hydrated TiO<sub>2</sub> anatase surfaces (2010) submitted.

A.R. Almeida, J.T. Carneiro, J.A. Moulijn, G. Mul, Improved performance of TiO<sub>2</sub> in the selective photo-catalytic oxidation cyclohexane by increasing the rate of desorption through surface silylation, J. Catal. 273 (2010) 116.

J.T. Carneiro, A.R. Almeida, J.A. Moulijn, G. Mul, Cyclohexane selective photo-catalytic oxidation by anatase TiO<sub>2</sub>: influence of particle size and crystallinity, Phys. Chem. Chem. Phys. 12 (2010) 2744.

M.D. Hernandez-Alonso, A.R. Almeida, J.A. Moulijn, G. Mul, Identification of the role of surface acidity in the deactivation of TiO<sub>2</sub> in the selective photo-oxidation of cyclohexane, Catal. Today 143 (2009) 326.

T.J.A. Renckens, A.R. Almeida, M.R. Damen, M.T. Kreutzer, G. Mul, Product desorption limitations in selective photo-catalytic oxidation, Catal. Today, 155 (2010) 302.

J. Gascon, M.D. Hernandez-Alonso, A.R. Almeida, G.P. van Klink, F. Kapteijn, G. Mul, Isorecticular MOFs as efficient photo-catalysts with tunable bandgap: an operando FTIR study of the photo-induced oxidation of propylene, Chemsuschem 2008, 1, 981.

P. Du, A. Bueno-Lopez, M. Verbaas, A.R. Almeida, M. Makkee, J.A. Moulijn, G. Mul, The effect of surface OH-population on the photo-catalytic activity of rare earth-doped P25-TiO<sub>2</sub> in methylene blue degradation, J. Catal. 2008, 260(1), 75.

A.R. Almeida, J.A. Moulijn, G. Mul, *In situ* ATR-FTIR study on the selective photo-oxidation of cyclohexane over anatase TiO<sub>2</sub>, J. Phys. Chem. C, 2008, 112(5), 1552.

## ORAL PRESENTATIONS

A.R. Almeida, F. Tielens, M. Calatayd, J.A. Moulijn, G. Mul; Cyclohexanone adsorption on TiO<sub>2</sub>: *in situ* ATR-FTIR and DFT calculations; American Chemical Society (ACS), San Francisco, USA, March 2010.

A.R. Almeida; Mul, G.; Moulijn, J. A.; Cyclohexanone adsorption on TiO<sub>2</sub>: *in situ* ATR-FTIR and DFT calculations; Netherlands' Catalysis and Chemistry Conference (NCCC), Noordwijkerhout, The Netherlands; March 2010.

A.R. Almeida; J.T. Carneiro; G. Mul.; J.A. Moulijn; Primary steps of TiO<sub>2</sub> deactivation upon cyclohexane photo-catalytic oxidation; International Symposium on Catalyst Deactivation (CatDeact), Delft, The Netherlands; October 2009.

A.R. Almeida; G. Mul; J. A. Moulijn; *In Situ* ATR-FTIR study on the selective photo-catalytic oxidation of cyclohexane; International Conference of Catalysis (ICC), Seoul, South Korea; July 2008.

A.R. Almeida; G. Mul; J. A. Moulijn; *In Situ* ATR-FTIR study on the selective photo-catalytic oxidation of cyclohexane; Netherlands' Catalysis and Chemistry Conference (NCCC), Noordwijkerhout, The Netherlands; March 2008.

A.R. Almeida, G. Mul. J.A. Moulijn; *In situ* ATR-FTIR characterization of photo-catalytic reactions, Infrarood en Raman discussie groep, Oss, The Netherlands, November 2007.

## POSTER PRESENTATIONS

A.R. Almeida, G. Mul, J.A. Moulijn, Increasing the hydrophobicity of TiO<sub>2</sub> to enhance performance in the selective photo-catalytic oxidation of cyclohexane, Netherlands' Catalysis and Chemistry Conference (NCCC), Noordwijkerhout, The Netherlands, March 2009.

A. R. Almeida, G. Mul, J.A. Moulijn, Time resolved *in situ* ATR-FTIR characterization of liquid phase photo-catalytic oxidation; Nanoporous materials in energy environment (NAPEN), October 2008.

A.R. Almeida, G. Mul, J.A. Moulijn; ATR-FTIR characterization of photo-catalytic reactions, DCT Science Day, De Uithof, The Hague, December 2007.

A.R. Almeida, G. Mul, J.A. Moulijn; ATR-FTIR characterization of cyclohexane photo-catalytic oxidation; Netherlands' Catalysis and Chemistry Conference (NCCC), Noordwijkerhout, The Netherlands, March 2007.



# CURRICULUM VITAE

Ana Rita Martins Guerreiro Rocha Almeida was born on May 27<sup>th</sup> 1982 in Lisbon, Portugal. She grew up in Loulé (Algarve), where she graduated from high school in the year of 2000. In the same year she initiated the Chemical Engineering degree (equivalent to BSc + MSc) in Faculdade de Ciências e Tecnologia of Universidade Nova de Lisboa. Graduated with a final CPD project entitled “EuroPA S. A. - Production of Phthalic Anhydride”. Her first contact with the Technical University of Delft was in 2005, with an Erasmus project entitled “CeO<sub>2</sub>-promoted Rh-Al<sub>2</sub>O<sub>3</sub> and Rh-SiO<sub>2</sub> catalysts for N<sub>2</sub>O decomposition”. She took a PhD position in the *in situ* monitoring of photo-catalytic reactions using Infrared Spectroscopy, under the supervision of Prof. dr. Jacob A. Moulijn and Prof. dr. Guido Mul. Her PhD work, presented in this thesis, resulted in publications in international journals and in oral presentations at several international conferences. During her PhD she applied for a short term scientific mission of two months in the Université Pierre et Marie Curie in Paris, France. In the Laboratoire de Réactivité de Surface, she had the opportunity of combining her experimental knowledge on catalysis with molecular modeling.



# ACKNOWLEDGEMENTS

Many people have contributed to this thesis, with their work, friendship, or support. First of all I would like to thank my promoters, Guido Mul and Jacob Moulijn, for their support even though in the final stages of my PhD they were not working at TUDelft anymore. Your interest in my work kept me motivated throughout these four years. Jacob, I'd like to thank you for your optimistic approach, and the broader perspective you've given to my work. Guido, I'd like to thank you for your constant good mood and the opportunities you've given me during my PhD.

I acknowledge the committee members of my PhD defense, Prof. Freek Kapteijn, Prof. Isabel Arends, Prof. Bert Weckhuysen, Prof. Jim Anderson, Dr. Frederik Tielens, and Prof. Herman van Bakkum. Thank you for accepting the invitation, for the attention you've provided to my thesis and the valuable comments.

I'd like to thank Frederik Tielens and Monica Calatayud for the great time spent in Université Pierre et Marie Curie, which was way beyond my expectation both in terms of work and in social terms. I'd also like to thank Noelia, Ana Lucia, Rui, Colin, Marc, Margerie, Patrick, Ronja, Jingying and Laura for their friendship during those two very enjoyable months in Paris.

Thanks to Freek Kapteijn for the opportunities provided. Thanks to Michiel Makkee for always being nice and readily signing my safety assessment sheets. Thanks to Michiel Kreutzer for the nice discussions and collaboration. Thanks to Patricia Kooyman for always being very pleasant and for the TEM. Thanks to Wim Buijs for his help on DFT calculations. Big thanks to Els and Elly for being always extremely helpful and friendly. Big thanks to Bart (van der Linden), Bart (Boshuizen), Harrie, Kevin and Willy for their support and for helping me with the technical problems, which insisted on popping up every now and then. Thanks to Joana, Dirk, Jorge, Loli, Rob, Chieh-Chao, Ugo, Gerard, and Jorrit for your help and fruitful collaborations. Thanks to Mariette, Martijn, Arjan, Melvin and LO2 students for being such good students and making my supervision such a rewarding experience.

I'd like to thank all the remaining members of the CE group for the good environment and for always making me feel at home in the lab: Christa, Jiarong (Li), Jasper, Alberto, Enrique, Malles, Bandar, Johan, Canan, Jana, Hossein, Christian, Pita, Sina, Oscar, Maarten, Emmanuel, Soren and Johan (Groen). Thanks also to the ex-members of the CE group or R&CE group as it used to be called: Hiro (and Cristina), Nathalie, Alexandre, Sergio, Asun, Pedro, Sonia, Leticia, Christophe, Mila and Eli. A special thanks to Sander for his friendship, nice time in the office and for his help in the Dutch translations.

I'd like to thank Professor Isabel Fonseca from FCT-UNL, for giving me the opportunity of doing an Erasmus project in TUDelft, which has allowed me to continue with the PhD research presented in this thesis.

When doing a PhD it is important to know when to stop thinking about work and external activities are really helpful for that. Very big thanks to the people Capoeira Liberdade in particular to Marquinhos, who made really tough trainings! Special thanks to some capoeiristas in particular: Melanie (Carapeta), Alper (Caracol), Gary (Divino) and Anouk (Ratinha), my companion in The Netherlands for the last 5 years.

Very big thanks to the all the people from the organizing committee (and friends) of Festibérico (Portuguese and Spanish film festival), for their friendship and good times: Telma, Casimiro, Pedro, Mafalda, João, Pieter, Silvia, Mercedes, Mario, Maria, Marta and Horácio. Special thanks to Mafalda for the very interesting experience while shooting the short movie "A Promessa".

Thanks to Bram, for giving me his old bass guitar and to Bobby Jacobs for teaching me how to play it.

When living abroad it's common to become homesick and to receive visits from old friends is really appreciated. Big thanks to my portuguese friends who paied me a visit in The Netherlands: Rita (Neto), Claudio, Vera (apesar de a visita ter sido por uma ocasião vulcânica, foi bom poder estar contigo mais uma vez por territórios holandeses), Susana, Emanuel, Roni, Vânia, Sara, Guia, Iris, Rui, Henrique, Célia (apesar de nos termos desencontrado), Rita, Patrícia, Marta, Cliff, Daniel e Veralisa.

A PhD research is a series of ups and downs, and the downs can sometimes be very frustrating. On those occasions the help of my friends and family was essential. Big thanks to Joana Torres, one of my childhood friends who shared with me my first years in the Netherlands and has helped so much. Big thanks to Daniel, Veralisa, Rita (Neto),



Nuno (Neto), e Luís for being such good friends. Thanks to my friends in Amsterdam who helped me adapt fast into my new hometown, Cláudia, Miguel, Lúcia and Alex.

Agradeço aos meus pais por terem sido sempre muito exigentes comigo e pelo apoio que sempre me deram e acima de tudo, por acreditarem nas minhas capacidades. À minha mãe, Nídia, agradeço em particular a forte amizade e a confiança que sempre teve em mim. Ao meu pai António agradeço ter-me dado o gosto pela qualidade no trabalho e dedicação. Um agradecimento muito especial à minha avó Maria Manuela que me apoiou na vinda para a Holanda mas que infelizmente já não está cá para me ver acabar o doutoramento. Agradeço ao meu avô Zé Ruivo e à família Moreira. Agradeço o forte apoio dado pelos pais do meu namorado, Nuno e Celeste. Finalmente, um obrigado gigantesco para o meu namorado Nuno, que largou tudo para vir comigo para a Holanda, que me ajudou tantas vezes a ultrapassar os períodos mais complicados e ver os lado positivo das coisas. Obrigada por acreditares em mim e me ajudares a acreditar nas minhas capacidades.

Now I will cite the words of the wise Monty Python, and leave a message to everyone who helped me throughout these years:

“Always look on the bright side of life”

